

Problems of Planetology, Cosmochemistry and Meteoritica

Alexeev V.A., Kalinina G.V., Pavlova T.A. Ablation of the ordinary chondrites by the track data

V.I. Vernadsky Institute of Geochemistry and Analytical Chemistry RAS, Moscow (AVAL37@mail.ru)

Abstract. Distribution of the ablation values of H- and L-chondrites was studied with using of the new track research results in the Laboratory of cosmochemistry. The obtained data showed that the meteorites with low found weight had the higher degree of ablation. This effect is more clearly shown for the H- chondrites. Such difference may be due to the difference of the parent body orbits of these chemical meteorite groups.

Keywords: tracks, cosmic rays, chondrites, ablation.

Introduction. While moving through the atmosphere with a cosmic velocity, the meteoroids may lose a significant part of their mass due to ablation, by which we usually understand a loss of mass, resulting from the melting of the outer layer and the successive liquid film blowing by an incident air flow, as well as evaporation of the substance and its removal in the form of vapours. The data on ablation can be useful when the exposure history of meteorites and time and space variations of cosmic radiation are studied.

To estimate the ablation, we can involve data on the content and depth distribution of cosmogenic stable and radioactive isotopes in a meteorite. These data provide the possibility of estimating the preatmospheric size and, hence, the mass of the meteorite and, thus, calculating the ablation (A , %) by the formula:

$$A = (1 - r^3/R^3) \times 100 \quad (1),$$

where r is an equivalent radius of a meteorite with fallen (collected) mass m . It should, of course, be appreciated that the collected mass is not always corresponds to the fallen mass, especially for finds. Some fragments of the meteorite could be lost after its destruction in the atmosphere. In this case, the ablation calculated by the formula (1) will correspond to the upper limiting value.

The possibility of involving the data on the distribution of cosmogenic Ne isotopes for estimating the meteorite ablation was thoroughly examined by Alexeev [2003]. However, this method has some limitations, associated with the fact that the depth dependence of the $^{22}\text{Ne}/^{21}\text{Ne}$ ratio changes its form under high shielding conditions in meteorites with preatmospheric radius $R \geq 60$ cm. It leads to an uncertainty in the estimated ablation of meteorites with large preatmospheric masses when the average

$^{22}\text{Ne}/^{21}\text{Ne}$ ratio in the meteorite is less than ~ 1.08 [Alexeev, 2003].

The track method is also often applied to determine the ablation [Bagolia et al., 1977; Bhandari et al., 1980; Cantelaube et al., 1969; Fleischer et al., 1967]. Heavy nuclei of galactic cosmic rays produce tracks in meteorite minerals (olivine, pyroxene, etc.). The density of these tracks (ρ , cm^{-2}) depends on both the duration of irradiation (exposure age t , million years) and the depth (d , cm) at which the study sample occurs in the preatmospheric meteorite body. A strong depth dependence of the rate of track formation (ρ/t) allows a more accurate estimation of the degree of the sample shielding than in the case when cosmogenic isotopes are used for this purpose. Thus, for example, the value ρ/t in a body with a chondrite composition and preatmospheric radius $R = 100$ cm decreases by more than three orders of magnitude with a depth varying from 1 to 20 cm [Bhattacharya et al., 1973], while, for example, the corresponding variation of the ratio of the rates of formation of cosmogenic isotopes $^{22}\text{Ne}_c/^{21}\text{Ne}_c$, which is also used to estimate the shielding degree, is only about 20% in this case. The rate of track formation is mainly determined by the depth of the sample and - to a considerably smaller extent - by the meteorite radius. Thus, the rates of track formation ρ/t at a depth of 5 cm from the surface in meteorites with $R = 20$ cm and $R = 50$ cm differ only by 5% [Gupta and Lal, 1978].

Fleischer et al. [1967] were the first to determine ablation by the track method when studying samples of 30 meteorites. Later many meteorites were investigated by this method. Cantelaube et al. [1969] determined the preatmospheric size of the Saint-Severin LL6 meteorite with a high accuracy (to 1-2 cm). The meteorites Pribram, Lost City, Innisfree, and Peekskill, whose falls had been instrumentally recorded, were thoroughly examined also. A detailed track data for about 160 meteorites of different types were presented by Bhandari et al. [1980]. Bagolia et al. [1977] successfully applied the track method to the examination of the exposure history of the Dhajala H3.8 meteorite, which had fallen as a meteorite rain. The authors determined the track density in more than 250 fragments of this meteorite, which made up about 70% of the total fallen mass. Involving also the data on the exposure age of the meteorite, they determined the preatmospheric radius of the meteorite (38 ± 2 cm) and its ablation ($86.7 \pm 2.1\%$) within small limits. In many of these studies the depth distribution of the track density in recovered fragments of the meteorite was thoroughly considered, the shielding degree was determined for each sample examined, the preatmospheric size of

Problems of Planetology, Cosmochemistry and Meteoritica

the meteorite was restored, and the ablation degree was estimated.

Based on the information about the depth dependence of the rate of track formation, the

nomogram has been developed [Alexeev, 2004]. This nomogram allows estimating the meteorite ablation on the found mass and measured average rate of track formation.

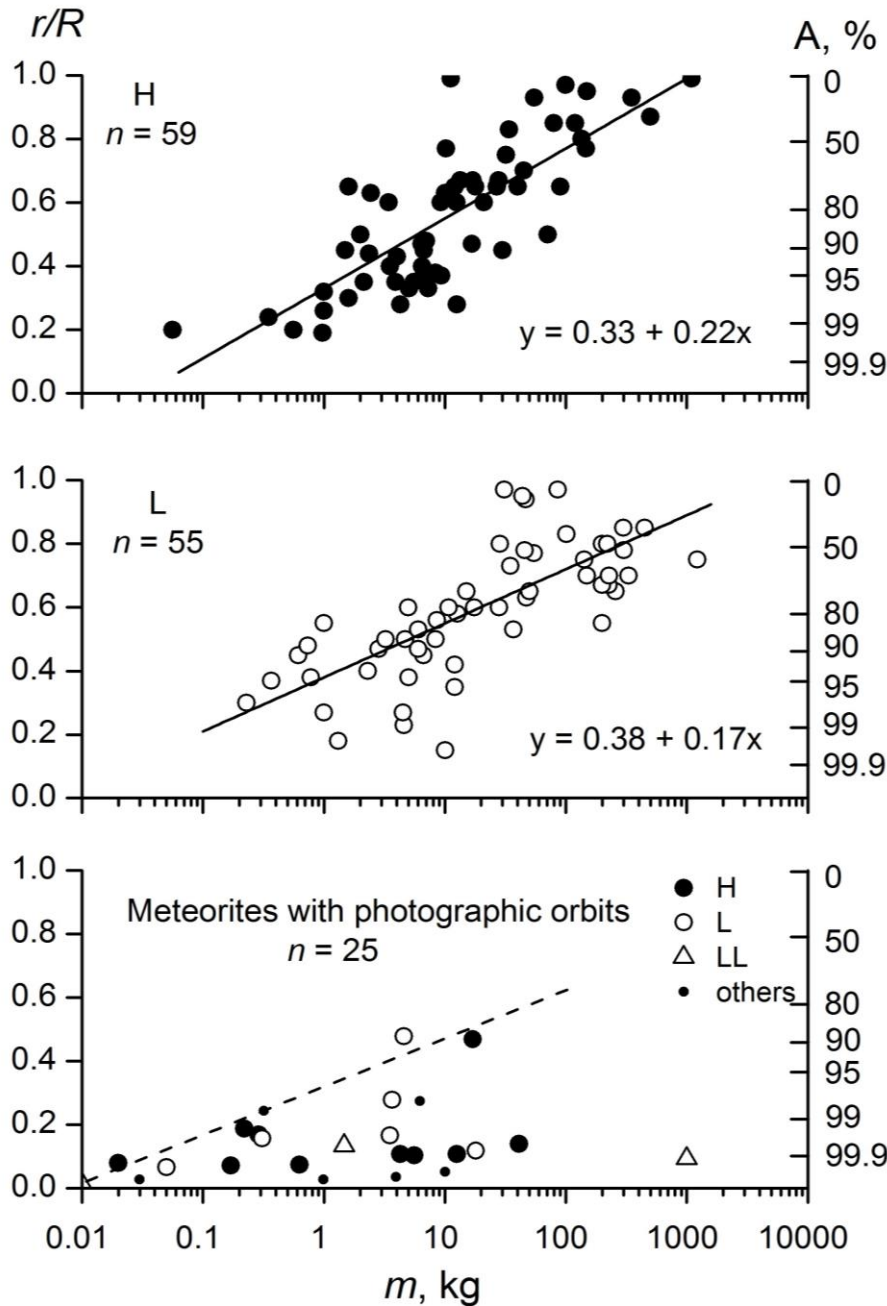


Fig. 1. The r/R ratio depending on the found mass (m , kg) of H and L chondrites and meteorites with photographic orbits. Straight lines and corresponding equations relate to the regression lines. A is the value of ablation; n is the number of meteorites.

Table 1. Parameters of the regression lines for the dependence of $r/R = a + b \lg m$.

Chondrites	n	a	b	Notes
H	59	0.33 ± 0.03	0.22 ± 0.03	1
	25	0.41 ± 0.05	0.15 ± 0.04	2
	84	0.35 ± 0.03	0.20 ± 0.02	3
L	55	0.38 ± 0.04	0.17 ± 0.02	1
	23	0.50 ± 0.04	0.09 ± 0.04	2
	78	0.43 ± 0.03	0.14 ± 0.02	3

Notes: 1 - our data; 2 - the data according to Bhandari et al. [1980]; 3 - all data; n is the number of meteorites

Table 2. Distribution (in %) of H and L chondrites on the r/R ratio.

Chondrites	n	$r/R < 0.5$	$r/R \geq 0.5$	Notes
H	59	46 ± 9	54 ± 10	1
	25	40 ± 13	60 ± 16	2
	84	44 ± 7	56 ± 8	3
L	55	31 ± 8	69 ± 11	1
	23	26 ± 11	74 ± 18	2
	78	29 ± 6	71 ± 10	3

Notes as for Table 1.

The results of analyses of r/R distributions and, respectively, ablation for 114 H and L chondrites, are given in this work on the basis of previously obtained data and also with the involvement of new measurement results obtained at the Cosmochemistry Laboratory. We compared these results with the results of the analysis of the Bhandari et al. [1980] data. The data for 25 meteorites with the known orbit parameters [Meier M.M., 2016] are also presented in the work.

Results and discussion

Results of the analysis of the obtained data are shown in the Figs 1 and 2 and in the Tables 1 and 2. The linear dependences of r/R from $\lg m$ in semi-log scale are shown in Fig. 1. It is typical, the parameters of the regression line equation ($y = a + bx$) describing this dependence for our data within $\sim(1-1.5)\sigma$ coincide with the parameters found on the data [Bhandari et al., 1980] (Table 1).

The analysis revealed a significant feature: the value of the parameter b in the regression equation for the H chondrites is significantly higher than for the L chondrites (for all data there are 0.20 ± 0.02 and 0.14 ± 0.02 , respectively). A similar trend of the r/R values increase with the increasing the found mass is also observed for meteorites of different chemical classes with the known orbital parameters and with independently calculated ablation (Fig. 1).

The difference between H and L chondrites is clearly seen when comparing the r/R distributions (Fig. 2 and Table 2). The share of H chondrites with $r/R < 0.5$ is $(44 \pm 7)\%$, whereas for L chondrites this value is substantially less $(29 \pm 6)\%$.

Note that for meteorites with the known parameters of orbits the major share (80%) suffered the ablation greater than 99%. As regards to track data like according to our calculations, and also according to Bhandari et al. [1980], less than 2% of meteorites suffered such ablation ($> 99\%$). This difference can be caused by overstating the value of meteorite preatmospheric mass at its estimation according to the observational data during the passage of meteoroid in the earth's atmosphere.

Conclusions

With the involvement of the new track data obtained at the Cosmochemistry Laboratory, the distribution of the r/R ratio and consequently the values of ablation of H and L chondrites were studied. The obtained results indicate the meaningful dependence of r/R and the ablation, also, from the found mass of a meteorite. Herewith the H chondrites with a small mass (less than about 10 kg) are characterized the higher degree of the ablation in comparison with L chondrites. The found effect is well confirmed by the results of the track data analysis of Bhandari et al. [1980] for ordinary chondrites. This difference can be caused by the

differences in the orbit parameters of the parent bodies of these chemical groups of meteorites.

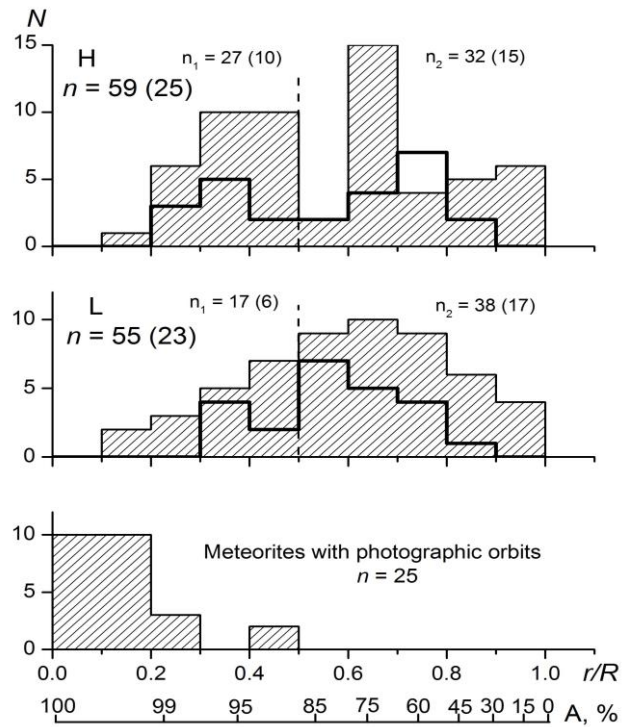


Fig. 2. Distribution of the r/R ratios and the corresponding values of ablation A for H and L chondrites and meteorites with the known orbital parameters; n is the number of meteorites; n_1 and n_2 are the numbers of meteorites with ratios $r/R < 0.5$ and $r/R \geq 0.5$, respectively; the interface is marked by dotted lines. Numbers in parentheses and distributions shown by bold lines are obtained according to the data of [Bhandari et al., 1980].

This work was supported in part by the Program of the Fundamental Research Number 7 of the Presidium of Russian Academy of Sciences.

References:

1. Alexeev V.A. 2003 Meteorite ablation evaluated from data on the distribution of cosmogenic neon isotopes // *Solar System Research*. V. 37. No. 3. P. 207-217.
2. Alexeev V.A. 2004 Meteorite ablation evaluated from the data on the density of cosmic-ray tracks // *Solar System Research*. V. 38. No. 3. P. 194-202.
3. Bagolia C., Doshi N., Gupta S.K. et al. 1977. The Dhajala meteorite shower: Atmospheric fragmentation and ablation based on cosmic ray track studies// *Nucl. Track Detection*. V. 1 P. 83-92.
4. Bhandari N., Lal D., Rajan R.S. et al. 1980. Atmospheric ablation in meteorites: a study based on cosmic ray tracks and neon isotopes. // *Nucl. Tracks*. V. 4. No. 4. P. 213-262.
5. Bhattacharya S.K., Goswami J.N., Lal D. 1973. Semiempirical rates of formation of cosmic ray tracks in spherical objects exposed in space: Preatmospheric and postatmospheric depth profiles // *J. Geophys. Res.* V. 78. No. 34. P. 8356-8363.

6. Cantelaube Y., Pellas P., Nordemann D., Tobalem J. 1969. Reconstitution de la meteorite Saint-Severin dans l'espace // Meteorite Research // Ed. Millman P.M. Dordrecht-Holland: D. Reidel Publ. Co. P. 705-713.
7. Fleischer R.L., Price P.B., Walker R.M., Maurette M. 1967. Origin of fossil charged-particle tracks in meteorites // *J. Geophys. Res.* V. 72. P. 331-353.
8. Gupta S.K., Lal D. 1978. On estimation of mass ablation of meteorites based on studies of cosmic ray tracks // *Nuclear Track Detect.* V. 2. No. 1. P. 37-49.
9. Meier M.M. 2016. <http://www.meteoriteorbits.info>.

Barenbaum A.A. Creating a chronological time scale for solar system UDC 523.2, 551.7.03

Oil and Gas Research Institute RAS, Moscow
(azary@mail.ru)

Abstract. Substantiates the applicability of modern geochronological table developed for the Earth in form chronological time scale for the Solar system. The main stages of creation the unified chronological scale for all planets of the Solar system are discussed.

Keywords: geochronological table, galactic model of geological cyclicity, Galactocentric paradigm

Introduction: Modern geology cannot be imagined without a geochronological table, which links the major past geological events in the Earth with absolute time. The same task today is relevant for other planets of the solar system, as well as their satellites, comets and asteroids.

The purpose of this article is to show that a geochronological scale constructed from data for the Earth is also applicable to other objects of the solar system. This principle conclusion is based on an analysis of the history of the creation of geochronological table relating to the interdisciplinary field of knowledge at the junction of geological and astronomical sciences. The creating of this table and its theoretical justification included a number of stages, what we will a brief examination.

Stages of geochronological table development: An empirical basis for building the geochronological table is the stratigraphic scale. The first stratigraphic scale as a reflection of the natural stages of the Earth's geological history was officially approved in geology in 1900. Generalizing data on extinctions of living organisms in the Phanerozoic, geologists empirically established and reflected in this table the fact existence of planetary geological cycles, which were named stratons. Further studies have shown that the main geological events in the history of the Earth occurred at the boundary of stratons of different rank.

Over the past hundred years, the stratigraphic scale has been constantly updated and refined [Zhamoyda, 2013]. At the present time in it, together with the Phanerozoic, two separate parts are

distinguished: Precambrian and Quaternary. Each of which is characterized by own interval of rocks age and leading methods of dismemberment. The Phanerozoic stratons are fixed by a biostratigraphic method. Precambrian subdivisions are determined on the basis of tectonomagmatic cyclicity, and for the Quaternary period, the leading is the climate-stratigraphic method.

All these improvements have become possible since the 1950s, when geologists began to use isotope methods for measuring the absolute age of rocks and meteorites. The use of these methods ensured a natural transformation of the stratigraphic scale into the geochronological time table. This dramatically increased the detail of study of the Earth geological history and also opened the possibility to measure the duration of the three main geological cycles, amounting to 20-40 million years, 200-300 million years and 1 billion years.

Hypothesis of Galactic year: The search for the causes of cyclicity quickly led geologists to the idea of connection geological cycles with the movement of the Sun in the Galaxy. The empirical basis of this idea was the proximity of the geological cycle with duration of 200-300 million years to the period of the Sun's orbital motion in the Galaxy according to P. Parenago calculations [1952]. This idea taken name the "galactic year" hypothesis was originally supported by geologists of our country. Later, his theoretical justification was continued by astronomers and physicists who offered their models. As the cause of geological cycles, such models in particular, offered the Sun fluctuates to relative to the galactic plane and Sun's entry into the spiral arms of the Galaxy.

However, because of the imperfection of astronomical models and ignorance of the spiral structure of the Galaxy, it was theoretically impossible to explain the origin of the geological cycles. As a result, many geologists ceased to consider cosmic processes in the Galaxy as the leading factor of cyclicity in the Earth geological development [Barenbaum, 2008].

The Galactocentric Paradigm: The situation radically changed by the beginning of the 2000s after the author attracted to explanation of geological cycles the astrophysical phenomenon of the jet flow of gas-dust substance from the center of spiral galaxies. Taking into account this phenomenon the author has constructed adequate physical models of our Galaxy and its spiral structure, which made it possible to dramatically increase the predictive power of theoretical calculations [Barenbaum, 2002].

These models, as well as the cosmogonical concept of the "Open Solar System" created by the author [Barenbaum, 1992] were the basis for the development of a more general representation system – the Galactocentric Paradigm [Barenbaum, 2010].

She discovered the very closest connection of processes on The Earth and in the Solar system with cosmic phenomena in the Galaxy. At present, this paradigm has well proved itself in solving a wide range of problems of cosmogony, geology and comparative planetology.

Galactic model of geological cyclicality: Unlike the "Galactic year" hypothesis, this model connects the geological cycles not with the Sun's orbital motion in the Galaxy, but by the fact that in the process of this movement the Sun intersects jet streams and galactic branches. It is then that the Earth and other planets are subjected to powerful cosmic impacts.

In this model, the Sun's orbit is an ellipse with an eccentricity of 0.36 and a major semi-axis of 10.17 kpc, which slowly rotates in the galactic plane in the direction of the Sun's motion with an angular velocity of 3.14×10^{-9} years⁻¹. The sidereal and anomalistic periods of the Sun's rotation around the center of the Galaxy, respectively, are $T_{\phi} = 223$ Ma and $T_R = 250$ Ma. In the epicenter of the orbit, the Sun moves away from the Galaxy center to a distance $R_{max} = 13.8$ kpc, and in the pericenter it approaches to it on a distance $R_{min} = 6.4$ kpc. At the same time the Sun performs vertical oscillations with respect to the galactic plane with a period of ~50 Ma and amplitude of 10 pc.

Moving along such an orbit the Sun occasionally at time ~2-5 million years crosses the spiral arms and jet streams of the Galaxy, and at such moments the Earth and other planets are exposed to powerful bombings by galactic comets, which are the main cause of geological cycles. The calculating times of comet falls are compared in Fig. 1 with the boundaries of the straton (periods and departments) of the Phanerozoic geochronological scale. The model allow calculating, with accuracy not inferior to isotopic methods, the times of the straton boundaries of the Phanerozoic and also to explain the principle of constructing the stratigraphic table itself.

It is established the nomenclature of straton is determined by the amount of energy and type of galactic comets falling to Earth in the moments of the Sun hitting in jet streams and galactic sleeves.

At this the boundaries of the departments correspond to the moments when the Sun to be in jet streams; the boundaries of periods – at the moments when the Sun to be in zones of star formation in spiral galactic sleeves, and the boundaries of Cenozoic, Paleozoic and Mesozoic eras – in the same zones, but when the Sun is located on deleting of Galaxy corotation radius of 13.5 kpc (see Figure 1).

The Precambrian geochronological scale: If we neglect the possible changes in the Sun's orbit due to the Galaxy evolution and the interaction of the Sun with other stars, then for the values of the parameters $T = 250$ Ma and $T = 222.22$ Ma, the built Galactic model of geological cyclicality is applicable not only to the Phanerozoic but also to the Precambrian [Barenbaum, 2015]. In this case the model makes it possible to clarify the times of the largest culminations of tectonic-magmatic processes and processes of ore formation occurred in the geologic history of our planet ~3.6, ~2.6, and ~1.6 billion years ago. The last two events determine in the Precambrian geochronology the boundaries of the Archean and Proterozoic. At the same time the Katarchean stratigraphic boundary with age of ~3.6 billion years, because of the scarcity of geological data has not yet received a geochronological status.

In this regard let us pay attention to the fact that if the parameters of the Sun's orbit remain unchanged, then the culminations of tectonic-magmatic processes, as well as the event at the Vendian-Cambrian boundary 0.57 billion years ago (beginning of Phanerozoic) occur in the same galactic arm (IV in Fig. 1), moreover in certain his place (corotation radius), where the processes of star formation in sleeve are characterized by the highest intensity [Marochnik, Suchkov, 1984].

Another consequence of the model is that all 4 extraordinary events in the Earth geological history are strictly repeated with a period of 1 billion years that exactly corresponds to 4 full revolutions of the Sun around the Galaxy center as well as 4.5 revolutions of the Galaxy around its own axis. This circumstance allows us to more accurately indicate the age of lower boundaries of the Katarchean, Archean and Proterozoic, which can be taken equal to 3.57, 2.57 and 1.57 billion years, respectively.

In Fig. 2 in the projection on the galactic plane we show of the position of the Sun relative to the Galaxy spiral sleeves at now and in the eras of major

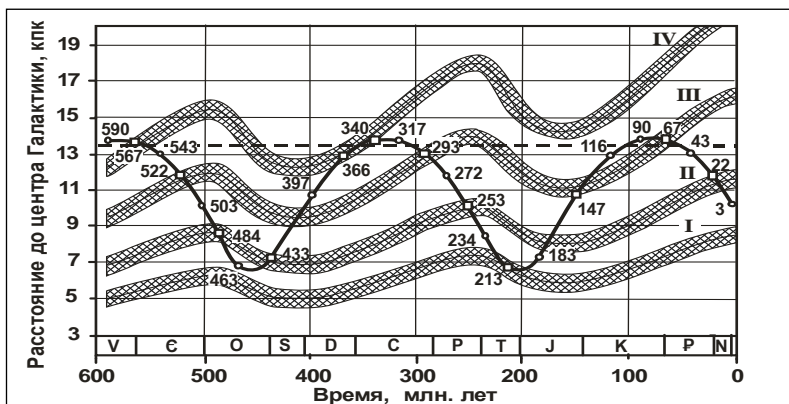


Figure 1. Removal of the Sun from Galaxy center and of 4 spiral galactic sleeves. Roman numerals – sleeve number; The solid curve – Sun's orbit; Circles and squares on the orbit – moments of hitting Sun in jet streams and in zones of star formation in sleeves, respectively; Dotted line – corotation radius of Galaxy

events in the Earth geological history.

"Pre-geological" time: This was the earliest period in the Earth development (previously ~3.8

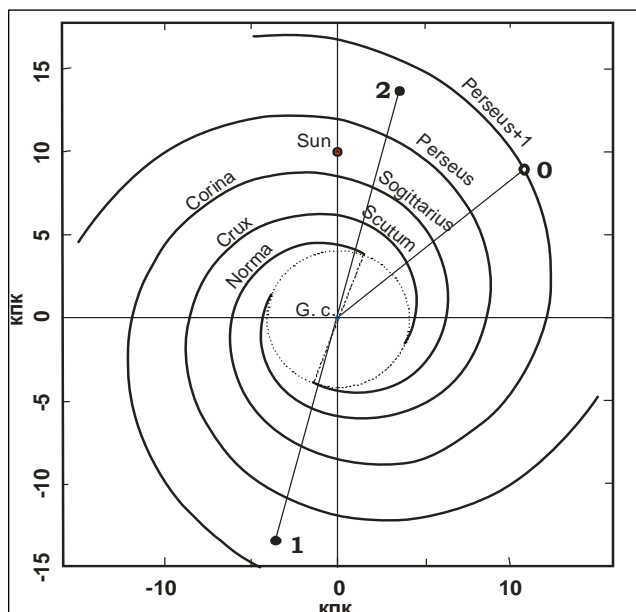


Figure 2. Spiral arms of the Galaxy in projection onto the galactic plane according to [Valle, 2002]. G.C. – Galaxy center. The sleeve of Perseus+1 corresponds to the branch IV in Figure 1. The figure shows: the current position of Sun – the point "Sun", the point "O" – area in Perseus+1 sleeve, where the main geological events occurred in the Earth history; Point "1" is the position of "O" point on galactic plane, when the Sun crossed the sleeve of Perseus+1 at times of 0.57, 2.57, and 4.57 billion years ago; Point "2" – the same at times of 1.57 and 3.57 billion years ago

billion years), reliable geological evidence of which at the present time on our planet is practically absent. Therefore, about the processes occurred at that time on the Earth and in the solar system we are today judged by studying the composition of substance and age of meteorites.

The measurements which most important for meteorites show the age of 4.5682 ± 0.0006 billion years, that is considered the time of formation of the solar system [Wikipedia].

At the same time, there is a group of iron meteorites whose isotope age is 0.9–2 billion years older [Sobotovitch, 1974]. However today this fact is usually ignored, as it contradicts the generally accepted notions. According to these notions based on the hypothesis of Kant-Laplace (XVIII century), the Sun, planets, their satellites, asteroids and comets were formed from the primary gas nebula 4.57 billion years ago. At this it is assumed that the Solar system in the era of its forming and later did not experience any significant influences of the Galaxy.

In fact, this is not so. Due to the Sun entering in the spiral sleeves and jet streams of Galaxy, the process of planetary formation was cyclic.

In reality, this is not the case. Due to the Sun regular entering in the spiral sleeves and jet streams

of the Galaxy, the process of planetary formation was cyclical. Based on the data of meteoritics, comparative planetology, geology and physics of the Earth, it was shown [Barenbaum, 2010] that the event 4.57 billion years ago was not the first but the second main cycle of planet formation in the Solar system. Judging by the age of iron meteorites, the Sun and planets arose at least 2 billion years earlier and, perhaps, even earlier. Moreover these key events for the Solar system occurred at the "0" point of the "Perseus + 1" sleeve in Fig. 2.

The second main cycle of planet formation was caused by the destruction of the planet Phaethon. In the cosmogony concept of the "Open Solar System" we shown [Barenbaum, 1992] that at the death moment the Phaethon was a quite formed planet with a mass of 14.7 masses of modern Earth, which was already stratified onto the system of mantle silicate shells and had a solid FeNi core.

Based on the composition and frequency of falls of all classes and groups meteorites [Dodd, 1986], which we consider as products of collisions of galactic comets with fragments of different shells of Phaethon, it differed from the present-day Earth with a greater content of iron in mantle silicates, by predominance of inner mantle shell over the outer, and by smaller dimensions of the metal core.

Fragmentation of Phaethon led to the formation from its wreck the asteroid belt, which became objects of intense collisions with galactic comets. Such collisions led to emission from the ring of large asteroid bodies as well as were accompanied by the formation of large quantities of gas and dust, which have formed gas-dust disk on the outer side of asteroid belt, in which happened the growth of gas shells of modern giant planets. The bodies that have been thrown out of the asteroid belt permeate into the interplanetary space from which they were scoop out by the planets for $\sim 10^8$ years. By falls of that bodies we explanation the culminations of tectonomagmatic processes on Earth of 3.57, 2.57 and 1.57 billion years ago.

The issues of the secondary formation of planets are discussed in books [Barenbaum, 2002, 2010]. In that books author justified the possibility of attracting the galactic model to the formation of a chronological scale of "pre-geological" time also for the solar system basing on the analysis of the successive formation of regular satellites of giant planets.

Conclusions: The modern geochronological scale constructed from the data of the Earth's geological study is fully applicable to the Solar system. This conclusion the author makes based an analysis of the history of the creation and the theoretical comprehension of that table, which included the following stages:

- Construction of the Phanerozoic and Precambrian stratigraphic tables based on the generalization of geological facts (late 19th century).
- Transformation of stratigraphic tables into geochronological tables using isotope methods for measuring the age of rocks. Identification of geological cycles different ranks in the Earth history and determination of their duration (mid-20th century).
- The emergence and justification of the hypothesis of "Galactic year", connecting the duration of geological cycles with the Sun orbital motion in the Galaxy (second half of the XX century).
- Discovery of the phenomenon of jet flow of gas-dust substance from the spiral galaxies center. The creation of: "Galactocentric paradigm", cosmogony concept of the "Open Solar System" and "Galactic model of geological cyclicity", which make it possible to theoretical calculate the time of boundaries different strata for the Phanerozoic scale (1990-2010).
- Justification of the applicability of the "Galactic model of geological cyclicity" for explanation of tectonic-magmatic cycles in the Precambrian, including the "pre-geological" period (2015)

References:

1. Barenbaum A.A. Origin of asteroids and meteorites (new cosmogony concept) // Conceptual bases of geology, Notes of St-Petersburg Mining Institute, V.134, 1992, P.9–27.
2. Barenbaum A.A. Galaxy, Solar system, Earth: Subordinated processes and evolution (Moscow: GEOS), 2002, 393 p.
3. Barenbaum A.A. Conception of "Galactic year in geology": history of formation and current state of problem // General and regional problems of tectonics and geodynamics: Materials of XLI Tectonic conference. V.1. (Moscow: GEOS), 2008, P.51–55.
4. Barenbaum A.A. Galactocentric paradigm in geology and astronomy (Moscow: LIBROCOME), 2010, 546 p.
5. Barenbaum A.A. Position of Sun in Galaxy in era of Phaeton destruction // Materials of XVI Intern. Conference: Physics-chemical and petrophysical studies in the Earth sciences (Moscow, IGEM RAS), 2015, P.39–42.
6. Dodd R.T. Meteorites: A petrologic-chemical synthesis (Cambridge Univ. Press), 1981.
7. Marochnik L.S., Suchkov A.A. Galaxy (Moscow: Nauka), 1984, 392 p.
8. Parenago P.P. On the gravitational potential of the Galaxy // Astron. Journal, Part I, 1950, V.27, Issue 6, P.329–340 and Part II, 1952, V.29, Issue 3, P.245–287.
9. Sobotovich E.V. Isotope cosmic-chemistry (Moscow: Atomizdat) 1974, 208 p.
10. Vallee JP Metastudy of spiral structure of our home Galaxy // Astrophysical J. 2002. V. 566. №1. P. 261–266.
11. Zhamoyda A.I. General stratigraphic scale adopted in USSR–Russia: Its meaning, purpose and improvement (St. Petersburg: VSEGEI), 2013, 24 p.

Demidova S.I.¹, Ryazantsev K.M.¹, Kononkova N.N.¹, Ntaflos Th.², Brandstätter F.³ Phosphorus zoning in lunar P-bearing olivines.

¹V.I. Vernadsky Institute of Geochemistry and Analytical Chemistry RAS, Moscow (demidova.si@yandex.ru);

²Vienna University, Austria,

³Natural History Museum, Vienna, Austria

Abstract. Olivine is a common liquidus phase in lunar magmas. Slow diffusion rate of P in silicate melts and crystals makes it promising indicator of magmatic processes. Here we report about P-zoning observed in lunar P-bearing olivines and discuss P incorporation mechanism in some of them. Two types of zoning were found. Similar to typical igneous olivine oscillatory type of zoning is present in that of anorthositic-noritic-troctolitic rocks of Luna-20, -16, and possibly Apollo-14 lunar samples. Fine-scale zoning of Luna-20 olivine suggests the formation period from several days to months. Conversely, concentric P zoning was observed in olivine grain containing oriented low-Ca pyroxene inclusions of Dhofar 961 lunar meteorite that implies its slow reaction with surrounding impact melt. Coupled Cr and P substitution mechanism (Milman-Barris et al., 2008) is strongly preferred for the olivine of Luna-20 anorthositic troctolites.

Keywords: lunar rocks, lunar meteorites, phosphorus-bearing olivine, phosphorus zoning.

Phosphorus is an important minor element of lunar rocks which is mainly concentrated in phosphate (merrillite, apatite) and phosphide (schreibersite) minerals. However another lunar P-bearing phase – olivine – has been recently found. Olivine is a common liquidus phase of lunar magmas. Occurrence of P-zoning in olivine as well as low P diffusion rate makes this element important indicator of magmatic processes. Rare grains of P-bearing olivine (containing up to 0.5 wt.% P₂O₅) were documented in some lunar samples and meteorites. Three types of P-bearing olivine were observed (Demidova et al., 2017): 1) P-bearing olivine (Fo₅₁₋₈₈) is present in rock and mineral fragments of anorthositic-noritic-troctolitic (ANT) composition of Luna-20, -16, Apollo 14 sites and Dhofar 961 (Dho 961) lunar meteorite; 2) P-bearing fayalite (Fo₂₋₄) was found in the late-stage mesostasis of Dho 287A mare olivine basalt and in Luna 16 Fe-rich rock; 3) Mg-rich P-bearing olivine (Fo₈₄₋₉₅) was found in central parts of two unusual zoned olivine grains with oriented inclusions of low-Ca pyroxenes from the Dho 025, 961 lunar meteorites. P zoning was studied in Type 1 and 3 olivines.

Samples and methods. Polished sections of Luna-20, -16, Apollo 14 fragments and Dho 961

lunar meteorite were studied by standard methods of optical microscopy. Chemical composition of mineral phases was measured using Cameca SX100 (Vienna University, GEOKHI RAS) and JEOL JXA-8530F (Natural History Museum of Vienna) microprobes at an accelerating voltage of 15 kV and a beam current of 10 nA. P X-rays distribution maps

in Luna-20 olivines were acquired with Cameca SX-FIVE (Vienna University) accumulating information from 4 detectors simultaneously at an accelerating voltage of 15 kV and a beam current of 60 nA. P, Cr and Fe X-rays distribution maps of other samples were performed at an accelerating voltage of 15 kV and a beam current of 80 nA (Cameca SX100).

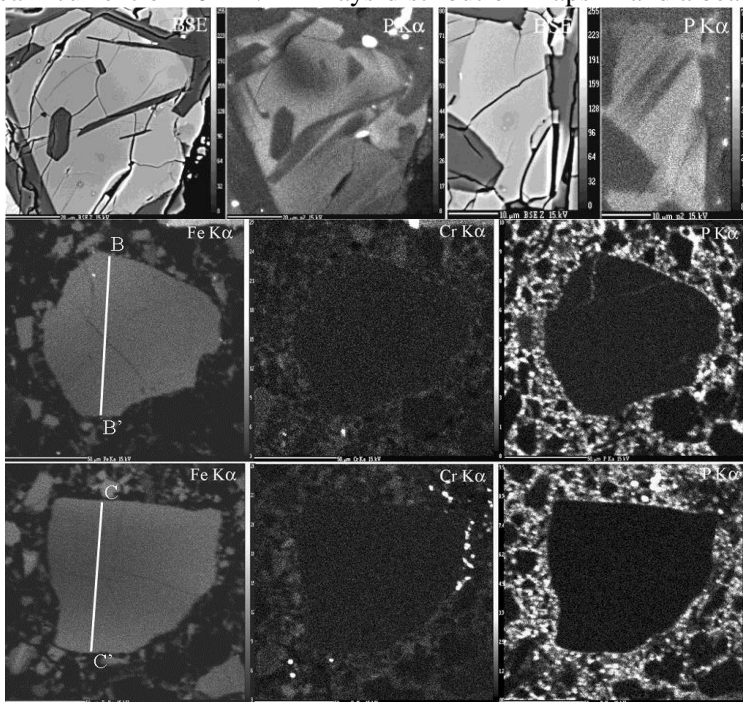


Fig. 1. BSE images and P X-ray maps of P-bearing olivine from the Luna-20 anorthositic troctolite fragment.

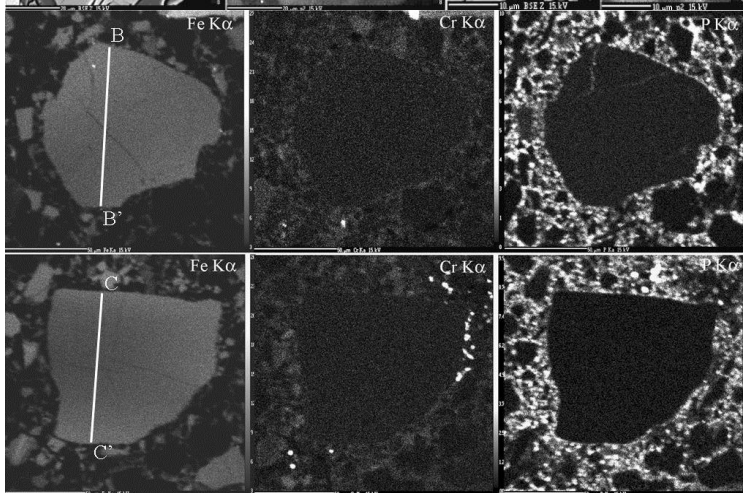


Fig. 2. X-ray maps of P-bearing olivine fragments of the sample 14321 (Apollo 14).

Results. P zoning patterns were studied in following samples:

1) Two fragments of Luna-20 pyroxene anorthositic troctolites have rather coarse-grained ophitic texture. Olivine Fe_{76-81} contains 0.2-0.5 wt.% Cr_2O_3 and CaO and up to 0.4 mac.% P_2O_5 . Olivines with oscillatory P zoning, patchy zoning and areas with tapering oscillations were observed (Fig. 1). The size of the P-rich bands varies from 2 to 10-15 mm (Demidova et al., 2016).

2) Two olivine fragments (80x80 and 100x110 μm in size) were found in a fragmental microbreccia of Apollo-14 sample 14321. Olivines Fe_{79-83} contain 0.1-0.3 wt.% P_2O_5 , up to 0.1 wt.% Cr_2O_3 and up to 0.2 wt.% CaO. They are slightly zoned in MG# number however P zoning is nearly absent on the X-rays maps (Fig. 2) occurring only on the profiles of P content (Fig. 5).

3) Luna-16 troctolite anorthosite fragment has porphyritic intersertal texture. Two coarse olivine relics (50x80 μm) Fe_{69-76} contain up to 0.3 wt.% P_2O_5 and Cr_2O_3 , 0.1-0.4 wt.% CaO. P zoning pattern is characterized by the gradual transition from P-rich to P-poor zones in one grain and sharp boundary between them in another one (Fig. 3). Width of the zones is about 30 μm .

4) Coarse P-bearing olivine (370x370 μm) contains oriented inclusions of low-Ca pyroxene in the lunar highland meteorite Dho 961. The object is

situated in the clast of crystalline impact melt of olivine noritic composition, and has sharp boundary with the surroundings. Flattened concentric zoning is observed in the olivine grain (Fig. 4). From the core to the rim olivine shows a gradual increase in Fe content (from Fe_{84} to Fe_{68-78}), P_2O_5 content decreases from 0.4-0.5 to 0.1-0.3 wt.%, as well as Cr_2O_3 content which reduces from 0.1 wt.% to below detection limit. At the same time CaO increases from 0.1 (in the core) to 0.2 wt.% in the rim. Such a zoning pattern points to the reaction with surrounding impact melt of a highland composition resulting in formation of the rim (Demidova et al., 2015).

Discussion. Complex P zoning patterns has been recently discovered in the natural and experimental olivines most of which reveal oscillatory type of zoning (Milman-Barris et al., 2008; Welsch et al., 2014; McCanta et al., 2016). The authors attributed the fine-scale zoning to kinetic influences during the growth of the host crystal. Formerly oscillatory P zoning in lunar olivines was documented in NWA 032 mare basalt meteorite (Burger et al., 2009; Elardo, Shearer, 2014) and in basaltic lunar sample 12002,162 (Welsch et al., 2014), however P content in them was ~200 ppm. Similar to previously described, Luna-20 olivine shows mostly oscillatory P-zoning similar to typical igneous one. Sharp boundary between P-rich and P-poor bands in one olivine relic of the Luna-16 olivine anorthosite

Abstracts

suggests the presence of rather coarse oscillations too (>30 μm bands). According to (Watson et al., 2015) the size of the P-rich and P-poor bands varying from 2 to 15 μm points to their formation during the period of only days to months if it was not multi-stage. The formation of >30 μm bands requires longer time. On the contrary, P-bearing olivine of Dho 961 demonstrates flattened concentric zoning similar to that of olivine porphyroblasts from metasomatized spinel peridotite xenoliths (Mallmann, 2009), which is thought to be formed during a few hundred thousand years (Watson et al., 2015). As it was

previously suggested, Dho 961 olivine-orthopyroxene object could be the product of lunar serpentine dehydration (Demidova et al., 2015). A gradual decrease of MG# and the P content from the core to the edge of the grain indicates a slow reaction of olivine with the host Fe-rich and P-poor impact melt. Despite the lack of visible P zoning pattern in the Apollo-14 olivines which may be explained by insufficient resolution of the applied method, the study of the minor element content profiles suggests the presence of the oscillations as well.

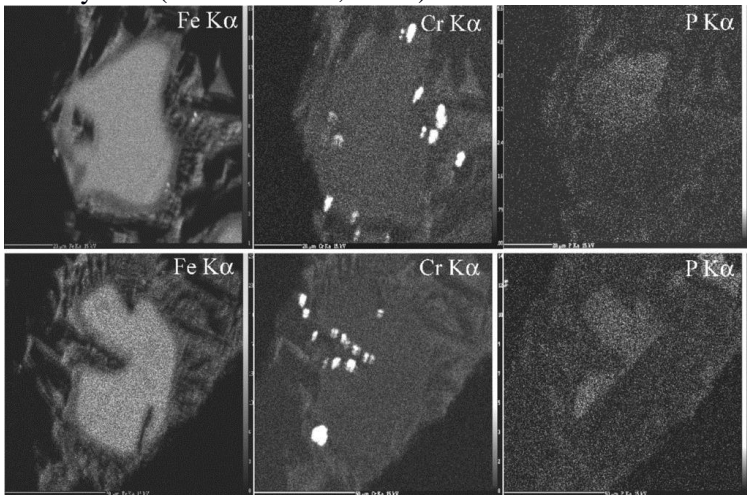


Fig. 3. X-ray maps of P-bearing olivine relics from the Luna-16 troctolitic anorthosite fragment

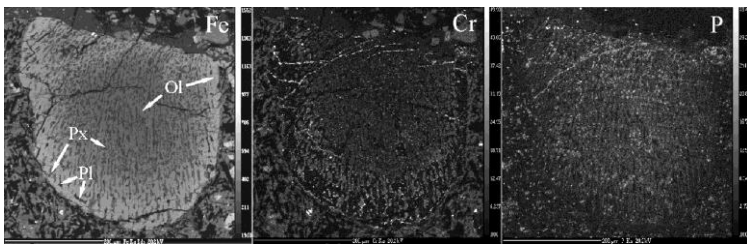


Fig. 4. X-ray maps of P-bearing olivine with oriented inclusions of low-Ca pyroxene from the Dho 961 lunar meteorite.

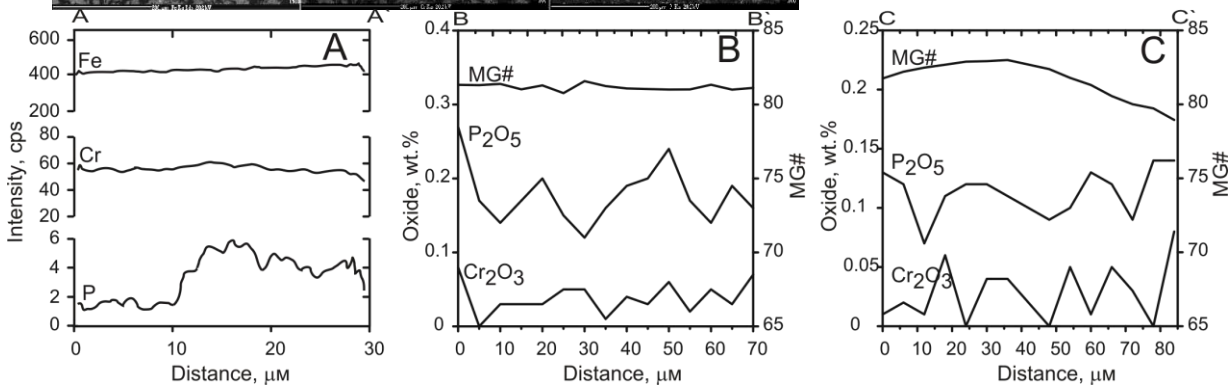


Fig. 5. The profiles of (A) Cr, P and Fe signal intensity of Luna-20 P-bearing olivine; (B,C) Cr_2O_3 , P_2O_5 contents and Mg# number of Apollo-14 P-bearing olivines.

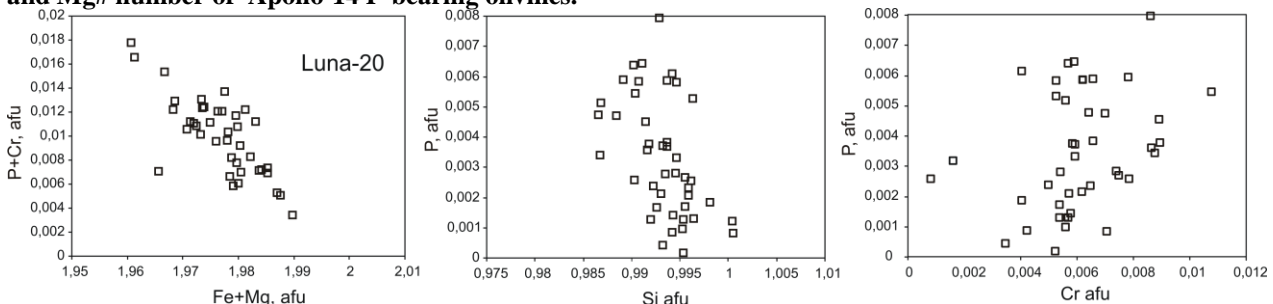


Fig. 6. Chemical composition of P-bearing olivines from Luna-20 anorthositic troctolite fragments (in formula units).

Rapid growth of olivine crystal may result in both P and Cr and Al capture. At the same time growth rate has little effect on the incorporation of divalent cations into the olivine structure, so no relation between P, Al, Cr and Fe content should be expected. The observation is consistent to the most studied P-bearing olivines (Fig. 2-5) except for the Dho 961 olivine grain with oriented inclusions of low-Ca pyroxene. Besides that, terrestrial and chondritic olivines frequently show spatial correlation of P and Cr and/or Al zoning (Milman-Barris et al., 2009; McCanta et al., 2016), while most P-bearing lunar olivines do not (Fig. 5).

It is generally accepted that due to the proximity of ionic radius and charge P^{5+} substitutes for Si^{4+} in tetrahedral coordination in olivine. To compensate for the positive charge excess a set of mechanisms was suggested (see e.g., Milman-Barris et al., 2008 and references therein). All of them are accompanied by the formation of vacancies and participation of monovalent or trivalent cations. In addition coupled substitution may occur: $2^{IV}Si^{4+} + 4^{VI}(Fe,Mg)^{2+} = 2^{IV}P^{5+} + 2^{VI}Cr^{3+} + \square$ (Milman-Barris et al., 2008). This mechanism is possibly responsible for the P incorporation into olivine of Luna-20 anorthositic troctolites. It is strongly supported by the presence of negative correlation between sum of divalent cations and P and Cr sum ($r = -0.74$). A weak negative correlation of Si and P and a weak positive correlation of P and Cr confirm this statement as well (Fig. 6). The lack of significant correlations in the other studied olivines may indicate either an influence of annealing, or interaction of different P incorporation mechanisms in olivine.

Conclusions. P-bearing olivines of ANT rocks of Luna-20, -16 and possibly Apollo-14 have oscillatory type of zoning similar to terrestrial and extraterrestrial igneous olivines. Delicate P-zoning must have been formed during the period of several days to months and longer. Similar to terrestrial igneous olivines no relation between zoning in P, Cr and Fe content was observed in most studied ones. The only exception is the Dho 961 P-bearing olivine which shows flattened concentric zoning similar to that of metasomatized spinel peridotite xenoliths. Negative correlation between sum of divalent cations and P and Cr sum in Luna-20 P-bearing olivines suggests the presence of coupled P and Cr substitution mechanism proposed by Milman-Barris et al. (2008). The absence of the correlation in other P-bearing olivines may be explained either by annealing or interaction of different P incorporation mechanisms.

Acknowledgments: The study was supported by RFBR (16-05-00695) and Russian Academy of Sciences (Program №7).

References:

1. Burger P.V., Shearer C.K., Papike J.J. The multi-stage cooling history of lunar meteorite NWA 032 as recorded by phenocrystic olivine and pyroxene // Lunar Planet. Sci. Conf. 40. 2009. Abs. #2043.
2. Demidova S.I., Nazarov M.A., Ntaflos Th., Brandstätter F. Possible Serpentine Relicts in Lunar Meteorites // Petrology. 2015. V. 23. P. 116-127.
3. Demidova S.I., Ntaflos Th., Brandstätter F. P-bearing Olivines in Rocks from the Luna 20 Site // Lunar Planet. Sci. Conf. 48. 2017. Abs. #1409.
4. Demidova S.I., Ntaflos Th., Brandstätter F. Kononkova N. N. P-bearing Olivines in Lunar Rocks: A New View on Lunar Phosphorus // Workshop New Views of the Moon 2 – Europe. 2017. Abs. #6010.
5. Elardo S.M., Shearer C.K. Magma chamber dynamics recorded by oscillatory zoning in pyroxene and olivine phenocrysts in basaltic lunar meteorite Northwest Africa 032 // American Mineralogist 2014. V. 99. P. 355–368.
6. Mallmann G., O'Neill H.St.C., Klemme S. Heterogeneous distribution of phosphorus from otherwise well-equilibrated spinel peridotite xenoliths and its implication for mantle geochemistry of lithium // Contributions to Mineralogy and Petrology. 2009. V. 158. P. 485–504.
7. McCanta M.C., Beckett J.R., Stolper E.M. Correlations and zoning patterns of phosphorus and chromium in olivine from H chondrites and LL chondrite Semarkona // Meteoritics and Planetary Science. 2016. V. 51. №3. P. 520-546.
8. Milman-Barris M. S., Beckett J. R., Baker M. B., et al. Zoning of phosphorus in igneous olivine // Contributions to Mineralogy and Petrology. 2008. V. 155. P. 739–765.
9. Watson E.B., Cherniak D.J., Holycross M.E. Diffusion of phosphorus in olivine and molten basalts // American Mineralogist. 2015. V. 100. P. 2053-2065.
10. Welsch B., Hammer J., Hellebrand E. Phosphorus zoning reveals dendritic architecture of olivine // Geology. 2014. V. 42. №10. P. 867-870

Ivanov A.A., Dolgonosov A.A., Sevastyanov V.S., Voropaev S.A., Dnestrovsky A.Y., Ivanova M.A. Young Earth-Moon system as the machine of life. UDC 550.47

V.I. Vernadsky Institute of Geochemistry and Analytical Chemistry RAS, Moscow (aiva@geokhi.ru)

What could be the next step on the way to the first living organism, after the formation of the primordial environment with organic broth? Could this step not happen, even under all favorable conditions on Earth, and why? Answers to these questions can be obtained if one understands exactly what should this step become. And what provoked and pushed it. In this paper, a number of arguments are presented not in favor of an accidental, and therefore long, search of various combinations of chemical compounds on the way to the biological level of organization of

matter. A possible variant of the events that preceded and predetermined the further history of the Earth on the way to the formation of a cradle for spontaneous generation, development and evolution of life is shown. Based on the material above, it was concluded that the Moon played a decisive role in the emergence of life on Earth! Theoretical reasoning in this work is supported by results of experimental studies, which were obtained by scientists and specialists of scientific and practical occupation from different fields of knowledge.

Keywords: abiogenic synthesis, hydrodynamic cavitation, asymmetric synthesis of isomers, microspheres, probionts, complementary structures, cell membranes.

To date, much has been known and experimentally verified from the history of the organic evolution of matter. Recently it became known that the synthesis of organic compounds occurs not only on planets, in interstellar and intergalactic spaces, but even on the periphery of hot stars. Therefore, there was no problem with the primary synthesis of organic compounds.

Abiogenously in modeling the conditions of primitive Earth most of the basic organic compounds that could be the initial building material for nucleoprotein complexes have been obtained. Efforts have been made to demonstrate experimentally the possibility of self-replication of primitive prebiotic information structures placed in artificially created membrane envelopes, emitting protocells. Based on the results, models of the possible nature of mechanisms of structural self-formation of the simplest, capable of independently existing and reproducing cells are constructed. However, until a complete understanding of the nature of the abiogenic self-forming of a living cell is yet to be overcome, it is not an easy way to realize how it's possible, when it's even impossible to imagine. How it's happened, that in microvolume of such primitive but already capable of replication cell was everything that is minimally necessary for mandatory functions? Gradual, sequential assembly of individual complex components for a future cell, such as separate assemblies for building an airplane, is not practical for inanimate nature. And the main thing is that everything must be produced for the assembly, and at the same time at once! But it is known that even the most primitive cell studied so far, contains millions of components of its essence. One part of the constituent components is responsible for isolation from the environment, i.e. for the creation of a cell membrane, since life begins with the cell. The other part is responsible for the energy of each biochemical reaction and the process as a whole. The third is for storage, the fourth is for reproduction, the fifth is for transfer of genetic and epigenetic information. And so on. Thus, for such a cell to spontaneously appear,

one has to come up and answer the next question. How could molecular complexes different in chemical and physical properties, having clearly specialized functions, simultaneously and in an active state and the necessary proportion, be synthesized and gathered in one place, forming the first native structure that laid the foundation for all life on Earth?! It is impossible to imagine this, or at least very difficult, since the randomness of such event is unimaginably unlikely! And it is impossible, for many reasons. First of all, the time of existence of different organic compounds in unchanged form in aggressive prebiological environment is different. Secondly, each class of organic compounds has its own individual synthesis route, its own individual building reagents and by-products. Thirdly, the conditions for individual synthesis are individual. Fourthly, the synthesis products must have the necessary isomerism, excluding symmetrical isomers, and also not have any third-party pollutants. And so on, and so much more. Therefore, if we do not find the right way to a comprehensive solution of the one-time formation of prebiological structures in the micro-volume of a separate space, the problem will not have an answer. And, generally, most investigators bypass this stage of the problem of the origin of life, relying on the duration of random processes. But because of the serious time limitation in the history of Earth, the process could not go infinitely long. And time is a negative component due to instability of organic compounds. Therefore, it is required to find a way to the regularity of the simultaneous formation of the necessary prebiological structures, capable of forming, at least, a protocell. And the first approach to this is available.

So, it is necessary to define the process and environmental requirements.

The object, as yet not a living organism, must be detached from the environment by a membrane.

In the volume (and for a greater probability of interaction, in the micro-volume of the object) simultaneously all and simultaneously in the active state must be complements in the correct proportion, and as part of all other necessary components.

It is very important that all of the interacting structures have the desired isomerism.

For primitive probionts - cells, though not independently, but still capable of multiplying, these conditions are sufficient. And if we find such process that these conditions will be met, it will be a firm step in the right direction for a serious and major breakthrough in understanding events that self-organize the emergence of the biological level of interactions. But what could lead to the creation of this non-random circumstance, to give energy and provide the necessary conditions for the coincidence of many events, and is still on the early Earth?!

Problems of Planetology, Cosmochemistry and Meteoritica

It seems that this should be something fundamental that can spin the wheel of life.

For the process of origin of life, in addition to the conditions and the necessary substrate, regular sources of a wide range of energy are required.

Until now the presumed energy sources, which ensure primary synthesis of organic compounds, were: hydrothermal, solar UV - generation, electrical atmospheric discharges and meteorite impacts (E. M. Galimov 2001). However, to a full and sufficient extent, these sources could not provide a regular spectrum of energies required for the synthesis and destruction of organic compounds. Most likely they were important for the primary synthesis of compounds of organic broth, and not for the formation of structural subunits of the protocell.

In the present paper, it is proposed to consider a new source of energy, which also existed in the prebiological phase of the Earth's history.

At the stage of the Young Earth (about 4 billion years ago) the Earth-Moon system was a powerful source of energy generation for tidal waves, which caused a wide range of secondary energy due to

cavitation. Such a powerful and regular source of energy is able to provide the synthesis and destruction of organic compounds, which required for the prebiological stage.

In addition, with cavitation generation of energy, its source is a point source, which has a number of advantages in the formation of chemically active complementary structures and microspheres. It is very important that isomers are formed in this process.

For some time, the formation of complementary structures was considered random, which made the process of their joint participation in the replication of information structures low-probable. With a much greater probability, the complements could be formed by the destruction of high molecular weight organic compounds, such as polyheterocyclic compounds, which present in the primary organic broth. The mechanism of this process has been proposed earlier (Ivanov A. A. A pre-biotic nature of complimentary, ISSOL-2008) (for example, pencil breakage sites are highly complementary).



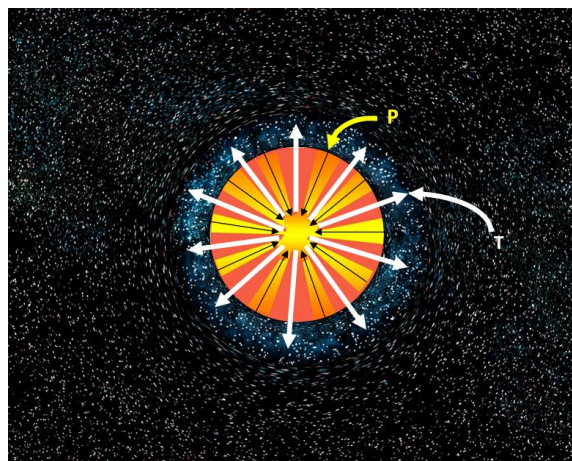
Cavitation in water-peptide solutions forms microspheres. In this case, microspheres can immediately include the necessary prebiological reagents contained in solutions. It is the mechanism of appearance and localization in the micro-volume of the protocell with the necessary pre-biological reagents for replication is the primary issue in the problem of the nature of the origin of life! The mechanism of microsphere formation is probably connected with thermochemical coagulation of peptides at the boundary of the cavitation bubble shell.

Thus, a cavitation source of energy can immediately solve three main problems:

1. Synthesis and destruction of organic compounds.
2. Formation of microspheres with reagents.
3. Approach the solution of the question of isomerism.

The possibility to experimentally confirm or disprove the theoretical premises and arguments of the concept makes it possible to advance in fully understanding the nature of the origin of life.

And today there are such opportunities. Using cavitation in aqueous and other liquids solutions, synthesize both organic substances, and diamonds, and, very importantly, microspheres. Deep nanodiamonds in the rocks of the young Earth can be witnessed by the alleged events.



When a cavitation bubble forms, the pressure force vector tends to its center, forming a

temperature gradient from the center to its boundaries.

References:

1. Galimov E. M., *Nature* 243, 389 (1973)
2. Ivanov A.A., Pre-biotic nature of complimentary., ISSOL-2008
3. Khramtsova M.S., Wiebe D.S., Boley P.A., Pavlyuchenkov Ya.N., Polycyclic aromatic hydrocarbons in spatially resolved extragalactic star-forming complexes, *MNRAS*, 2013
4. Suslick K. S. and others, Acoustic cavitation and its chemical consequences, 1998
5. Galimov E. M., Phenomenon of life, URSS, Moscow, 2001 (in Russian)
6. Dnestrovsky A.Y., Voropaev S.A., Zabrodina E.A., Modeling the compression of a cavitation bubble in benzol., 2016 (in Russian)
7. Ivanov A.A., The nature of the regularity of ontogeny., Moscow, IKAR, 2013 (in Russian)
8. Simakov S.K., Oil - is a potential source of nanodiamonds, 2010 (in Russian)
9. Marov M.Y., From the Solar System into the Universe, Fizmatlit, 2016 (in Russian)

Dorofeeva V.A. Main results of the investigation of the chemical composition of the 67P/Churyumov-Gerasimenko comet by the "Rosetta" mission and cosmochemical consequences from them.

Moscow, V.I. Vernadsky Institute of Geochemistry and Analytical Chemistry RAS, Moscow (dorofeeva@geokhi.ru)

Abstract. The study of the short-period comet 67P/Churyumov-Gerasimenko ("Rosetta", ESA, 2014–2016) showed that the results of measurements of cometary coma composition depend on many factors – the position of the comet relative to the Sun, its geometric parameters and dynamic characteristics, the degree of heterogeneity of the core material, as well as from secondary processes during degassing associated with a change in the structure of ice water. The influence of these factors on the experimental results of the composition of comet coma is analyzed.

Keywords: comets, composition of comets, 67P/C-G

Within 25 months (August, 2014 – September, 2016) the features of the structure and composition of the Jupiter family comet 67P/Churyumov-Gerasimenko (hereinafter 67P) were studied using numerous instruments installed on the ESA spacecraft "Rosetta" during the passage of the comet in orbit from $r \approx 5$ AU through perihelion ($r = 1.24$ AU) to $r \approx 3$ AU was investigated. The orbital period of the comet is 6.44 years, the aphelion is 5.68 AU, and the density is 0.47 g/cm^3 .

In the initial observation period, when low level of cometary activity was noted, images of the surface

of its core were obtained. They were taken from a distance of 6-10 km that is commensurable with the size of the comet itself (4.5×3.4 km). It turned out that the comet surface is very diverse – in places it is strewn with boulders which size reaches 30-40 m, and sometimes covered with a thick layer of sand and dust that explains the low albedo of comets: 3-6%. Objects the size from 0.05 m and higher have been identified. For the first time, a layered structure of the cometary nucleus was found at a scale of 1-10 m to a depth of the order of a kilometer. At the same period of observations, inert gases – ^{36}Ar , ^{38}Ar , Kr, Xe, were found in the coma of 67P for the first time in comets. In addition, there was not only molecular nitrogen detected in the composition of the coma, but also established a linear correlation of the contents of N_2 and ^{36}Ar (Balsiger *et al.*, 2015). Since the sublimation temperatures of ice N_2 and Ar are close ($\approx 20\text{K}$), we can assume that they accumulated simultaneously in the form of ice. At the same time, no correlation was found between the content of N_2 and another high-volatility component – CO (T sublimation of $\text{CO}_{\text{ice}} \approx 25\text{K}$); in a set of 138 measurements the ratio of N_2/CO varied from $1.7 \cdot 10^{-3}$ to $1.6 \cdot 10^{-2}$ (Rubin *et al.*, 2015). It may indicate secondary processes occurring in the cometary nuclei and related, for example, to a change of aggregate state of water ice caused by an intensification of heating by the Sun: $\text{H}_2\text{O}_{\text{ice}}$ is transformed from an amorphous form to a crystalline one and crystalline hydrates therewith are formed, in particular $\text{CO} \cdot 5.75\text{H}_2\text{O}$, which sublimation temperature is approximately 20K higher than that of CO_{ice} . Another important result of the initial observation period was the discovery of molecular oxygen in the coma, the relative content of which turned out to be very high – from 1 to 10%, averaging $3.8 \pm 0.8\%$, with a high correlation between the abundances of O_2 and H_2O (Bieler *et al.*, 2015). We note that for the comet 1P/Halley, a close $\text{O}_2/\text{H}_2\text{O}$ value of $3.7 \pm 1.7\%$ was defined (Rubin *et al.*, 2015). It is known that the content of O_2 in the interstellar medium is extremely small, and therefore its origin in cometary coma is attributed either to the photolysis of $\text{H}_2\text{O}_{\text{ice}}$ (Mousis *et al.*, 2016) or to the decomposition of H_2O_2 ; its relative content in interstellar ice is estimated as $\text{H}_2\text{O}_2/\text{H}_2\text{O} = 9 \pm 4\%$ (Dulieu *et al.*, 2017).

Evidence of complex mechanisms of formation and evolution of the cometary nucleus was obtained when at $r \approx 3$ AU the descent vehicle *Philae lander* carrying 10 scientific instruments for the first time made a soft landing to the surface of the comet. For 57 hours of work, 6 photographs were taken as well as soil samples while investigation of which organic molecules were found. A scaly structure of the surface on a scale of ~ 10 cm was first revealed.

The main scientific purpose of the "Rosetta" mission is to find out whether the comets could bring

life to Earth and to other bodies of the Solar system. On the 67P surface, 16 different organic substances have been identified, including methyl isocyanate (CH_3NCO), acetone (CH_3COCH_3), propionic aldehyde ($\text{CH}_3\text{CH}_2\text{COH}$) and acetamide (CH_3CONH_2); these substances were not previously found in comet matter. Some of them play a leading role in the synthesis of amino acids, sugars and nucleins, which are necessary components for the origin of life. For example, formaldehyde CH_2O found on comet 67P participates in the formation of ribose, the derivative of which is a component of DNA. In seven solid particles of the 67P coma solid macromolecular compounds were found, similar to those found in carbonaceous chondrites. The results obtained will help to evaluate the possible role of comets in the origin of life on the Solar System bodies.

The heterogeneity of the cometary nuclei composition on a scale of the first hundred meters is evidenced by numerous data obtained during the “Rosetta” experiment.

1. The surface of 67P is covered with dust, but near the Sun an intense gas flow blew it out and exposed areas of water ice and even of CO_2 ice, with a length of 60-80 m, were fixed on some sections of the comet, but the mixture of the ice of these volatile components wasn't noted.

2. As with other comets (1P/Halley, 19P/Borrelly, 81P/Wild 2, 9P/Tempel, 103P/Hartley 2), degassing at 67P occurs from local areas, from pits whose area is $\sim 10\%$ of the total area of the comet. Their diameter of pits ranges from several tens to several hundred meters, and the depth can reach two hundred meters. Part of the pits were active, the activity of others was significantly reduced, and some pits were inactive at all. The formation of pits comes most likely according to this scenario: a) a local reduction of the volume of matter in the subsurface layer due to the sublimation of ice of CO_2 or CO, or due to the transition of amorphous ice to crystalline one as a result of heating by the Sun; b) the formation of cavity through this process; c) caving of the upper layer and degassing from the cavity walls. The close location of active and inactive pits (at a distance of ≈ 100 -150 m) indicates the heterogeneity of the composition of cometary nuclei on a scale of $n \times 100$ m.

3. The heterogeneity of the cometary nuclei composition is also indicated by data on the variations in the contents of H_2O , CO_2 , and CO in the 67P coma, obtained during the period from September 2014 to February 2016 (Hoang *et al.*, 2017). They confirmed the suggestion presented in a number of works that the sublimation of CO_2 and especially of CO occurs from a greater depth than H_2O ; in addition, its intensity depends on the seasonal and diurnal illumination of the region, as

well as on the structural features of individual parts of the surface.

The representativeness of the data is an important issue in the study of comets. The comet 67P has a large inclination of the rotation axis (52°) so that there is a seasonal change on it. Summer in the southern region, unlike the northern region, is short (it lasts only 10 months) but quite hot, so when the temperature of sunlit areas of the surface reaches ~ 250 -350K in the daytime, a large (up to twenty meters deep) erosion occurs. Fresh nondegassed layers are exposed, resulting in increased gas activity. For example, the rate of discharge of water a week after the passage of perihelion has more than doubled. Besides, the relative abundance of other gases has increased substantially. Thus, the contents of CH_4 and OCS in coma in relation to water doubled, reaching 0.47% and 0.18%, respectively (Bockelée-Morvan *et al.*, 2016), and $\text{CO}_2/\text{H}_2\text{O}$ increased from 1-4% obtained in the pre-perihelion period, when the northern hemisphere was illuminated (Migliorini *et al.*, 2016) to 32%. This is the highest $\text{CO}_2/\text{H}_2\text{O}$ value ever observed in cometary coma. Therefore, the data obtained in the post-perihelion period for 67P are interpreted as representative, in contrast to the pre-perihelion values.

The main questions of cosmogony coming out from the results of the study of comets, including 67P.

1. The formation region of comets. Until quite recently, it was generally agreed that comets were formed in the trans-Neptunian region at radial distances $r \sim 15$ -25 AU from the Sun in the circumsolar gas-dust protoplanetary disk at the earliest stages of its evolution – in the first 1-3 million years (Emel'yanenko *et al.*, 2013). Part of the comets was subsequently thrown out to the periphery of the Solar system into the Oort cloud region ($r \sim 50$ -100 thousand AU); at present it is a source of long-period comets (LPC). The other part of them was concentrated in the region of the Edgeworth-Kuiper belt ($r \sim 30$ -50 AU). In the evolution of the Solar system, some of the comets from this region could move to smaller orbits, due to the gravitational influence of the giant planets, and form families; the largest of these is the Jupiter family of comets (JFC – Jupiter family comet). Comets move around the Sun along elliptical orbits, and the perihelion point (it corresponds to the minimum distance to the Sun) is often located inside the orbits of the terrestrial planets that makes possible their experimental study.

The isotopic data on the D/H value in the water molecule available at the time of this hypothesis development, experimentally determined for 9 long-period comets, confirmed this viewpoint – all D/H values were close to the $\text{D}/\text{H}_{\text{H}_2\text{O}}$ value for the protosolar nebula and were $\approx (3$ -5) $\cdot 10^{-4}$. This

indicated that the water ice that had entered the comet composition never evaporated; otherwise, its D/H should decrease due to interaction in the gas phase with molecular hydrogen that was isotopically by an order of magnitude more light and worked out ~ 90% of the mass of the protosolar nebula: $D/H_{H_2} = 2 \cdot 10^{-4}$ (Geiss, Gloecker, 2003). However, in 2011, for the 2 short-period comets: 103P/Hartley and 45P/Honda-Mrkos-Pajdušakova, D/H_{H_2O} values were obtained that coincided with the standard mean ocean

water (VSMOW) of $1.56 \cdot 10^{-4}$ (see Fig.1). Contrary to expectations, for the third short-period comet 67P, the D/H value was more than three times higher than the VSMOW: $D/H_{H_2O \text{ 67P}} = (5.3 \pm 0.7) \cdot 10^{-4}$ (Altwegg et al., 2015). It is partly possible to explain this fact in the context of the existing models for the formation of cometary nuclei, assuming the family of short-period comets can be replenished by capture of LPCs, but the reasons for the low D/H_{H_2O} value of the other two short-period comets remain undefined.

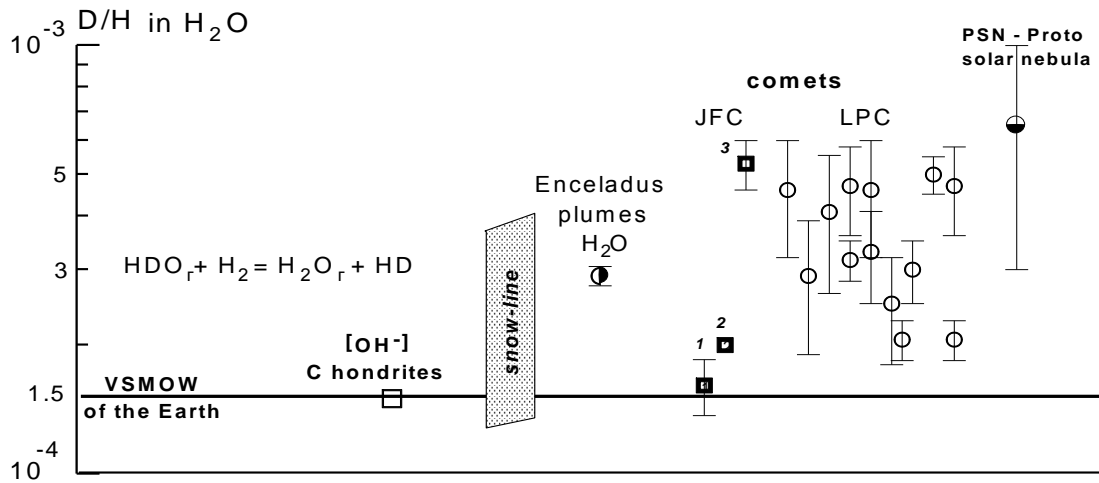


Fig. 1. The values of the hydrogen isotope composition in the water molecule in various objects of the Solar system and in the protosolar nebula. Conventions: snow line – position of the conditional border of water ice evaporation in a circumsolar gas-dust disk; JFC and LPC are short- and long-period comets, respectively.

2. Formation mechanism of comets. It turned out that the nuclei of comets have a layered structure, often consist of two bodies heterogeneous in composition but depleted in relation to solar proportions by the most volatile components (N₂, Ar, Xe, Kr). This brings up the question: whether such a structure was originally inherent in cometary nuclei, or is it the result of the periodic thermal action of the Sun and the associated processes of ice sublimation in the inner layers of cometary nuclei and their condensation in the outer layers? Or the nuclei of comets were formed in a larger body, and then as a result of internal heat due to ²⁶Al lost some of the most volatile components, then were shock-crushed, and subsequently combined as a result of mutual collisions at low speeds? If comets originally have such a structure, then they really are extremely ancient objects and reflect the chemical, mineralogical and physical properties of the protoplanetary nebula that makes it possible to use cometary data in describing the early stages of the evolution of a gas-dust protoplanetary disk. If, on the other hand, the composition and structure of cometary nuclei is the result of their post-accretive evolution or they arose for a reason of collisional processes of small-scale bodies, i.e. could be formed quite recently, in this case, comets do not necessarily store information about conditions in the early Solar

system and the data obtained during their study may have limited significance. In the literature, arguments are advanced in favor of both hypotheses (Davidsson et al., 2016, Jutzi et al., 2017), but the answer to this and other equally important questions requires further experimental studies of the composition of comet matter, especially young ones, and development of theoretical models of the matter formation and evolution in the early Solar system.

Conclusions

The results of the study of the comet 67P/Churyumov-Gerasimenko by the “Rosetta” spacecraft are the structural features of its core, in particular, the stratification and heterogeneity of the composition at a level of tens of meters. These features require for the formation of comets special physical conditions that were not previously considered in any cosmogonic work.

While developing a new model it must be taken into account that

- the survival conditions of cometary nuclei require that their formation be separated in time and/or place with other trans-Neptunian objects, much larger in scale even in comparison with comet C/1995 O1 (Hale-Bopp);
- the comet formation zone should be located at such a radial distance from the Sun that during the period of formation of the circumsolar disk, gas

from its inner areas propagated to it with low D/H_{H₂O} and delivering dust containing including CAIs experimentally found in cometary matter (Joswiak, Brownlee, 2014).

This work was partially supported by the Basic Research Program no. 7 of the Presidium of the Russian Academy of Sciences.

References:

1. Altwegg K., Balsiger H. and 30 coauthors. 67P/Churyumov-Gerasimenko, a Jupiter family comet with a high D/H ratio. 2015. *Science*, V. 347, Is. 6220, id. 1261952.
2. Bieler A., Altwegg K., Balsiger H. and 30 coauthors. Abundant molecular oxygen in the coma of comet 67P/Churyumov-Gerasimenko. 2015, *Nature*, 526, 678
3. Bockelée-Morvan D., Crovisier J., Erard S. and 19 coauthors. Evolution of CO₂, CH₄, and OCS abundances relative to H₂O in the coma of comet 67P around perihelion from Rosetta /VIRTIS-H observations. 2016. *Monthly Notices of the Royal Astronomical Society*, vol. 462, issue Suppl 1, pp. S170-S183.
4. Davidsson B. J. R., Sierks H. and 46 coauthors. The primordial nucleus of comet 67P/Churyumov-Gerasimenko. 2016. *Astronomy & Astrophysics*, V. 592, id.A63, 30 pp.
5. Dulieu F., Minissale M., Bockelée-Morvan D. Production of O₂ through dismutation of H₂O₂ during water ice desorption: a key to understanding comet O₂ abundances. 2017. *Astronomy & Astrophysics*, V. 597, id.A56, 5 pp.
6. Emel'yanenko V. V., Asher D. J., Bailey M. E. A Model for the Common Origin of Jupiter Family and Halley Type Comets. 2013. *Earth, Moon, and Planets*. V. 110. Issue 1-2. P. 105-130.
7. Hoang M., Altwegg K., Balsiger H. and 25 coauthors. The heterogeneous coma of comet 67P/Churyumov-Gerasimenko as seen by ROSINA: H₂O, CO₂, and CO from September 2014 to February 2016. *Astronomy & Astrophysics*, Volume 600, id.A77, 13 pp. 2017
8. Migliorini A., Piccioni G., Capaccioni F. and 14 coauthors. Water and carbon dioxide distribution in the 67P/Churyumov-Gerasimenko coma from VIRTIS-M infrared observations. 2016. *Astronomy & Astrophysics*. V.589, id.A45, 12 pp.
9. Jutzi M., Benz W., Toliou A., Morbidelli A., Brasser R. How primordial is the structure of comet 67P/C-G? Combined collisional and dynamical models suggest a late formation. 2017. *Astronomy & Astrophysics*, Volume 597, id.A61, 13 pp.
10. Mousis O., Ronnet T. and 14 coauthors. Origin of Molecular Oxygen in Comet 67P/Churyumov-Gerasimenko. 2016. *The Astrophysical Journal Letters*, V. 823, Issue 2, article id. L41, 5 pp.

Dunaeva A.N., Kronrod V.A., Kuskov O.L. Total H₂O content in titan at a varying degree of silicates hydration.

V.I. Vernadsky Institute of Geochemistry and Analytical Chemistry RAS, Moscow (dunaeva.an@gmail.com)

Abstract. In this paper, the total content of H₂O in the partially differentiated Titan was estimated. It has been shown that this value lies within the limits of 37.6-53.5% and depends on extent of silicates hydration in the satellite. When the amount of hydrous minerals in Titan is not higher than 30%, the H₂O(water, ice)/rock ratio in the satellite is equal to 1.0-1.15, which is close to the Solar proportion.

Keywords: Titan, water/rock ratio, internal structure.

It is assumed in a number of papers studying Saturn's icy satellite Titan internal structure, that the satellite contains a significant amount of hydrated silicates, since hydration of silicate minerals is a common process in icy space objects, the formation of which is associated with the melting of ice. In academic literature the models are discussed that allow the long-term stability of hydrous silicates in Titan's core (Sohl et al., 2014), as well as the models that take into account the possible dehydration of a portion of the hydrated substance, leading to the formation of a large silicate core in the center of the satellite (Castillo-Rogez and Lunine, 2010). In such models, Titan is assumed to consist of an external water-ice shell (H₂O-ice ± internal water ocean) and a lower-lying layer of low density represented by hydrated minerals of the serpentine group (antigorite, chrysotile, lizardite) ± innermost iron-silicate core.

Alternative models represent Titan as a partially differentiated body in which the separation of ice and rock components was not complete. In this case, the internal structure of the satellite includes an outer water-ice shell below which there is an extended layer (mantle) consisting of a homogeneous mixture of rock and water ice in the form of corresponding H₂O polymorphs stable at the satellite's pressures. In the center of Titan, under the rock-ice mantle, an iron-silicate core of uniform density is assumed to be (Tobie et al., 2012; Dunaeva et al., 2016).

Both groups of models are in a good agreement with the measured physical characteristics of Titan (mass, density, moment of inertia). However, preliminary calculations (Dunaeva et al., 2014) showed that the estimates of the total H₂O content in Titan obtained for each group of models differ significantly. However, the total H₂O content, as well as the water/rock ratio, could be important criteria when choosing a certain model for studying the internal structure of the satellite.

In the present paper we continue our earlier studies of this issue. The internal structure of Titan in terms of partially differentiated model was calculated in more detail. In setting the task, the composition of

Titan's rock-iron material was estimated by analogy with the ordinary L/LL chondrites. An additional requirement was to determine the possible extent of silicates hydration in the satellite. Since the degree of Titan's chondrites hydration (the amount of hydrous silicates) is not reliably known, in the performed calculations this value was used as a varying parameter with respect to which the whole density profile in the satellite was built. Thus, the task was to calculate the range of possible models of Titan's internal structure, characterized by varying degrees of silicates hydration and satisfying the data on the satellite's mass and moment of inertia.

To solve this problem, a number of procedures have been added to existing software algorithms (Dunaeva et al., 2016), which allow us to calculate the density of the rock component in the satellite's mantle and inner core more accurately using the equations of state for silicates and hydrous silicates. When calculating the density of the inner core, the processes of hydration/dehydration of silicates which take place at 900 K under the satellite's pressures were also taken into account. The water density (ice and liquid water) in the water-ice shell and rock-ice mantle was determined by the equations of state for the individual H₂O-phases.

Apart from the H₂O component, other volatile compounds such as CH₄, CO₂, CO, NH₃, H₂S, etc. could also compose Titan (Tobie et al., 2012). Being captured by Titan during its formation from the accretion gas-dust circumplanetary disk, these volatiles became the part of the satellite's icy shell in a form of clathrate ices, gas hydrates and dissolved salts in inner ocean. The above estimates suggest that the total content of all light impurities in Titan does not exceed 10% of bulk content of H₂O. In this case, all volatiles, regardless of the form of existence, are concentrated in the upper ice crust of the satellite and in its internal ocean, whereas the ice underlying the subsurface water ocean and included into the rock-ice mantle mainly contains pure H₂O ice.

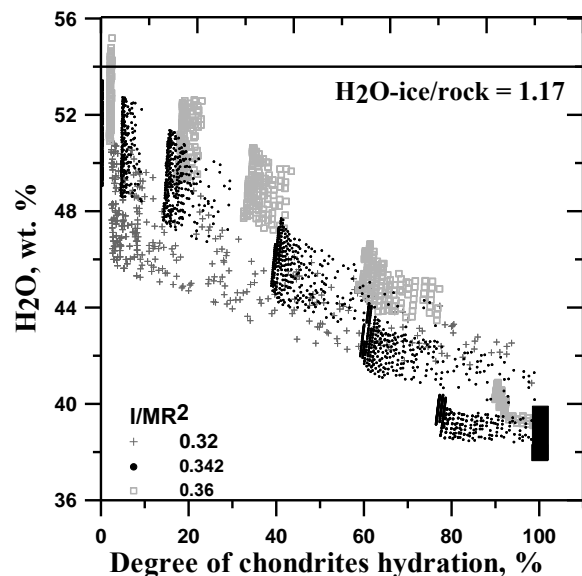
crust and the water ocean does not exceed 400 km (1/5 of the satellite radius) at Titan's heat flux of 7 mW/m². No changes are expected in the properties of other H₂O-containing layers of the satellite: in the extended rock-ice mantle (up to 1500 km) and in high-pressure ices below the ocean floor. Furthermore, the test calculations of Titan's internal structure using the models with up to 15% of volatiles (by the example of NH₃) have shown that the addition of light impurities to the water-ice shell leads mainly to changes in its phase composition and has practically no influence on its total thickness. Thus, at this stage of the study when determining the total H₂O content in Titan, the presence of other volatile ice and compounds in the satellite can be neglected.

The total water content in Titan was determined as the bulk concentration of H₂O in the outer water-ice shell (liquid water + H₂O-ice) and in the rock-ice mantle (H₂O-ice + bound water in hydrous silicates). The proportion of bound water in the hydrated minerals was assumed equal to 13 wt%, which corresponds to the average content of H₂O in the minerals of the serpentine group. The calculations were carried out at various moments of inertia of Titan in the interval of 0.32 < I/MR² < 0.36. On the one hand, it makes it possible to take into account the errors in the experimental measurements of the moment of inertia, and on the other hand, it makes it possible to determine the relationship between the moment of inertia value and the number of low-density (hydrated) minerals in the satellite.

Research findings show that in chosen interval of moments of inertia the amount of H₂O in partially differentiated Titan is 38.5-55.21% (Fig. 1). For the moment of inertia I/MR² = 0.342 (Iess, 2010), the water content in the satellite does not exceed 53.5% (the ratio of H₂O (liquid, ice)/rock is equal to 1.15). The figure also shows that the minimum values of the water content in Titan correspond to the complete

Fig. 1. Total H₂O content in partially differentiated Titan at different degree of chondrites hydration in the moments of inertia interval of 0.32-0.36. The line indicates the solar ratio of H₂O/rock (Lodders, 2003). The black rectangle corresponds to the H₂O content in Titan calculated for models of the fully differentiated satellite with a hydrous silicate mantle.

Strictly speaking, even the presence of small amounts of volatile components in the watery or icy layer of Titan can significantly change the properties of the medium, affecting its composition and density. However, the localization of volatiles in a rather narrow inner region of Titan leads to the properties change of only a small part of the satellite (according to our estimates, the total thickness of the outer Ih-



Problems of Planetology, Cosmochemistry and Meteoritica

hydration of the satellite's substance. The maximum content of H₂O is achieved in the complete absence of hydrated phases in Titan. Thus, increase in the substance hydration in Titan leads to decrease in the total water content in it. In this case, there is no essential linkage between the moment of inertia of the satellite and the amount of hydrous silicates in it.

According to the data on solar water abundance in the Solar system (Lodders, 2003), the solar abundance of H₂O is generally higher than the abundance of the metallosilicate substance: the solar H₂O-ice/rock ratio is 1.17. The results obtained in the present study show that partially differentiated Titan is slightly depleted of H₂O ice compared to the ice/rock ratio in the solar composition. Deviations from the solar proportion reach 15% and may indicate ice loss during accretion processes (for example, as a result of the collision and ablation of planetesimals in the gaseous medium of the accretion disk). Another explanation for the low content of H₂O component in Titan may probably be the initial difference from the solar proportions of the amount of H₂O-ice in the ice planetesimals accreted by the satellite. Water loss could also be associated with the mechanical removal of surface ice after intensive meteorite bombardment of Titan about 4 billion years ago.

Against the background of the general decrease in the water content in Titan compared with solar abundance, it is nevertheless possible to build the satellite's models that are close to the solar ratio (in Fig. 1 this models are represented by an area of points corresponding to the water content of more than 50%, the ratio of H₂O-ice/rock is ≥ 1). As can be seen from the figure, the total degree of silicates hydration obtained in these models does not exceed 30%. Moreover, the calculations show that all the

hydrated material is located in the rocky component of the satellite's mantle. The inner iron-silicate core of the satellite does not contain any hydrated silicates and has an average density of 3.4-4.0 g/cm³ at a radius of up to 1300 km. The thickness of Titan's outer water-ice shell obtained for these models is 420-440 km.

Fig. 1 also shows the water content in Titan, typical for the satellite models with a purely mineral hydrous silicate mantle, implying a complete differentiation of the satellite matter into an ice and rock component (Sohl et al., 2014; Castillo-Rogez and Lunine, 2010). The expected water content in such models does not exceed 38-40%, the water/rock ratio is about 0.6, which is almost two times lower than the solar one (Dunaeva et al., 2014).

The mass fraction of water in Titan calculated in this paper for the partially differentiated satellite model was compared with similar estimates obtained for other ice satellites of the gas giant planets Jupiter, Saturn and Uranus (Fig. 2). It can be seen that all three large icy satellites (Ganymede, Callisto and Titan) have an upper limit of water content close to solar abundance. Along with this, Ganymede has a fundamentally different internal structure than Titan and Callisto: its substance has been completely differentiated into a water-ice shell, a silicate mantle and a metal core. This means that the structure of Ganymede eliminates any variation in the choice of models, which can affect the assessment of the water content in the satellite, as it was in the case with Titan. This implies that the water content in Ganymede does not depend on the type of model used and could reflect the real H₂O content typical for the proto satellite disk material participating in the satellite formation.

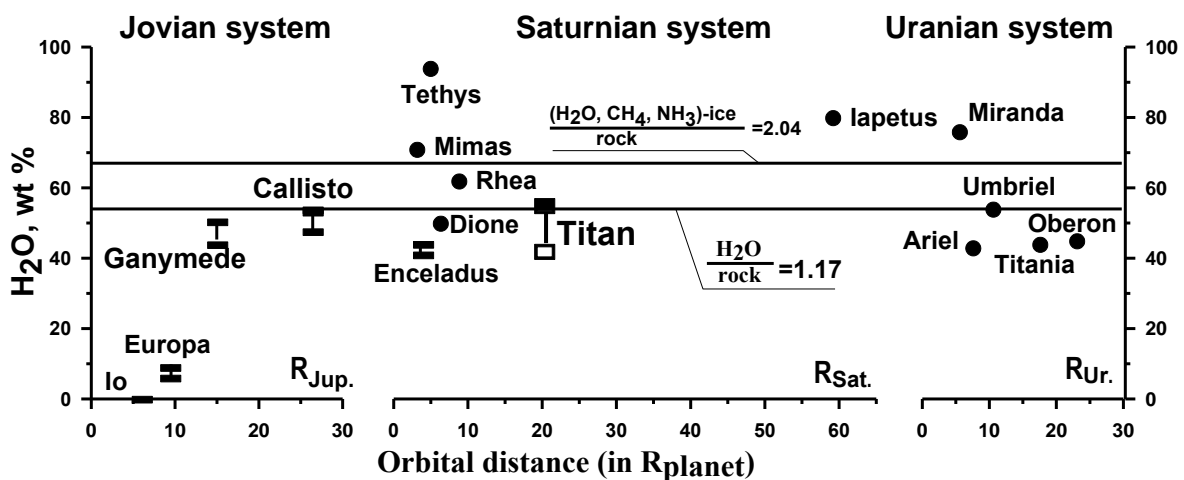


Fig. 2. H₂O content in the icy satellites of Jupiter, Saturn and Uranus (Kuskov and Kronrod, 2001, 2005; Sekine, 2012). The lines show the cosmic (H₂O)-ice/rock and (H₂O, CH₄, NH₃)-ice/rock ratios (Lodders, 2003). The upper limit of water content in Titan corresponds to the model without the silicates hydration, the lower one is the model with the maximum silicates hydration. The H₂O content in Callisto is shown for the model with the minimum degree of chondrites hydration. Ganymede does not contain any water-containing minerals.

If we assume that Ganymede, Callisto and Titan were formed in accordance with the uniform regularities of satellite formation in the gas-dust accretion disks, the disks substance composition in different planetary systems did not differ significantly in water and iron-silicates content, and the temperature conditions were favorable for the water ice condensation, then the water content in Callisto and Titan should roughly correspond to the total H₂O value obtained for Ganymede. Thus, for the satellite systems of Jupiter and Saturn it is logical to suggest that the ice/rock ratio in the satellites can remain identical (or non-decreasing, at least) as the distance of the central planet from the Sun increases. In this connection, the models of partially differentiated Titan look more reliable than "hydrous silicate" models which lead to undervalued water content in the satellite.

Conclusions. The total content of H₂O in the models of partially differentiated Titan inversely depends on the degree of the satellite's iron-silicate material hydration. Depending on the amount of hydrous silicates, the water content in Titan is 38.5-55.21% in the range of moments of inertia of 0.32-0.36. The models of Titan with the hydrous silicates content which does not exceed 30% comply with the solar H₂O-ice/rock proportion most of all. The H₂O-ice/rock ratio for these models is 1.0-1.15.

Acknowledgements: This research was supported by the RFBR grant № 15-05-02572.

References:

1. Dunaeva A.N., Kronrod V.A., & Kuskov O.L. (2016). Physico-chemical models of the internal structure of partially differentiated Titan. *Geochemistry International*, 54(1), 27-47.
2. Dunaeva A., Kronrod V., Kuskov O. (2014). Models of Titan with rock-ice or hydrous silicate mantle. In European Planetary Science Congress 2014, EPSC Abstracts, Vol. 9, id. EPSC2014-663 (Vol. 9).
3. Kuskov O.L., Kronrod V.A. (2001) Core Sizes and Internal Structure of Earth's and Jupiter's Satellites, *Icarus*, V. 151, pp. 204–227.
4. Kuskov O.L., Kronrod V.A. (2005) Internal structure of Europa and Callisto, *Icarus*, V. 177, pp. 550–569.
5. Castillo-Rogez J.C., Lunine J.I. (2010) Evolution of Titan's rocky core constrained by Cassini observations // *Geophys. Res. Lett.* 37, L20205.
6. Iess L., Rappaport N.J., Jacobson R.A., Racioppa P. et al. (2010) Gravity field, shape, and moment of inertia of Titan // *Science*. V. 327, No 5971. pp. 1367-1369.
7. Lodders K. (2003). Solar system abundances and condensation temperatures of the elements. *The Astrophysical Journal*, 591(2), 1220.
8. Sekine Y., Genda H. (2012) Giant impacts in the Saturnian system: A possible origin of diversity in the inner mid-sized satellites // *Planetary and Space Science*, V. 63-64, pp. 133-138.

9. Sohl F., et al. (2014) Structural and tidal models of Titan and inferences on cryovolcanism // *Journal of Geophysical Research: Planets*, 119(5), 1013-1036.
10. Tobie G., Gautier D., Hersant F. (2012) Titan's Bulk Composition Constrained by Cassini-Huygens: Implication for Internal Outgassing. *The Astrophysical Journal* 752(2), 125.

Kadik A.A., Tsekhonya¹ T.I., Lukanin¹ O.A., Pavlova¹ L.F., Koltashev^{1, 2} V.V., Kryukova^{1,2} E.B., Kononkova¹ N.N., Senin¹ V.G. Influence of C–O–H components on fractionation of Ni, CO, P between silicate melt and metal Fe phase: experimental study at 4 GPa, 1550°C, and low oxygen fugacity

¹- V.I. Vernadsky Institute of Geochemistry and Analytical Chemistry RAS, Moscow, ²-Fiber Optics Research Center RAS, Moscow (tsekhonya@geokhi.ru; lukanin@geokhi.ru)

Abstract. A series of experiments was performed in the model system NaAlSi₃O₈+FeO+SiC+NiO+CoO+Na₂HPO₄ at 1550°C, 4 GPa and oxygen fugacity (*f*O₂) by 1–3.6 log units below the iron-wüstite buffer (*IW*) to evaluate the influence of C–O–H volatiles on Ni, Co, and P fractionation between the silicate melt and liquid metal phase under redox conditions corresponding to segregation of the metal phase in the global melting of the reduced early Earth. It is found that the partition coefficients of Ni, Co, P between silicate melts containing C–O–H volatile components and Fe–Ni–Co–P–C alloys (*D*_{met/sil}) have lower values than *D*_{met/sil} for silicate melt-metal equilibria without volatiles in the system at similar values of *f*O₂, *P*, *T* and NBO/T. With decreasing *f*O₂ and, accordingly, with increasing the carbon and hydrogen content in silicate melts these differences grow up. At Δlog*f*O₂(*IW*) = -3.6 *D*_{met/sil} decreases, approximately, by an order of magnitude for Ni and Co, and almost by two orders of magnitude for phosphorus. Thus, the formation of molecules and C–O–H species in silicate liquid leads to a significant reduction of siderophilicity of these elements.

Keywords: Experiment, Low oxygen fugacity, C, Ni, Co, P, Silicate melt, Metal Fe phase.

Experimental data on the distribution coefficients *D*_{met/sil} of siderophile elements between liquid metal and silicate phases, which would allow estimating the effect of the presence in the melt of dissolved volatile components, are very limited and contradictory (Jana, Walker 1999; Richter, 2015, et al.). To evaluate the possible influence of C–O–H volatiles on the distribution of Ni, Co, P between the silicate melt and liquid iron-enriched metal phase, we performed a series of experiments in the model system NaAlSi₃O₈+FeO+SiC+NiO+CoO+Na₂HPO₄ at 1550°C, 4 GPa and oxygen fugacity (*f*O₂) by 1–3.6 log units below the iron-wüstite buffer *IW* (*IW* -1...-3.6), characteristic of global melting processes of the

early Earth's. In the experiments pressure conditions match to the near-surface parts of hypothetical magmatic ocean (at a depth of ~ 150 km), considered to be related to the planetary core formation and the early chemical differentiation of siderophile mantle elements.

Methods. Starting materials for the experiments were a finely ground mixture of synthetic albite glass NaAlSi₃O₈, FeO, NiO, CoO oxides, and phosphorus in the form of Na₂HPO₄ with addition of finely powdered silicon carbide (SiC). The chemical composition of initial mixtures is given in Table 1.

The test mixture weighing 200-300 mg was placed in a sealed Pt capsule. SiC as a source of carbon was unstable under the experimental conditions and completely consumed according to the oxidation reaction: SiC+2FeO(melt) → SiO₂(melt) +2Fe(metal) + C(graphite). As a result, the *f*O₂ values inside the Pt capsule appear to be well below *f*O₂(IW) and proportional to the amount of SiC in the initial mixture. Addition of ~ 1, 2, 5, and 7 wt. % SiC to the initial mixture allows to achieve low *f*O₂ values in the experiments owing to oxidation of SiC interacting with iron-bearing silicate melt and H₂.

Table 1. Compositions of initial mixtures used in the experiments, wt. %.

Runs	SiO ₂	Al ₂ O ₃	FeO	Na ₂ O	Si	C	NiO	CoO	P ₂ O ₅	H ₂ O	Sum
L1	49.89	14.12	18.15	10.51	0.68	0.29	1.93	1.93	2.21	0.28	99.99
L2	49.36	13.97	17.96	10.42	1.35	0.58	1.93	1.93	2.21	0.28	99.99
L3	47.77	13.52	17.38	10.15	3.38	1.44	1.93	1.93	2.21	0.28	99.99
L4	46.71	13.22	16.99	9.97	4.74	2.02	1.93	1.93	2.21	0.28	100.00

The experiments were carried out on a high-pressure anvil-with-hole apparatus of a large volume 6 cm³ at 4 GPa and 1550±25°C under controlled hydrogen fugacity, using the method described earlier in (Kadik et al., 2004; 2013). The chemical compositions of glasses and metal phase were analyzed by electron microprobe. Hydrogen and low concentrations of Ni, Co, P in glasses were determined by secondary ion mass spectrometry. To estimate the mechanisms of carbon and hydrogen dissolution in reduced silicate liquids, the quenched glasses were investigated by Raman spectroscopy.

Results. The experimental products consist of transparent glass with inclusions of Fe metal phase globules <50 μm in size and graphite crystals. The color of glasses depends on experimental conditions and varied from golden-yellow to greenish. The spherical shape of Fe metal phase (Fig. 1) suggests its liquid state during the experiments. A characteristic feature of the chemical composition of glasses is the decrease in FeO concentration with *f*O₂ decreasing as a result of FeO reduction in the melt to form liquid Fe phase. At IW-1.0 it is 13.9 wt.% FeO, and at IW-3.6 it equals to 2.1 wt. % FeO.

The decrease in *f*O₂ is accompanied by a decrease in the melt concentrations of Ni, Co, and P

(Fig. 2a). The change of the chemical composition of metal globules as *f*O₂ decreases is characterized by an increase in Fe concentration and decrease in the concentration of Ni, Co, P (Fig. 2b).

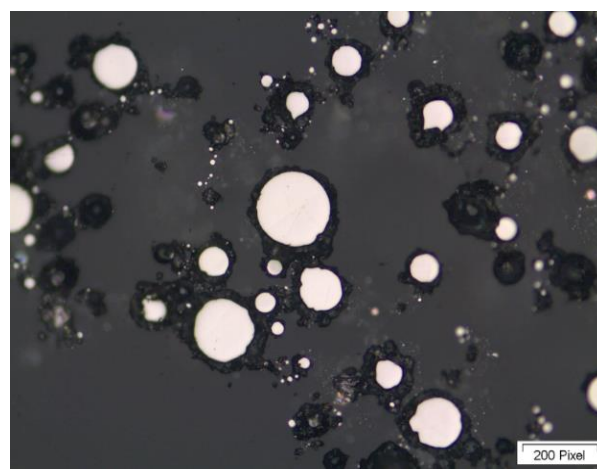


Fig.1. Back-scattered electron image of quenching sample products after the experiment at 4 GPa, 1550±25°C, and *f*O₂(IW-3.6): silicate glass (grey field) with droplets of metal phase (white circles) surrounded by black graphite.

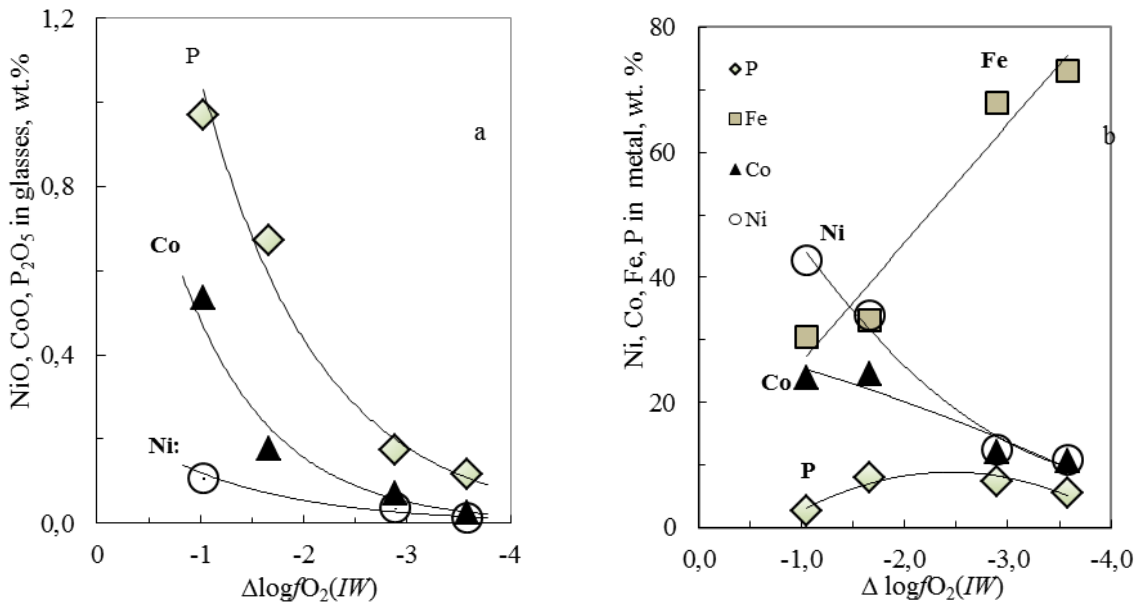


Fig. 2. Ni, Co, P contents versus fO_2 in silicate glass (a), in metal phase (b), $\Delta \log fO_2(IW) = \log fO_2(\text{experiment}) - \log fO_2(IW)$.

Raman spectroscopy. Raman spectra of glasses reveal a series of peaks in the range of 2500–4500 cm^{-1} (Fig. 3). A wide asymmetric band at 3567–3583 cm^{-1} corresponds to O–H bonds in H_2O molecule or OH^- groups in the structure of silicate melts (Mysen and Virgo, 1986, Luth et al., 1987). A weak Raman band at 4124 cm^{-1} is assigned to molecular H_2 (H–H bond) dissolved in glass (Luth et al., 1987). According to (Pouchert, 1981), the peaks at 2909 cm^{-1} and 3287–3291 cm^{-1} correspond to stretching vibrations of molecular CH_4 or other hydrocarbon groups, such as CH_3^- or CH_2^{2-} . The peaks at 1042–1045, 883, 655, 487–495, 75 cm^{-1} are related to the vibrations of aluminosilicate bonds in the glass network. Change in the nature of the Raman spectra of glasses within 20–1200 cm^{-1} (Fig. 3 a, b) indicates significant variations in the melt structure with fO_2 decrease, dissolution of C–O–H species and changes in the melt composition relative to Fe, Ni, Co, P contents. Their nature requires further research.

Thus, spectral studies indicate the formation of reduced (H_2 , CH_4 , CH_2^{2-}) and oxidized (OH^- , H_2O , CO_2) forms of hydrogen and carbon during their interaction with silicate melt. The ratios between oxidized and reduced species significantly depend on fO_2 value. In the range of $\Delta \log fO_2(IW) = -1.0 \dots -1.7$, the predominant hydrogen species in the melt are OH^- groups and H_2O . Some amount of hydrogen is dissolved in the molecular form. Carbon is dissolved in the form of the species with bonds of the C–H type (CH_4 , CH_2^{2-} etc.). At lower values of $\Delta \log fO_2(IW) = -3.6$ the solubility of hydrogen in the form of OH^- and H_2O decreases, while the solubility of carbon in the form of C–H species increases.

Distribution coefficients for Ni, Co, Fe, and P between silicate melt and equilibrated metal phase. Basing on the experimental data obtained, we calculated the distribution coefficient values ($D_{\text{met/sil}} = \text{wt. \% metal} / \text{wt. \% silicate melt}$) for Fe, Ni, Co, P between silicate melt in the presence of C–O–H volatiles

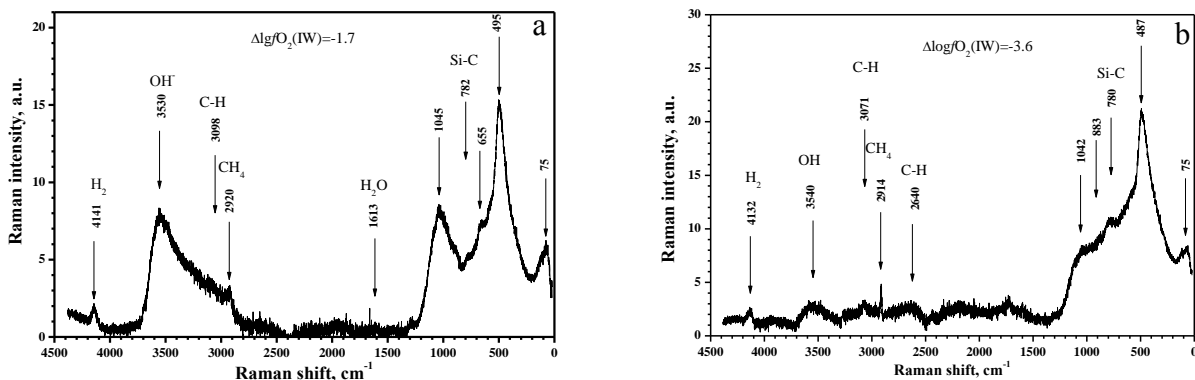


Fig. 3. Raman spectra of glasses containing C–O–H species within 4500–20 cm^{-1} after the experiments at 4.0 GPa, 1550±25°C, and $\Delta \log fO_2(IW) = -1.7$ (a) and -3.6 (b).

and equilibrated metal phase. Fig.4 demonstrates these data in comparison with ($D_{\text{met/sil}}$) for the systems without C–O–H species at similar T , P , $f\text{O}_2$, and NBO/T parameter values. The values of $D_{\text{met/sil}}$, used for a comparison, were calculated on the basis of regression equations describing the experimental data on metal – silicate equilibrium as a function of T , P , $f\text{O}_2$, and NBO/T for silicate liquids (Righter et

al., 1997; Righter and Drake, 2000; Righter, 2003). The NBO/T ratio characterizes a degree of silicate melt polymerization, where NBO is the number of nonbridging oxygen atoms, and T is the number of tetrahedral cations. A decrease in NBO/T corresponds to an increase in the degree of silicate melt polymerization (Mysen, 1991).

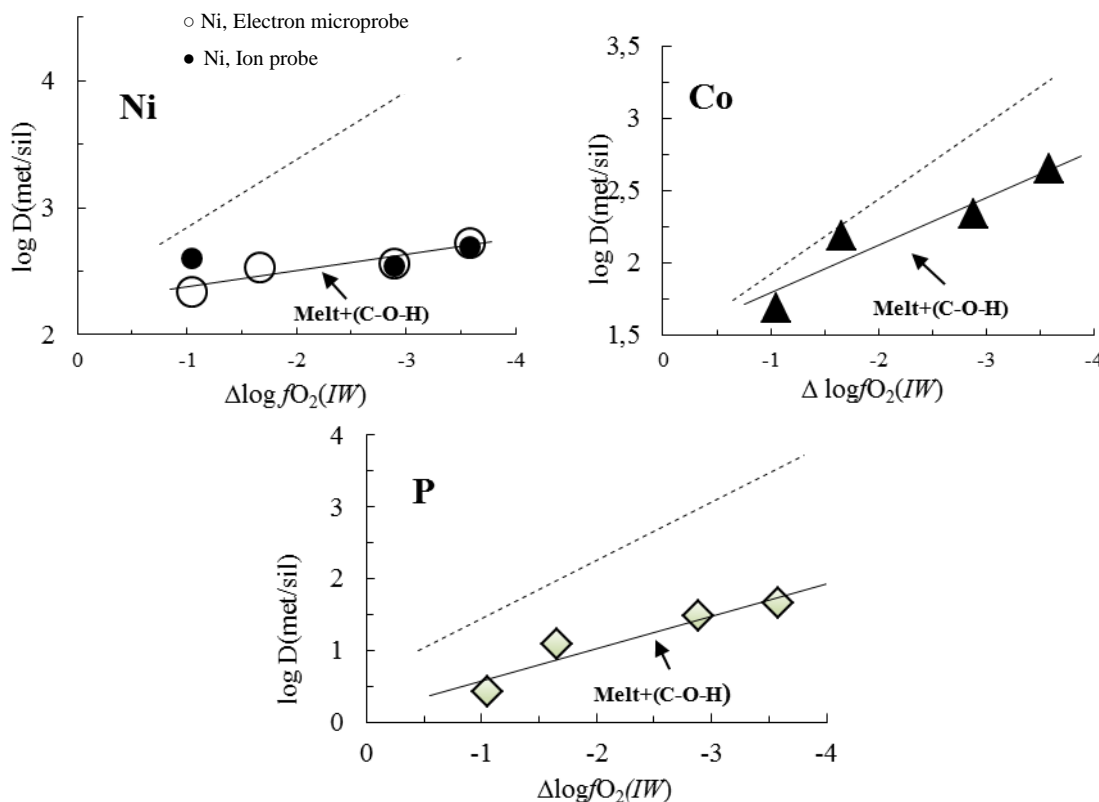


Fig. 4. Distribution coefficients ($D_{\text{met/sil}}$) for Ni, Co, and P between silicate melt, containing C–O–H volatiles, and equilibrated liquid metal phase at 4 GPa, 1550°C are shown as a function of $\Delta\log f\text{O}_2(IW)$. The obtained experimental data were compared with ($D_{\text{met/sil}}$) for the systems without C–O–H species at similar T , P , $f\text{O}_2$, and NBO/T (dotted lines) parameter values.

For all $f\text{O}_2$ values studied Ni, Co, P clearly exhibit their siderophile properties, being distributed mainly into the metal phase. With $f\text{O}_2$ decreasing $D_{\text{met/sil}}$ increases, especially for cobalt and phosphorus, and to a much lesser extent for nickel. However, in the same system in presence of C–O–H species $D_{\text{met/sil}}$ values become lower compared to the system without them. With a decrease in $f\text{O}_2$ and, accordingly, with an increase in C and H content in silicate liquids, the differences increase (Fig. 4). At $\Delta\log f\text{O}_2(IW)=-3.6$ the differences are about one order of magnitude for $D_{\text{met/sil}}$ of Ni and Co (Fig. 4 a, b). The presence of C–O–H volatiles in the system is especially significant: at $\Delta\log f\text{O}_2(IW) = -3.6$ $D_{\text{met/sil}}$ for phosphorus falls down by about two orders of magnitude.

Conclusion. Thus, the formation of C–O–H molecules and complexes in silicate liquids leads to a certain decrease in siderophile properties of Ni, Co, and P. With decreasing $f\text{O}_2$ and, consequently, increasing carbon and hydrogen content, these

differences increase. The obtained result requires further research. Apparently, it is related to significant changes in the structure of silicate melt at low $f\text{O}_2$ values, which were found by Raman spectroscopy. The decrease in siderophile properties of Ni and Co is possibly due to the formation of bonds of the Me–C, Me–H type in reduced silicate melts, where Me is the metal element. In silicate liquid phosphorus can also form the complexes, involving carbon, hydrogen, and oxygen, unidentified by Raman spectroscopy. A certain effect can also have a change in the composition of the metal phase resulting from the dissolution of carbon and hydrogen in it.

This study was supported by the Russian Foundation for Basic Research, project no. 17-05-00713 a, and Program 22 of the Presidium of the Russian Academy of Sciences.

References:

1. Jana D., Walker D., 1999. Core formation in the presence of various C–H–O volatile species. *Geochim. Cosmochim. Acta*, 63, 2299-2310.
2. Kadik A.A., Litvin Y.A., Koltashev V.V., Kryukova E.B., Plotnichenko V.G., Tsekhnonya T.I., Kononkova N.N., 2013. Solution behavior of reduced N–H–O volatiles in FeO–Na₂O–SiO₂–Al₂O₃ melt equilibrated with molten Fe alloy at high pressure and temperature. *Phys. Earth Planet. Inter.*, 214, 14-24.
3. Kadik A.A., Pineau F., Litvin Y., Jendrzewski N., Martinez I., and Javoy M., 2004. Formation of carbon and hydrogen species in magmas at low oxygen fugacity. *J. Petrol.*, 45, 1297-1310.
4. Luth R.W., Mysen B.O., Virgo D., 1987. Raman spectroscopic study of the solubility behavior of H₂ in the system Na₂O–Al₂O₃–SiO₂–H₂. *Amer. Min.*, 72, 481-486.
5. Mysen B.O., 1991. Relations between structure, redox equilibria of iron, and properties of magmatic liquids. In L.L. Perchuk and I. Kushiro, Eds., *Physical Chemistry of Magmas*, Springer-Verlag, New York, 9, 41-98.
6. Mysen B.O., Virgo D., 1986. Volatiles in silicate melts at high pressure and temperature. 2. Water in melts along the join NaAlO₂–SiO₂ and a comparison of solubility mechanisms of water and fluorine. *Chem. Geol.*, 57, 333-358.
7. Pouchert C. G., 1981. *The Aldrich Library of Infrared Spectra*, 3rd ed. (Aldrich Chemical Co, 1981).
8. Righter K., 2003. Metal-silicate partitioning of siderophile elements and core formation in the early Earth. *Ann. Rev. Earth Planet. Sci.*, 31, 135-174.
9. Righter K., 2015. Modeling siderophile elements during core formation and accretion, and the role of the deep mantle and volatiles. *Amer. Min.*, 100, 1098-1109.
10. Righter K., Drake M.J., 1999. Effect of water on metal-silicate partitioning of siderophile elements: a high pressure and temperature terrestrial magma ocean and core formation. *Earth Planet. Sci. Lett.*, 171, 383-399.
11. Righter K., Drake M.J., Yaxley G., 1997. Prediction of siderophile element metal-silicate partition coefficients to 20 GPa and 2800°C: the effects of pressure, temperature, oxygen fugacity, and silicate and metallic melt compositions. *Phys. Earth Planet. Inter.* 100, 115-134.

¹Kadik A.A., ¹Lukanin O.A., ¹Kurovskaya N.A., ¹Ignat'ev Yu.A., ¹Kryukova E.B., ^{1,2}Koltashev V.V. Experimental study of the solubility and speciation of N–C–O–H volatile components in basic silicate melts in equilibrium with liquid iron alloys at 1.5 GPa, 1400°C.

V.I. Vernadsky Institute of Geochemistry and Analytical Chemistry RAS, Moscow, ²Fiber Optics Research Center RAS, Moscow (lukanin@geokhi.ru; Kurum46@mail.ru)

Abstract. The contents and speciation of nitrogen, carbon, and hydrogen were determined in basic silicate melts in equilibrium with liquid Fe alloys at 1.5 GPa, 1400°C, and oxygen fugacities (f_{O_2}) 1.4–1.9 log units below that of the Fe–FeO buffer (IW). FTIR and Raman spectroscopy of quenched experimental glasses indicates the formation in the silicate melts of molecules and complexes with bonds to N–H (NH₃, NH₂[–], NH₂⁺, NH₄⁺), H–OH (H₂O, OH[–]), C–H (CH₄), C=O, C–N, and the molecules N₂, H₂, and CO₂. The data obtained confirm the conclusion made earlier on the basis of the study of model silicate melts of the FeO–Na₂O–Al₂O₃–SiO₂ system (Kadik et al., 2011, 2015), about the possibility of presence of relatively large amounts of water (OH[–], H₂O) in silicate magmatic melts, even under strongly reduced conditions. These data are important for understanding the formation of the early reduced atmosphere of the Earth enriched with CH₄, H₂, NH₃, CO, as a result of global melting and magmatic degassing, and also to estimate the quantities of carbon and nitrogen, which remain in the mantle after the formation of the metallic core.

Keywords: *experiment, solubility of N–C–O–H volatiles, Fe-bearing silicate melt, Fe-alloy, oxygen and hydrogen fugacity, IR and Raman spectroscopy.*

Introduction. Global melting of matter of the early Earth, associated with the formation of a magma ocean and iron core, despite the short duration in geological history (Galimov, 2005, etc.), could play a decisive role in the formation of the N–C–O–H volatile compounds in the mantle, as well as in the emergence of the early reduced atmosphere of the planet. It is assumed that the gas regime of the early Earth could be determined by dissolution of volatiles in magmatic melts and liquid iron alloys at f_{O_2} by 4-8 orders of magnitude below than values typical for the modern mantle-derived magmas (Wood et al., 2006; Frost et al., 2008, etc.). Such low f_{O_2} values determine the presence of reduced carbon, nitrogen, and hydrogen compounds in melts. The mechanisms of their formation are not clear enough. The knowledge reactions of interaction of volatiles with reduced silicate melts and their partitioning between silicate and metallic phases is a key for understanding the role of melting of reduced primary mantle in the formation of the early Earth atmosphere, enriched in CH₄, H₂, NH₃, CO, and also for estimating the amounts of carbon, nitrogen, and other volatiles that remained in the mantle of the Earth after the completion of the formation of the metallic core.

The purpose of this study is to reveal the peculiarities of the simultaneous dissolution of N–C–O–H volatile compounds in natural Fe-bearing silicate melts at low f_{O_2} , which could correspond to the conditions of differentiation and melting of the

Early Earth during its melting and segregation of the iron-rich metal phase.

Methods. The starting material for the experiments was a finely dispersed mixture of natural ferrobasalt glass and silicon nitride (Si_3N_4) (1, 3, 5, and 7 wt %) as a source of nitrogen in the system. The experiments were performed in a piston–cylinder apparatus in a welded Pt capsule in the presence of excess C (graphite) at 1.5 GPa, 1400°C, and $f\text{O}_2$ by 1.4–1.9 log units below the IW buffer (Kadik et al., 2017). The duration of the experiments was 60 min. The products of quenching experiments, which are glasses with spherical inclusions of the iron alloy, were analyzed by electron microprobe analysis, Raman and FTIR spectroscopy. With the increase of Si_3N_4 in the initial mixture and, consequently, the decrease of $f\text{O}_2$ in the system, the silicate melt, formed during the experiments, was enriched with SiO_2 , varying in composition from basalt to basaltic andesite. The value of $f\text{O}_2$ during the experiment was calculated from the ratio of the equilibrium concentrations of Fe in the silicate melt (glass) and the metallic phase (Kadik et al., 2014). The hydrogen fugacity in the capsule was buffered externally as a result of the diffusion of hydrogen forming during thermal dissociation of traces of water absorbed by the solid assemblage of high-pressure cell through the walls of Pt–capsule (Kadik et al., 2011).

Results. The performed studies reveal some important features of the dissolution of nitrogen,

carbon and hydrogen in magmatic melts of basic composition and coexisting with them liquid iron-rich alloys in a strongly reducing environment, which are characteristic of the mantle of the early Earth. Among the main results of this study are the following.

The concentration of nitrogen in basalt-basaltic andesite melts with decrease $\Delta\log f\text{O}_2(\text{IW})$ from -1.4 to -1.7 increased from 0.13 to 0.41 wt.%. In the interval $\Delta\log f\text{O}_2(\text{IW})$ from -1.7 to -1.9, it remains almost constant at the level of 0.44–0.47 wt.% (Fig. 1a). Similar N concentration (0.4–0.6 wt.%) was determined earlier in the melts of the $\text{FeO-Na}_2\text{O-Al}_2\text{O}_3\text{-SiO}_2$ model system in equilibrium with liquid Fe alloy and graphite, in the experiments carried out by the same method under similar P-T- $f\text{O}_2$ parameters (Kadik et al., 2011). This indicates the relatively weak influence of silicate melt composition on the solubility of nitrogen. In more reducing conditions ($\Delta\log f\text{O}_2(\text{IW}) = -3.4$) the solubility of nitrogen in the melts of the model system increases by almost three times. It can be expected that further decreasing of the $f\text{O}_2$ will lead to a significant increase in the concentration of nitrogen in the melts of basalt-basaltic andesite composition. As shown by the data for the $\text{FeO-Na}_2\text{O-Al}_2\text{O}_3\text{-SiO}_2$ system the increase of pressure up to 4 GPa (1550°C) at a constant $f\text{O}_2$ leads to a significant increase in nitrogen solubility in silicate melt (Kadik et al., 2015).

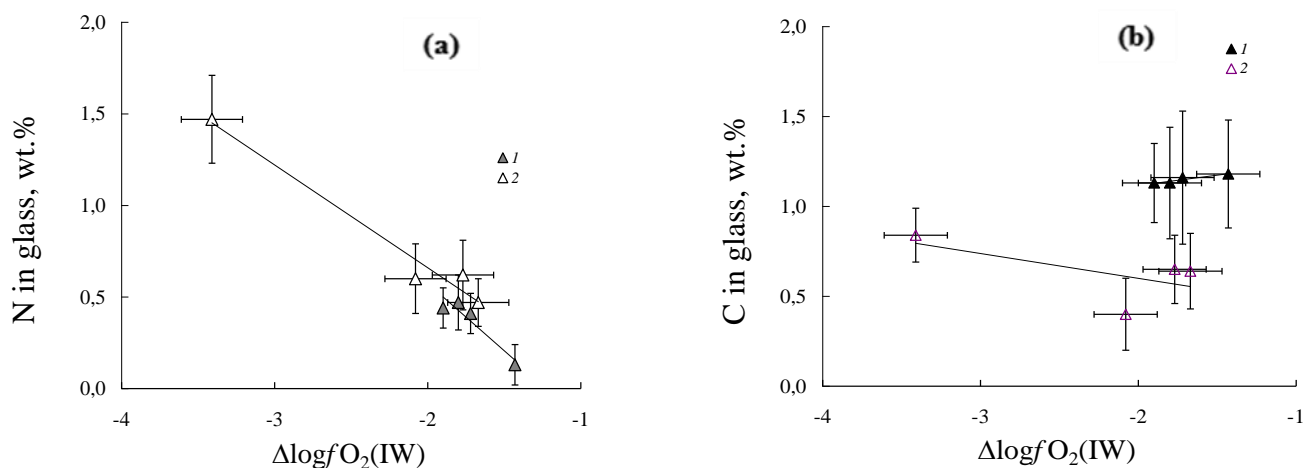


Fig. 1. Nitrogen (a) and carbon (b) in silicate melts as function of oxygen fugacity: 1 - basaltic melt (this study); 2 - melt system $\text{FeO-Na}_2\text{O-Al}_2\text{O}_3\text{-SiO}_2$ (Kadik et al., 2011)

The concentration of carbon in basalt-basaltic andesite melts is 1.18–1.13 wt.% and in a first approximation constant throughout the studied interval $f\text{O}_2$. It is about 0.5 wt.% higher than in the melts of the system $\text{FeO-Na}_2\text{O-Al}_2\text{O}_3\text{-SiO}_2$ under similar P-T- $f\text{O}_2$ parameters (Fig. 1b).

Hydrogen is present in the melt as OH^- -groups and H_2O and H_2 molecules. The total water content

($\text{OH}^- + \text{H}_2\text{O}$) determined by FTIR spectroscopy decreases from 4.91 to 1.20 wt.% with decreasing $\Delta\log f\text{O}_2(\text{IW})$ from -1.4 to -1.9. These data confirm previously obtained conclusions for model $\text{FeO-Na}_2\text{O-Al}_2\text{O}_3\text{-SiO}_2$ melts (Kadik et al., 2011, 2015) that OH^- and H_2O are highly stable species, the relatively large amounts of which could occur in silicate melts even under reducing conditions.

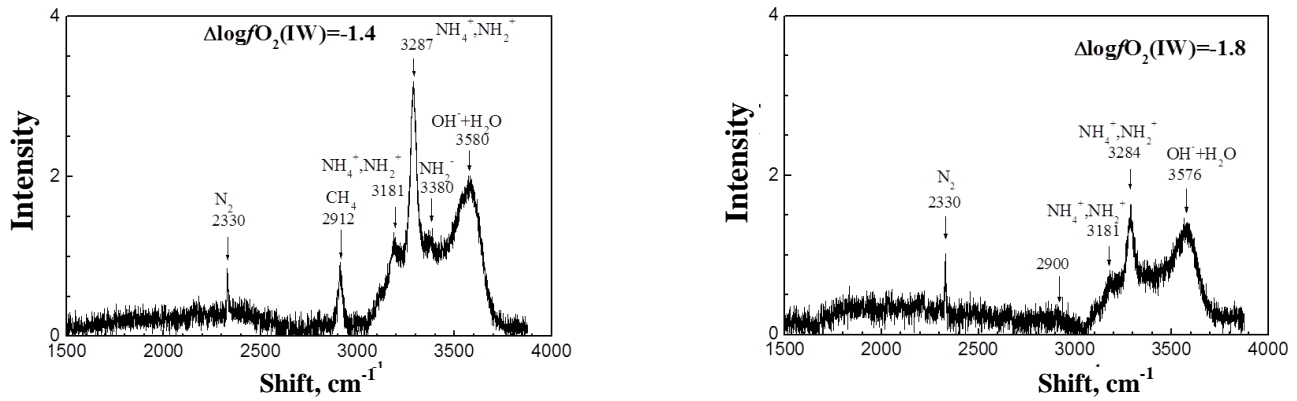


Fig. 2. Raman spectra of glasses in the region 4000–1500 cm⁻¹ after the experiments at ΔlogfO₂(IW) = -1.4 and -1.8. Spectra were normalized to the fundamental band around 490 cm⁻¹.

The FTIR and Raman spectroscopic study of experimental glasses indicates the formation of molecules and complexes with bonds N–H (NH₃, NH₂⁻, NH₂⁺, NH₄⁺), H–O (H₂O, OH⁻), C–H (CH₄), and N₂ and H₂ molecules in the melts (Fig.2). FTIR spectra also revealed the presence of complexes with bonds C=O, C–N, and CO₂ molecules. The molecules and complexes of N–C–O–H volatiles in the basalt–basaltic andesite melts are similar to those found in the model FeO–Na₂O–Al₂O₃–SiO₂ melts at 1.5 GPa (1400°C) and 4 GPa (1550°C) at similar or close ΔlogfO₂(IW) (Kadik et al., 2011, 2015).

Oxygen fugacity significantly affects the proportions of different species of N–C–O–H in a melt, in spite of the sufficiently narrow range of ΔlogfO₂(IW) in the performed experiments. The intensities of Raman bands 2330, 2912, 3288 cm⁻¹, which characterize molecules and complexes N₂, CH₄, NH₄⁺, NH₂⁺ respectively, decrease with decreasing fO₂. The intensities of other bands 3115 (N–H), 3180 (NH₄⁺, NH₂⁺), 3380 (NH₂⁻) cm⁻¹ show non-linear behavior (Fig 3).

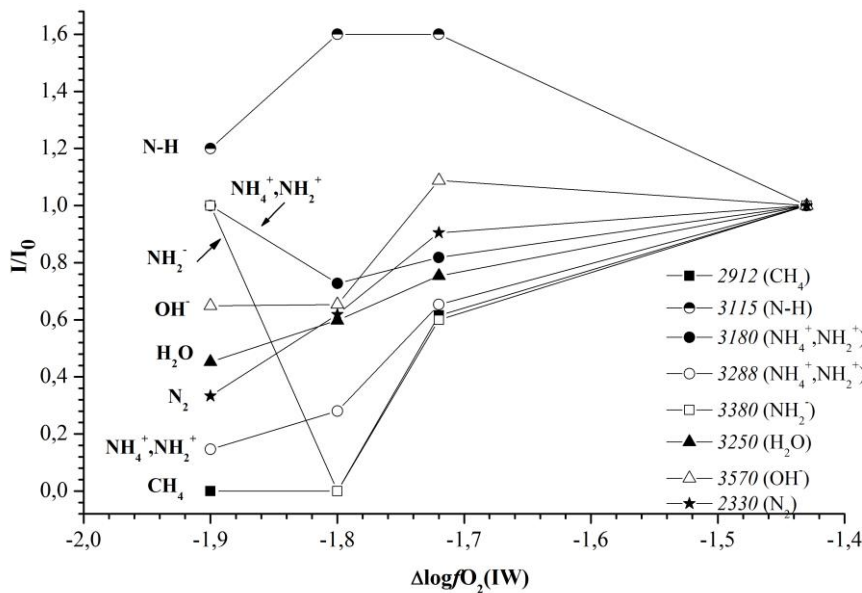


Fig. 3. Variations of integral intensities I/I₀ of Raman bands corresponding to N–C–O–H molecules and complexes in the basalt–basaltic andesite melts versus ΔlogfO₂(IW). I₀ - integrated intensity at ΔlogfO₂(IW) = -1.4.

Conclusions. The solubility of nitrogen in silicate melts in equilibrium with liquid alloy enriched with iron in the presence of H and C increases significantly with decreasing fO₂ and increasing the pressure. Thus, the oxidation of the melt during its ascent to the surface may be accompanied by removal of the gas phase enriched in nitrogen in N₂ and N–H compounds from the melt.

The data obtained confirm the conclusion about the high stability of OH⁻ groups and H₂O in a highly reduced silicate magmatic melts. This can explain the

formation of hydrous mineral phases in the reduced early mantle of the Earth.

This work was supported by the Russian Foundation for Basic Research (project no. 17-05-00713a) and Program 22 of the Presidium of the Russian Academy of Sciences.

References:

1. Frost D.J., Mann U., Asahara Y., Rubie D.C. (2008) The redox state of the mantle during and just after

- core formation. *Philosophical Transactions of the Royal Society*. **A 366**, 4315–4337.
- Galimov E.M. (2005). Redox Evolution of the Earth Caused by a Multistage Formation of Its Core. *Earth and Planetary Science Letters* **233**, 263–276.
 - Kadik A. A., Kurovskaya N. A., Ignat'ev Yu. A., Kononkova N.N., Koltashev V. V., and Plotnichenko V. G., (2011) Influence of oxygen fugacity on the solubility of nitrogen, carbon, and hydrogen in FeO–Na₂O–SiO₂–Al₂O₃ melts in equilibrium with metallic iron at 1.5 GPa and 1400°C,” *Geochem. Int.* **49** (5), 429–438
 - Kadik A. A., Koltashev V. V., Kryukova E. B., Plotnichenko V. G., Tsekhonya T. I., and Kononkova N. N., (2014) Solution behavior of C–O–H Volatiles in FeO–Na₂O–Al₂O₃–SiO₂ melts in equilibrium with liquid iron alloy and graphite at 4 GPa and 1550°C. *Geochem. Int.* **52** (9), 707–725.
 - Kadik A. A., Koltashev V. V., Kryukova E. B., Plotnichenko V. G., Tsekhonya T. I., and Kononkova N. N. (2015) Solubility of nitrogen, carbon, and hydrogen in FeO–Na₂O–Al₂O₃–SiO₂ melt and liquid iron alloy: influence of oxygen fugacity. *Geochem. Int.* **53** (10), 849–868.
 - Kadik A. A., Kurovskaya N. A., Lukanin O. A., Ignat'ev Yu. A., Koltashev V. V., Kryukova E. B., Plotnichenko V. G., and Kononkova N. N. (2017) Formation of N–C–O–H molecules and complexes in the basalt–basaltic andesite melts at 1.5 GPa and 1400°C in the presence of liquid iron alloys. *Geochem. Int.* **55** (2), 151–162.
 - Wood B. J., Walter M. J., Wade J. (2006) Accretion of the Earth and segregation of its core. *Nature* **441**, 825–833.

Lavrentjeva Z.A., Lyul A.Yu. EL6 enstatite chondrites: the peculiarities of trace element composition.

V.I. Vernadsky Institute RAS, Moscow (lavza@mail.ru).

Abstract. In the present paper the results of elemental abundances in separated grain-sized nonmagnetic fractions from Pillistfer EL6 and Atlanta EL6 enstatite chondrites are reported. Based on the study of the features of lithophile and siderophile element distributions in the fractions of meteorites a conclusion has been made that some of difficulties of unraveling metamorphic processes of the EL6 chondrites probably result from mixing effects of nebular fractionation, thermal metamorphism and shock.

Keywords: nonmagnetic fractions, fractionation of elements, enstatite chondrites.

The enstatite chondrites (EC) are most reduced meteorites and classified into the high-siderophile group EH and low-siderophile group EL [Sears et al., 1982], characterized by abundant Fe-Ni metal, nearly Fe-free silicates, and unusual sulfides [Keil, 1968]. Texturally the EL chondrites appear to have experienced much higher levels of metamorphic alteration than HL chondrites of similar equilibration

temperatures. Most EL6 chondrites have been strongly affected by impact melting and/or brecciation [Rubin et al. 2009]. Previous studies showed that EL6 chondrites exhibit specific REE patterns [Kallemeyn and Wasson, 1986, Rubin, 2009]. If all the EL chondrites belong to the same metamorphic sequence, then the particular REE abundances in EL6 chondrites were certainly achieved by complex parent body processes [Barrat et al., 2014]. To receive more information about features of composition of EL6 chondrites, to assess the effects of nebular fractionation and metamorphism, the trace element contents in nonmagnetic grain-sized fractions from Pillistfer EL6 and Atlanta EL6 chondrites was determined by INAA.

Samples and methods

The nonmagnetic fractions were selected by particle – size analysis and handpicking under microscope. The elemental composition of fractions was analyzed at the Central Laboratory of GEOKHI RAS using optimized version of neutron-activation analysis developed for analyzing extraterrestrial material (Kolesov, 2001).

Results and discussion:

Under consideration are peculiarities of elemental composition of nonmagnetic grain-sized fractions extracted from Pillistfer EL6 and Atlanta EL6 enstatite chondrite. The analysis of the chemical composition of the obtained data showed that:

(1) All “*ultra- and fine-grained*” fractions from Pillistfer EL6 (Fig.1) are enriched in lithophile and depleted in siderophile elements.

Such distribution of elements in these fractions a result of nebular metal-silicate fractionation. Distinctive feature of REE distribution in these fractions is the high abundances of light and heavy REE with negative and positive Eu-anomalies. Perhaps, the positive and negative Eu – anomalies in these fractions REE patterns are associated with oldhamite and plagioclase. In “*ultra-fine grained*” fractions (A,B,C) the abundance Ni (0.04 – 0.09 x CI) and Co (0.04 – 0.08 x CI) are lower than Au (0.1 x CI). A distribution of Au in these fractions is permanent. The (Ir/Au)_{Pillistfer} / (Ir/Au)_{CI} ratio in “*ultra-fine-grained*” fractions varies from 0.4 to 0.7. This fact supports the opinion that, the main processes controlling of composition “*ultra-fine-grained*” fractions was nebular fractionation and the fractionation in situ probably result from thermal metamorphism. “*Fine-grained*” nonmagnetic fraction (1 < d < 45 μm) from Atlanta EL6 chondrite (Fig.2) are enriched in lithophilic Sc (1.7 x CI); Cr (6.3 x CI), La (1.5x CI); Sm (1.8 x CI); Eu (2.0 x CI); Tb (2.1 x CI); Yb (2.2 x CI); Lu (2.0 x CI) and depleted in siderophilic Ni (0.3 x CI); Co (0.2 x CI); Au (0.05 x CI), Ir (0.04 x CI).

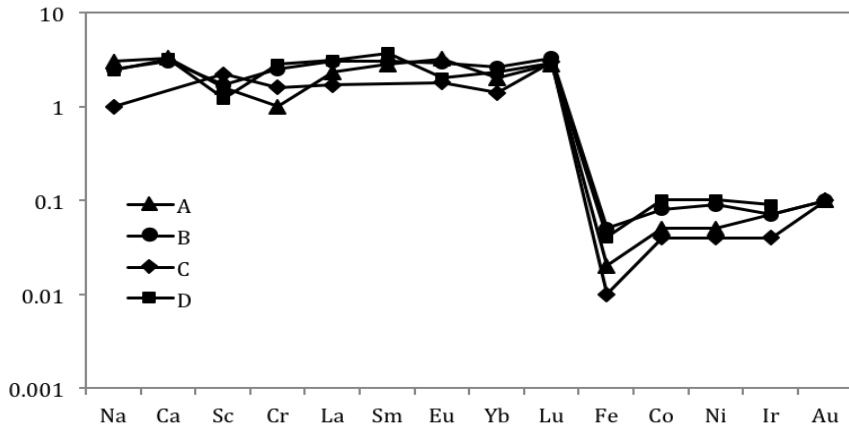


Fig.1. CI chondrite-normalized pattern of trace element abundance of nonmagnetic “*ultra - and fine - grained*” fractions from Pillistfer EL6 enstatite chondrite: A – fraction $1 < d < 25 \mu\text{m}$; B - fraction $25 < d < 45 \mu\text{m}$; C – fraction $35 < d < 45 \mu\text{m}$; D - fraction $< 45 \mu\text{m}$.

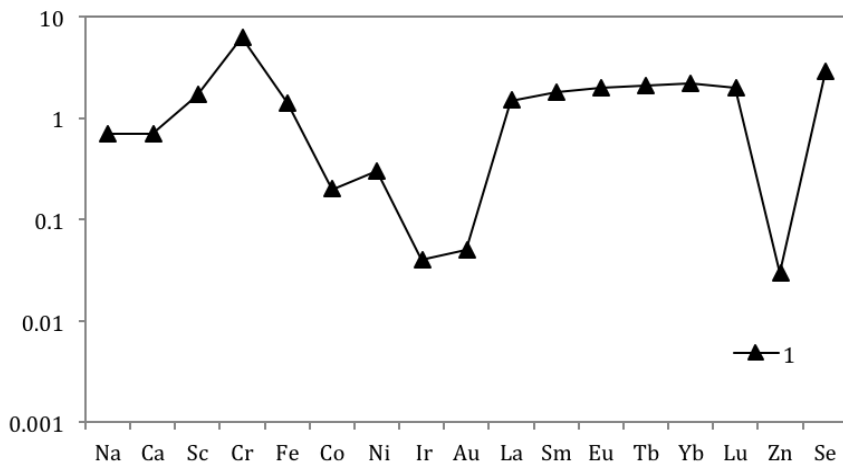


Fig.2. CI chondrite-normalized pattern of trace element abundance of nonmagnetic “*fine - grained*” fraction 1 ($1 < d < 45 \mu\text{m}$) from Atlanta EL6 enstatite chondrite.

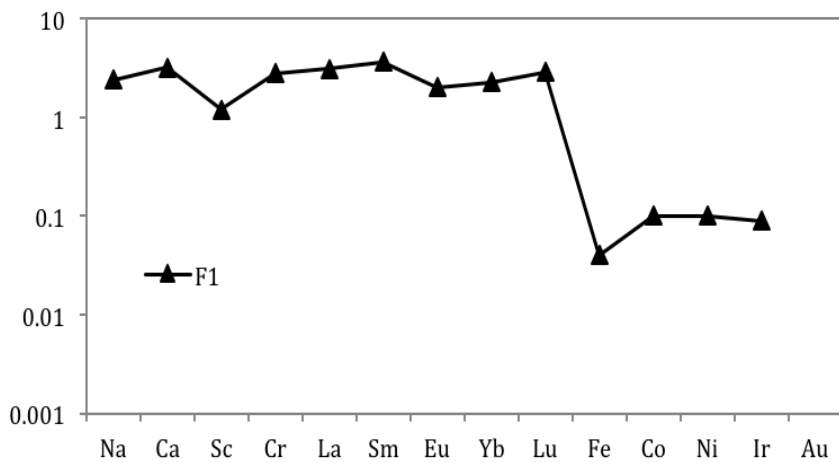


Fig.3. CI chondrite-normalized pattern of trace element abundance of nonmagnetic “*mean-grained*” fraction F ($71 < d < 100 \mu\text{m}$) (with accessory minerals) from Pillistfer EL6 enstatite chondrite.

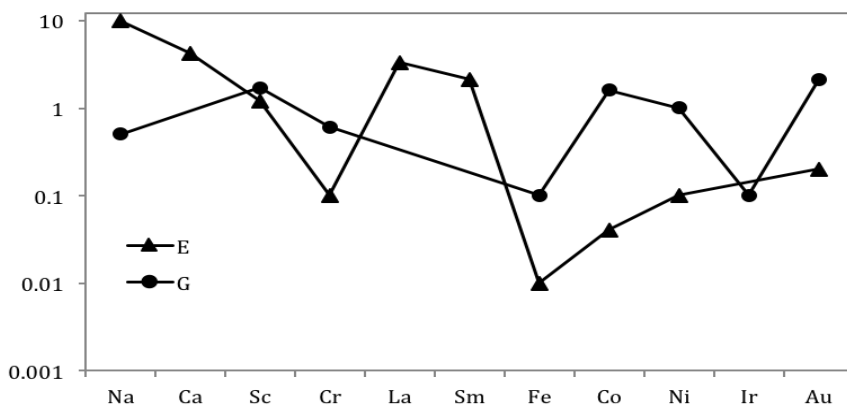


Fig.4. CI chondrite-normalized pattern of trace element abundance of nonmagnetic “*mean-grained*” fractions E ($45 < d < 71 \mu\text{m}$) and G ($71 < d < 100 \mu\text{m}$) (without accessory minerals) from Pillistfer EL6 enstatite chondrite.

Problems of Planetology, Cosmochemistry and Meteoritica

Distinctive feature of trace element distribution in this fraction ($1 < d < 45 \mu\text{m}$) is the high abundances of LREE ($1.5 \times \text{CI}$) and HREE ($2.0 \times \text{CI}$) with positive Eu-anomalies and much lower than those of Pillistfer EL6 chondrite. Perhaps, the positive Eu-anomalie in this fraction REE patterns are associated with plagioclase. Atlanta EL6 was examined by Keil [Keil, 1968] and are found to be free of oldhamite. Plagioclase, which is LREE enriched, displays much lower LREE abundances (about three orders of magnitude lower than those of oldhamite [Hsu, 1998]).

(2) “*Mean-grained*” nonmagnetic fraction F1 ($71 < d < 100 \mu\text{m}$) (with accessory minerals) from Pillistfer EL6 enstatite chondrite (Fig. 3.) are enriched in lithophilic (Na ($2.4 \times \text{CI}$); Ca ($3.3 \times \text{CI}$); Cr ($2.8 \times \text{CI}$); La ($3.1 \times \text{CI}$); Sm ($3.7 \times \text{CI}$); Eu ($2.0 \times \text{CI}$); Yb ($2.3 \times \text{CI}$); Lu ($2.9 \times \text{CI}$) and depleted in

siderophilic Fe ($0.04 \times \text{CI}$); Co ($0.1 \times \text{CI}$); Ni ($0.1 \times \text{CI}$); Ir ($0.09 \times \text{CI}$); Au ($0.1 \times \text{CI}$). This fraction (F) has a Eu minimum ($\text{Eu}_F/\text{Eu}_{\text{CI}}/\text{Sm}_F/\text{Sm}_{\text{CI}} = 0.5$), and are cosmic ($\text{La}_F/\text{La}_{\text{CI}}/\text{Lu}_F/\text{Lu}_{\text{CI}}$) ratio ~ 1.0 .

“*Mean-grained*” nonmagnetic fractions G ($71 < d < 100 \mu\text{m}$) from Pillistfer EL6 enstatite chondrite (Fig. 4.) (without accessory minerals), on the contrary, are depleted in lithophile elements and are enriched in siderophile elements.

(3) “*Coarse-grained*” nonmagnetic fraction H ($100 < d < 160 \mu\text{m}$) and fraction I ($160 < d < 260 \mu\text{m}$) from Pillistfer EL6 enstatite chondrite (Fig.5.) are enriched in lithophilic Na ($1.0 - 1.2 \times \text{CI}$); Ca ($1.0 - 1.3 \times \text{CI}$); Sc ($2.2 - 2.3 \times \text{CI}$); Cr ($0.5 - 1.0 \times \text{CI}$), Sm ($0.6 - 1.0 \times \text{CI}$); Eu ($1.3 - 1.8 \times \text{CI}$); Yb ($2.3 \times \text{CI}$) and depleted in siderophilic Fe ($0.02 - 0.03 \times \text{CI}$); Co ($0.08 - 0.2 \times \text{CI}$); Ni ($0.06 - 0.1 \times \text{CI}$); Ir ($0.1 \times \text{CI}$); Au ($0.1 - 0.2 \times \text{CI}$).

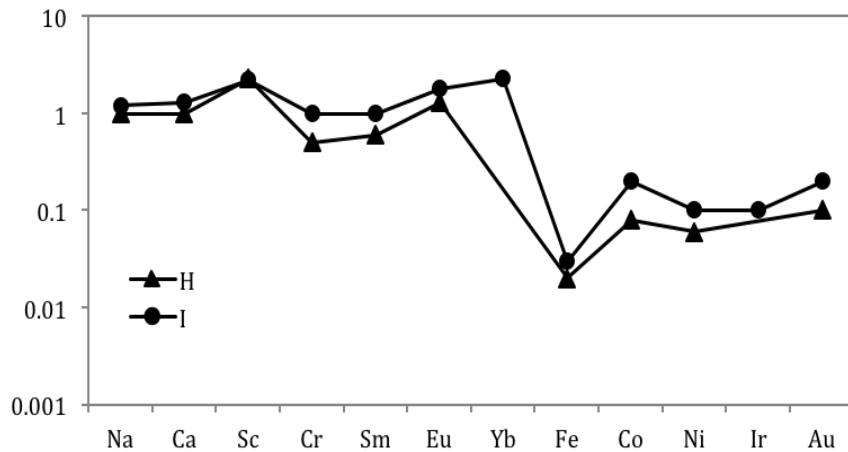


Fig.5. CI chondrite-normalized of trace element abundance patterns of nonmagnetic “*coarse-grained*” H - fraction ($100 < d < 160 \mu\text{m}$) and I - fraction ($160 < d < 260 \mu\text{m}$) from Pillistfer EL6 enstatite chondrite.

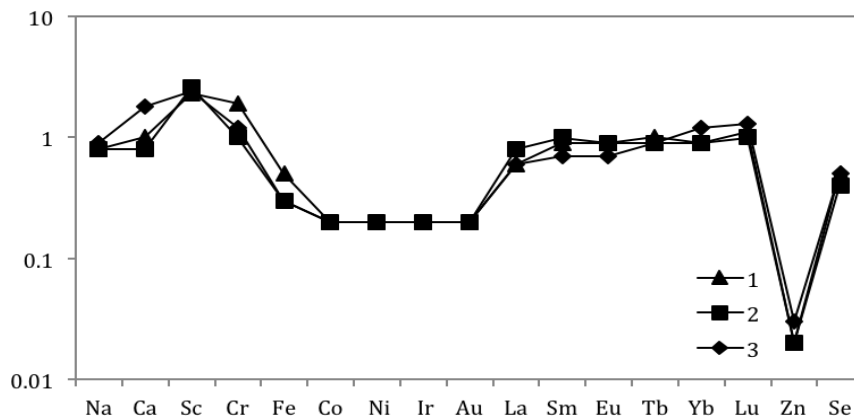


Fig.6. CI chondrite-normalized of trace element abundance patterns of nonmagnetic “*mean-grained*” fractions from Atlanta EL6 enstatite chondrite. 1 - fraction ($45 < d < 71 \mu\text{m}$); 2 - fraction ($71 < d < 100 \mu\text{m}$); 3 - fraction ($100 < d < 160 \mu\text{m}$)

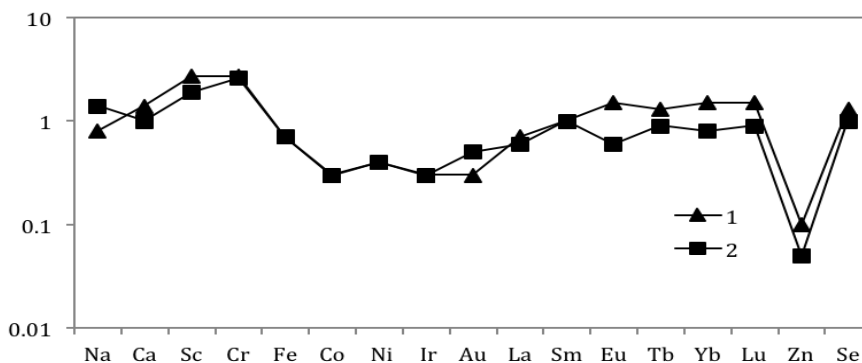


Fig.7. CI chondrite-normalized of trace element abundance patterns of nonmagnetic “*coarse-grained*” fractions from Atlanta EL6 enstatite chondrite. 1 - fraction ($160 < d < 260 \mu\text{m}$); 2 - fraction ($260 < d < 360 \mu\text{m}$).

Distinctive features of trace element distribution in “coarse-grained” fractions (H, I) from Pillistfer EL6 enstatite chondrite (Fig. 5) is the fact that the contents of lithophile and siderophile elements increase with increasing of the grain-size. These fractions have REE patterns with positive Eu – anomalies - $[(\text{Eu}/\text{Sm})_{\text{H,I}} / (\text{Eu}/\text{Sm})_{\text{CI}}] = 2.2; 1.8$, respectively.

“Mean-grained” (Fig. 6) and “coarse-grained” (Fig. 7) fractions from Atlanta EL6 chondrite are depleted LREE - La (0.6 – 0.8 x CI) and enriched HREE - Lu (1.0 – 1.5 x CI). These fractions have REE patterns with positive Eu – anomalies - $[(\text{Eu}/\text{Sm})_{\text{fractions}} / (\text{Eu}/\text{Sm})_{\text{CI}}] = 1.0 – 1.5$. Perhaps, the positive Eu – anomalies in these fraction REE patterns are associated with plagioclase. Atlanta EL6 was examined by Keil [Keil, 1968] and are found to be free of oldhamite.

Conclusions.

Based on the study of the features of lithophile and siderophile element distributions in the fractions from Pillistfer and Atlanta meteorites a conclusion has been made that some of difficulties of unraveling metamorphic processes of the EL6 chondrites probably result from mixing effects of nebular fractionation, thermal metamorphism and shock.

References:

1. Barrat J.A., Zanda B., Jambon C., Bollinger C. (2014) The lithophile trace elements in enstatite chondrites. *Geochim. Cosmochim. Acta* V.128. P. 71 – 94.
2. Hsu W. (1998) Geochemical and petrographic studies of oldhamite, diopside, and roederite in enstatite meteorites. *Meteorit. Planet. Sci.* V.33. P. 291–301.
3. Kallemeyn G.W., Wasson J.T. (1986) Compositions of enstatite (EH3, EH4,5 and EL6) chondrites: implications regarding their formation. *Geochim. Cosmochim. Acta* V.50. P. 2153 – 2164.
4. Keil K. (1968) Mineralogical and chemical relationships among enstatite chondrites. *Journal of Geophysical Research* V.73. P. 6945 - 6976.
5. Kolesov G. M., Shubina N.V., Lyul A.Yu. (2001) Optimizing instrumental neutron activation analysis of extraterrestrial materials: fragments of lunar rocks, meteorites, chondrules and ultrarefractory inclusions. *J. Anal. Chem.* V.56. P. 1022 – 1028.
6. Rubin A., Hubert H., Wasson J. (2009) Possible impact-induced refractory lithophile fractionations in EL chondrites. *Geochim. Cosmochim. Acta* V.73 . P. 1523 – 1537.
7. Sears D.W., Kallemeyn G. W., Wasson I. T. (1982) The compositional classification of chondrites II. The enstatite chondrite groups. *Geochim. Cosmochim. Acta* . V.46. P. 597 - 608.

Nikitin S.M.¹, Skripnik A.Ya.², Asanov V.A.³, Panykov I.L.³. Super-brittle and dynamical strength of the Tsarev stone meteorite

¹ Laboratory of mechanics of rocks and ores. Company of «JC-KAM», Moscow.

² V.I. Vernadsky Institute of Geochemistry and Analytical Chemistry RAS, Moscow.

³ Mining Institute of the Ural Branch of the Russian Academy of Sciens. Perm (archont@mail.ru).

Abstract. This paper presents the rationale to exploit a generalized strength passport in the form of the Mohr–Coulomb circles’ envelope to control the damage degree of SAU-001, Ghubara and Tsarev meteorites. The rationale is based on the complex definitions of ordinary chondrites’ physical and mathematical properties, which were conducted for samples with regular (25x25x50mm) and semi-regular (20x20x20mm) shapes. The interpretation of the stress-strain diagrams for samples, which were tested by the method of T. Karman in the uniaxial axial compression mode and in the unequal-component bulk compression mode using mineralogical-petrographic, geochemical and ultrasonic data, allows to consider abnormal (against the background of static strains) dynamic forms of extraterrestrial matter’s cramped movement under load, beginning from the stage of primary consolidation, which promotes the growth of the internal energy of the chondrites and the transition to a super-brittle state, and ending with self-sustaining destruction processes in the form of a rheological explosion. It is established, that the transition of an inhomogeneous, generally anisotropic meteorite substance with a structural hierarchy to a super-brittle state corresponds to the development of bulk forms of fragmentation in narrowly localized zones of microcracks within the main crack channel. The latter is emphasized by the data of electron and optical microscopy.

Keywords: *superbrittleness, crack, dynamic durability, explosion, the Tsarev meteorite, friction, crushing*

The basis for the paper was a widespread view about quasi-static forms of meteoroid solid destruction, which, taking into account the observed explosive processes of the Chelyabinsk bolide (Marov, Shustov, 2013), required a detailed study of cracks development dynamic effects against the background of static deformations.

It can be seen that the effects of geomaterials explosive destruction in the laboratory and the explosions of meteoroids at the entrance to the Earth's atmosphere have much in common (Grigoryan S.S. et al. 2013). Meteorites explosive destruction is associated with shear processes in brittle solids and is implemented in cramped conditions under static loading due to the dynamic activation of the shear processes on solids’ contact points and growing cracks. Uncontrolled explosive dynamic destruction of samples also occurs under static loads and is associated with the cracks brittle development processes following by the "rheological explosion" mechanism.

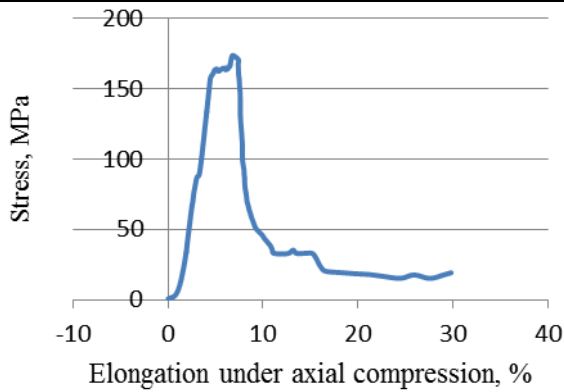


Fig.1. The strain characteristic of the Sayh Al Uhamir meteorite sample (20x20x20 mm)

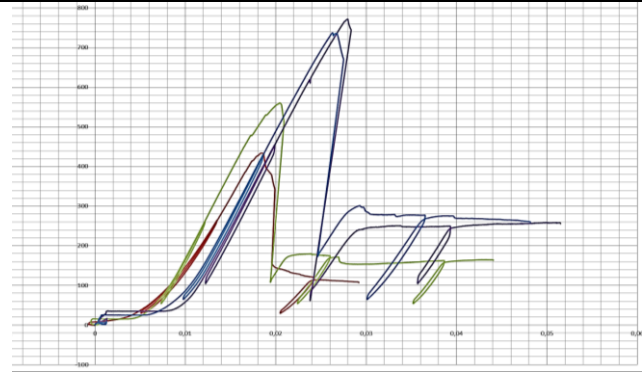


Fig.2. Summary diagram of the meteorite Tsarev deformation-strength characteristics under lateral compression 5, 15, 25 and 35 MPa

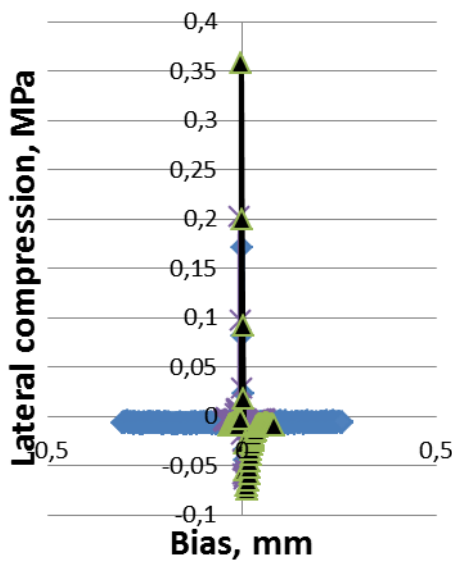


Fig.3. Explosive growth of lateral load on the sample at the limit of dynamic strength, the Tsarev meteorite, 5, 15, 25 and 35 MPa (summary diagram).

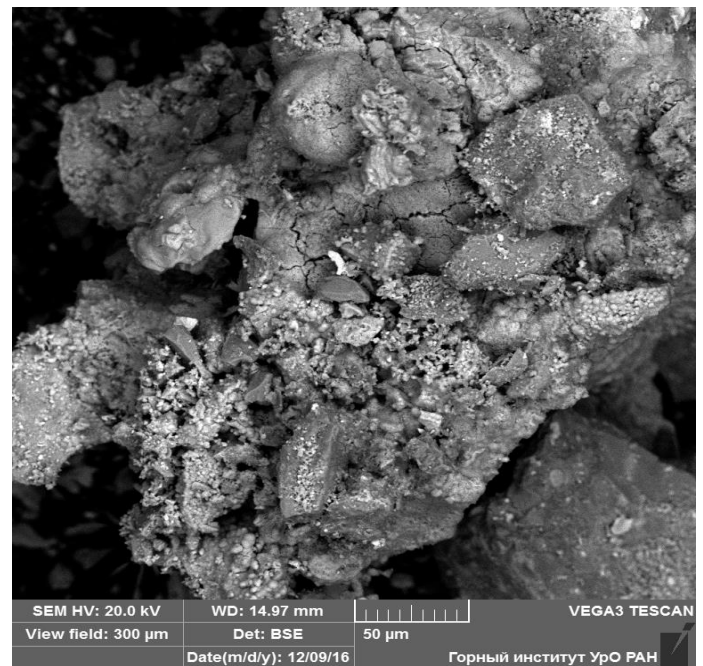


Fig.4. The structure of the particle from the debris of the Tsarev meteorite. Left on the lower edge vertically - aggregation of particles in the "domino" structure – an element of the main crack.

For the first time, explosive destruction of rock samples under high-pressure volumetric compression was indicated by P. Bridgman. His experiments on the rotary anvils allowed to draw attention to the need to take into account the effects of friction between the rotary plates and the sample, which provide a joint influence on the shear deformation nature of the latter (Bridgman, 1955). Frictional structures, which emphasize the role of shear deformations in the destruction of a meteoroid solid, were also found in the researches of the Chelyabinsk meteorite material composition (Galimov et al., 2013).

Research methodology involved the use of the testing machines for uniaxial and volumetric compression of the samples with semi-regular shape 20x20x20 - Sayh Al Uhamir 001 meteorite and parallelepipeds 25x25x50 mm in side load mode 5, 15, 25 and 35 MPa - meteorite Tsarev.

The deformation of the samples was carried out in three stages. To determine the static modulus of elasticity, E_{st} and Poisson's ratio, μ_{st} the samples were subjected to uniaxial compression without leading to destruction on a ZWICK Z250 press. Then, after the sealed packaging, they were placed in the high-pressure chamber of the MTS-815 press (Rock Mechanik Test Sistem) and tested in the axial compression mode under different lateral loads with recording of the full stress-strain characteristics, including the excessive deformation stage, fig. 1 and 2.

Interpretation of the loading diagrams was performed using the Coulomb-More and Drukker-Prager models, which underlie the presentation of data in the form of a generalized strength passport (Stefanov, 2014).

Analysis of the results of the tests in the form of a destroyed material was performed using optical

microscopy, atomic force microscopy (MEPI) and a scanning electron microscope VEGA 3 LMH with an X-ray energy dispersive microanalysis system (Oxygen Instruments INCA Energy 250 / X-max 20) (operator Korotchenkova O.V. (GI UB RAS)).

While testing samples for uniaxial and triaxial compression, main signs of deformation and destruction were set, such as dilatancy in proportional loading stage, elasticity, plasticity in the cataclastic current form, an abrupt lateral compression increase at the point of sample fracture in a dynamic form (rheological explosion), abnormal instability effects of deformation processes that reflect the transitions in the substance structural hierarchy, strain localization and super-brittle excessive state appearance in excessive state.

In general, the fragility of materials and rocks is considered as the ability of solids to collapse in the elastic deformation mode due to the growth of cracks and is estimated by different coefficients.

In the case of the Coulomb-More criterion usage, the brittleness is determined according to a strength passport which includes the results of determining the strength limits under tensile and compression, $K_{br} = \sigma_c / \sigma_t$. According to this coefficient, the L5 Tsarev chondrite, fragments No. 15384.1 and No. 15398.9, shows the highest brittleness, $K_{br} = 6.0$ and 6.1 respectively, relatively to the Sayh Al Uhamir $K_{br} = 5.82$ and Ghubara $K_{br} = 3.0$ chondrites.

In the case of testing the samples in the volumetric strain state with the lateral compression variation with the possibility to control the destruction under conditions of excessive deformation, the main attention is paid to the relations between the modulus of the excessive deformations, the M-modulus of the decay, and the Young's modulus of elasticity, E, so that $k = (E - M) / M$. (Tarasov, 2011).

And here it should be noted, that due to insufficient studies of meteorites' deformation properties in Russia, information about the decline modulus and the nature of the meteoritic matter behavior in the area of post-peak loads are known only for the Tsarev meteorite (Nikitin, Skripnik, et al. 2015).

The fragility coefficient of the Tsarev fragment No. 15383.5 varies in the range $k = 2.0 \dots 7.5$, under limit loads in the range from 174 MPa to 772 MPa, i.e. the material becomes less prone to plastic deformation. It can be noted that the chondrite brittleness changes non-linearly, under load of 5 MPa, an anomaly is observed, $k = 5.3$ against $k = 2.0, 3.9, 4.0$ and 7.5 for loads of 0, 15, 25 and 35 MPa, respectively. The latter is explained by the inhomogeneous character of the deformation. The effects of dilatancy, caused by the activation of the initial fracturing, the shear displacements along the elements of which (by microcracks) are accompanied by compaction of the material, are most clearly seen

in the region of comparatively small volume compression. A further change in brittleness with increasing lateral compression is accompanied by a change in the sign of the modulus of decay M, fig.2. Its value becomes comparable with the value of the elastic modulus E, at that the feature of this transition is the act of explosive destruction accompanied by impulse growth of lateral load, fig.3. The change in the brittleness of the material is the result of a "rheological explosion", which is responsible for the change in the mechanism of deformation and destruction of the material, which is realized when the sample reaches a certain limit, hereinafter referred to as the *dynamic strength limit*.

At this point of the deformation-loading characteristic, the material destruction mechanism changes and becomes characterized by an intense localization of deformations and an increase in main cracks leading to partial degradation of the material.

The material passes into a super-brittle state and microparticles aggregates are formed inside the fissure channels, the reorientation of which contributes to a local decrease in internal friction when the load increases, fig.4.

Thus, the destruction forms sequence has been established: - main cracks grow after microcracks germination around the stress concentrators, after defective microstructure stabilization, when the material passes into an equilibrium state, i.e. becomes quasihomogeneous.

It is shown fractographically that the fine fraction is concentrated in the main cracks development zones and is accompanied by the formation of the microcracks echelons of the highest chondrites structural organization level when transition to the super-brittle fracture mode occurs.

The main cracks are transform. And the stresses concentration at their tips is appeared by activation of transhierarchical forms of destruction that have deeper roots and include a mechanism of destruction of the self-sustaining type - grain boundaries and cracks can no longer be stoppers for main cracks, but serve as sources of internal energy expended on the growth of new surfaces.

According to the obtained mineralogical and petrographic data, when super-brittle dynamic fracture occurs, microcracks are opened and grown up to the highest energy level - when the level of deep accumulation of energy, which was accumulated while the cosmic solid was developed since the period of its formation - accretion, is revealed. The development of the main cracks occurs in the rheological explosion mode, when the external energy, adding up with the internal one, exceeds the limit of the material dynamic strength, leading to the realization of the kinematic forms of matter motion.

The sharply localized destruction occurs in the form of solid-phase mass transfer of the fracture products along the fissure channels.

The emerging macrocracks growth energy and increase in damage to their shores simultaneously has a mixed character, both thermomagnetic and athermal, with the removal of matter in the form of a gas-dust substance (plasma).

The obtained results broaden the understanding of the bolides destruction processes in the earth's atmosphere and contribute to the development of theoretical models of structural geomechanics which are aimed at solving the problems of space research.

References:

1. Бриджмен П. Исследование больших пластических деформаций и разрыва. М. 1955. 350 с.
2. Галимов Э.М. и др. Результаты вещественного анализа метеорита Челябинск. //Геохимия. М. 2013. №7. С.580-598.
3. Григорян С.С., Ибадов Ф.С.,Ибадов С.И. Челябинский суперболид: к физике взрыва. //Астрономический вестник, 2013, том 47, №4, с.292-298.
4. Маров М.Я., Шустов Б.М. Метеорит «Челябинск»: основные характеристики падения. // Вестник РФФИ №3(79) июль-сентябрь 2013г. С.11-14.
5. Никитин С.М., Скрипник А.Я и др. Деформация и разрушение образцов метеорита Царев при объемном сжатии. // Труды ВЕСМПГ-2015, М. 2015. С.311-315.
6. Тарасов Б.Г. Суперхрупкость горных пород при высоких всесторонних напряжениях. // Вестник инженерной школы ДВФУ. 2012. №1(10). Науки о Земле, с. 57-89.
7. Stefanov Yu.P. Dilatancy and compaction modes in shear zone. // International Conference on Physical Mesomechanics of Multilevel Systems 2014 AIP Conf. Proc. 2014.P/611-614.

Pechersky D.M.¹, Kazansky A.Yu.², Tselmovich V.A.³ Evidence of origin of terrestrial native iron particles in the lacustrine sediments, Zhombolok volcanic region, East Sayan.

1 O.Y. Schmidt Institute of Physics of the Earth RAS, Moscow,

2 M.V. Lomonosov Moscow State University, Department of Geology, Moscow,

3 Borok Geophysical Observatory Shmidt Institute of Physics of the Earth, RAS, Borok, Yaroslavl' Region (diamarmp@gmail.com)

Abstract. The article is dedicated to the only case of occurrence of terrestrial iron particles in the lake sediments from Zhombolok volcanic region, East Sayan Mountains (Russia). The particles of native iron, previously discovered in sediments of different ages from various regions are of extraterrestrial origin. The exclusivity of the results indicates a very limited distribution of native iron particles from its source - a volcanic eruption and / or fall of a large space body. The similarity of the composition, shape and size of native iron particles of terrestrial and

extraterrestrial origin testifies the uniform conditions during the planet formation.

Keywords: thermomagnetic analysis, microprobe analysis, terrestrial and extraterrestrial rocks, sediments, native iron, magnetite

The search for traces of the global spread of products from the fall and explosion of large space bodies in young sediments is a principle question in the study of global space disasters, which solution is possible primarily on the basis of the results of thermomagnetic research and microprobe analysis. Previously we have studied native iron particles in various sedimentary rocks of different ages and different origin from various regions of the world using thermomagnetic (TMA) and microprobe (MPA) analyzes [Pechersky and Sharonova 2012; Pechersky et al., 2011; Pechersky et al., 2013a; Pechersky et al., 2013b]. All sedimentary sections investigated using TMA and MPA contained particles of native iron with typical signs of extraterrestrial origin. And the only one object turned out to be abnormal: the particles of native iron of terrestrial origin were found in the young lacustrine sediments of Zhombolok volcanic region, East Sayan Mountains (Russia).

Zhombolok volcanic region is located in the eastern part of the East Sayan Mountains (south of Central Siberia) and is drained by the Zhombolok river (Fig. 1). The river bottom is completely overlapped by series of basaltic lava flows with a total thickness up to 150 m and a width up to 4 km comprising the lava field called Zhombolok flow. A number of cinder volcanic cones are located on the surface of upper lava flow (Kropotkin, Peretolchin and Stary volcanoes). Lava eruptions began in post-glacial time, at least 7000 years ago [Arzhannikov et al., 2013; Bezrukova et al., 2016], and probably have not ended yet. Volcanic eruptions were accompanied by the development of lava-dammed lakes. Lake sizes vary from 0.3 to 9 km². Three piston cores were taken from bottom sediments of three different lakes Hara-Nur (core length is 94 cm, age of the core base is 6881±53 yr), Tuhuren-Nur (core length is 98 cm, age of the core base is 13209±113yr) and Hikushka (core length is 87 cm age of the core base is 9333±79 yr) (Fig. 1) and we also have 5 samples from basaltic lava flows. Descriptions of sediment cores and absolute dates are given in accordance with [Shchetnikov et al., 2016]. The age of the lake sediments is determined by the radiocarbon method AMS 14C at 1-2 points of each core, Average sedimentation rate for each core was estimated using AMS data assuming its constancy along the core due to the uniform composition of sediments.

The histograms of Curie points (Tc) in sediments of all previously studied regions and ages (Fig. 3d) are closer to meteorites (Fig.3d) and differ markedly from Tc of terrestrial basalts and lunar basalts (Figures 3a, b) [Nagata et al., 1974] The histogram iron Tc from the lakes of Zhombonk region (Fig. 3c)

Abstracts

is completely different from the rest of the sediments and is similar to the terrestrial and lunar basalts (Fig. 3a, b). Exotic alloys contain FeCrNi (72-73% Fe, 16-18% Cr, 7-9% Ni), ZnFe (65% Zn, 31% Fe) grains, WFeCr grains, FeCoNd grains (54% Fe, 15% Co, 23% Nd), chromite grain ~ 2 μm, grain 7 μm of native zinc, nickel grains 1-3 μm, magnetite spherulas with a diameter of 4 ± 20 μm.

According to TMA data, iron concentration in basalts varies from zero to ~ 0.5x10⁻³%, that is noticeably less than in lake sediments (Fig. 2), while iron Curie points vary from 712 to 780°C. According to MPA, only sporadic small particles of native iron were found in basalt samples. As in sediments, chromium iron (10.7-17.7% Cr), FeCrNi, FeNiSn, and CuZn are found in basalts. A similar set of exotic metal particles in sediments and basalts, especially the great similarity of nickel particles, unusual both for basalts and for sediments, suggests that basalts are the source of such particles in the lake sediments

of the Zhombolok region. Such connection is also confirmed by the spatial regularity of iron distribution: the highest concentration of native iron is observed in the sediments of the Khara-Nur Lake, which is in direct contact with the Zhombolok basalt flow. Lake Hikushka is located ~ 800 m from the edge of the Zhombolok basalt flow and is much closer to volcanoes (~ 3 km), but the concentration of iron in its sediments is noticeably lower than in the sediments of Lake Khara-Nur. The lowest concentration of native iron is observed in the sediments of Lake Tuhuren-Nur, located behind the ridge ~ 3 km from the Zhombolok flow. However, despite the above, a very low concentration of iron in basalts, a predominance of titanomagnetite with Tc ≤ 120° C in basalt which is absent in sediments and vice versa - the presence of "pure" magnetite in sediments which is absent in basalts, indicates that the basalts of the region are not the only sources of metallic iron in the sediments.

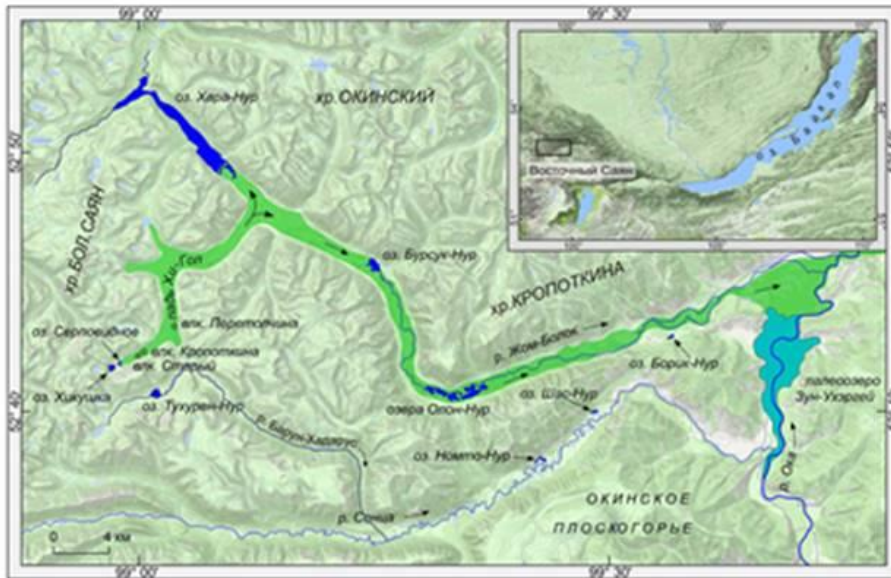


Fig.1. Geographic scheme of Zhombolok volcanic region [Shchetnikov et al., 2016] and studied lakes. Zhombolok lava flow is marked dark green/

TMA and MPA result shows that iron concentration in the sediments of the Zhombonok region (Fig. 2a) is an order of magnitude higher than in other sedimentary rocks (Fig. 2b), it is similar to the distribution of terrestrial magnetite (Fig. 2c) and differs sharply from the distribution of iron concentrations in previously studied sedimentary rocks of the Earth.

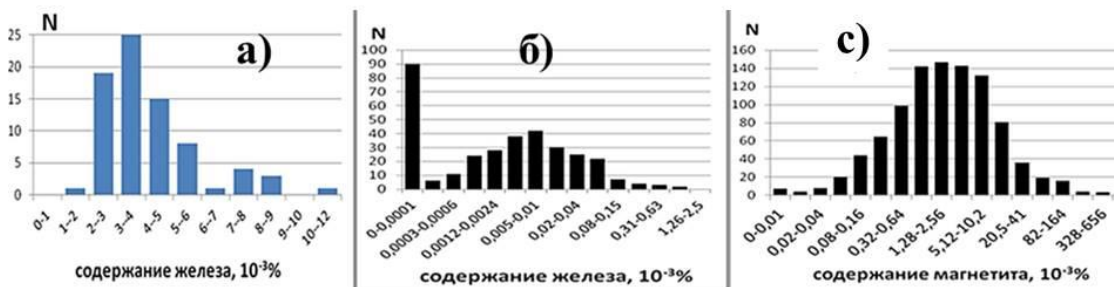


Fig. 2. Histograms of iron concentration (a, б) and magnetite concentration (в) in sediments of different regions of the world, Summarized TMA results from Zhombolok lakes (a) and all other previously studied sections (b,c).

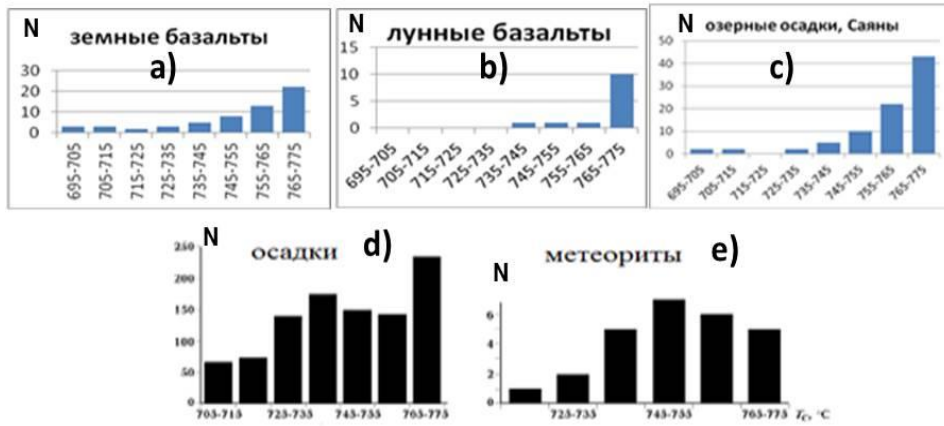


Fig. 3. Histograms of iron Tc in terrestrial (a) and lunar basalts (b), in lake sediments of Zhombolok region (c), in terrestrial sediments of different region of the world (d), in meteorites (e) [Pechersky et al., 2015; Nagata et al., 1974].

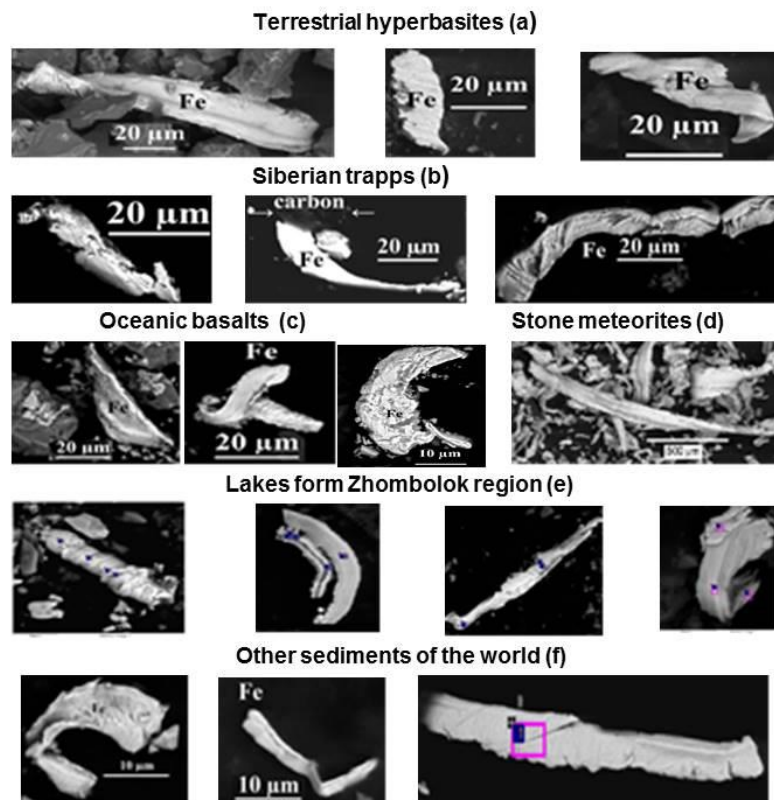


Fig. 4. Examples of terrestrial (a, b, c, e) and extraterrestrial (d, f) particles of native iron [Pechersky et al., 2013a; Pechersky et al., 2013b].

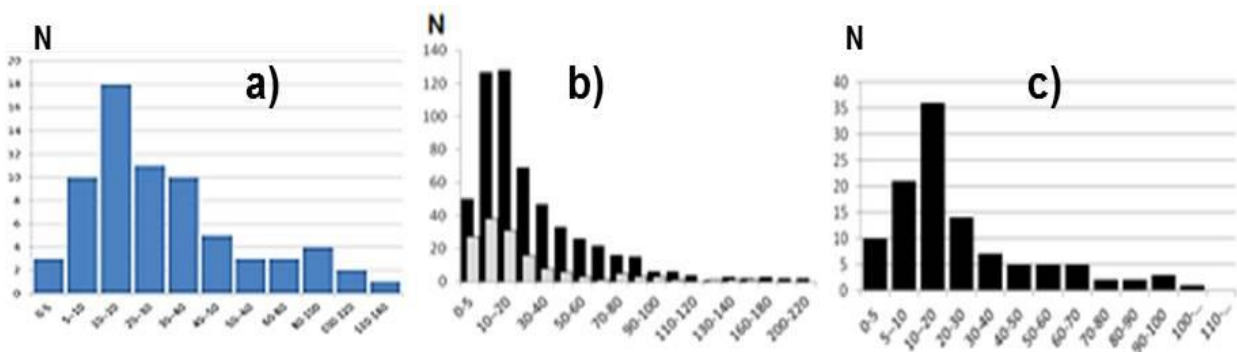


Fig. 5. Histograms of particle size of native iron in lake sediments from Zhombolok region (a), sediments from different regions of the world (b) and terrestrial basalts (c)

In terms of composition, shape (Fig. 4) and size (Fig. 5), the particles of iron of terrestrial and extraterrestrial origin are almost identical. The histograms in Fig. 5 repeat each other, especially in the same modes of particle size (10-20 μm). We explain this by the uniform conditions for the origin of iron particles during the formation of planets and other cosmic bodies, which are the source of native iron in interplanetary dust and in earth sediments. Accordingly, there are no specific genetic features of the difference between iron particles of terrestrial and extraterrestrial origin, there are only different in conditions for their formation. The terms "terrestrial or extraterrestrial" determine only the location of the source of iron particles. Obviously, particles of native iron during air transportation sharply deposit near the place of the eruption of the volcano: the concentration of magnetic particles decreases at a distance of 450 km by a factor of 10, at a distance of 880 km by a factor of 100 [Evans, 1999]. Such a conclusion should be attributed not only to volcanic sources of native iron but also to impact events. When such bodies fall and explode, the particles of native iron, as in the case of a volcanic eruption, will deposit on the Earth surface near the place of the fall of the cosmic body. In the case of weathering products of volcanic rocks, the halo of their separation will be even less than in the case of air separation. However, direct relationship between iron concentration and volcanic eruptions very frequent, and not single, volcanic eruptions during the accumulation of lake sediments, because iron particles are present in significant amounts in all samples of lake sediments.

Conclusions. The similarity of the compositions, shape and size of native iron particles of terrestrial and extraterrestrial origin is evidenced the unity of the conditions for the formation of iron particles in the formation of star-planetary systems formed from gas-dust clouds. The spread of metallic iron particles from the place of volcanic eruption and / or the fall of a large meteorite is limited in space. This follows from a striking example: from the many objects studied only in the Zhombolok region, in the immediate vicinity of large eruptions of basaltic lavas, a noticeable enrichment of sediments with particles of metallic iron of terrestrial origin was found. Consequently, it is unlikely to find global aureoles of the spread of metallic iron particles from the fall of large meteorites and other cosmic bodies, as well as from large eruptions of volcanoes. It follows that the global halos of spread of metallic iron particles from the impacts of large meteorites and other cosmic bodies, as well as from large volcanic eruptions are unlikely to detect. But we can successfully detect and track the local native iron anomalies from meteorite impacts and/or volcanic eruptions using thermomagnetic study of sediments and sedimentary rocks.

Acknowledgments. We are grateful to A.Shchetnikov and M.Kraynov for providing samples from lake sediments and basalts. We also thank G.Markov and A.Titov for the help in thermomagnetic measurements. The geological part of the research was supported by RFBR grant 15-05-01811 and RNF grant 16-17-10079, microprobe - RFBR 16-05-703a, thermomagnetic measurements - with the support of the RF Government grant No. 14.Z50.31.0017.

References:

1. Arzhannikov SG, Ivanov AV, Arzhannikova AV, Demonterova EI, Orlova LA et al. (2013) Stages of formation of Zhombolok lava fields (Eastern Sayan). Geodynamic Evolution of the Lithosphere of the Central Asian Mobile belt Irkutsk IZK SO RAN 11: 22-24 (in Russian).
2. Bezrukova EV, Shchetnikov AA, Kuzmin MI, Sharova OG, Kulagina NV et al. (2016) First Data on the Environment and Climate Change within the Zhombolok Volcanic Field (Eastern Sayan Mountains) in the Middle-Late Holocene. Doklady Earth Science 46: 527-531.
3. Evans ME (1999) Magnetoclimatology: a test of the wind-vigour model using 1980 Mount St Helens ash. Earth Planet Sci Lett 172: 255-259.
4. Nagata N, Sugiura N, Fisher RM, Schwerer FC, Fuller MD et al. (1974) Magnetic properties of Apollo 11-17 lunar materials with special reference to effects of meteorite impact. Proceedings of the Fifth Lunar conference
5. Pechersky DM and Sharonova ZV 2012 Thermomagnetic evidence for the presence of native iron particles in sediments. Izvestiya Physics of the Solid Earth 4: 38-44.
6. Pechersky DM, Gil'manova DM, Ivanov EV, Kuz'min MI, Markov GP et al. (2013b) Native iron in the sediments of Lake Baikal (borehole BDP-98): results of thermomagnetic analysis. Russian Geology and Geophysics 54: 1044-1054.
7. Pechersky DM, Gil'manova DM, Markov GP, Murdmaa IO, Nurgaliev DK et al. (2013a) Native Iron and Other Magnetic Minerals in the Sediments of the Northwestern Atlantic: Thermomagnetic and Microprobe Evidence. Izvestiya Physics of the Solid Earth 49: 426-447.
8. Pechersky DM, Nurgaliev DK, Fomin VA, Sharonova ZV, Gil'manova DM (2011) Extraterrestrial Iron in the Cretaceous-Danian Sediments. Izvestiya Physics of the Solid Earth, 47: 379-401.
9. Shchetnikov AA, Bezrukova EV, Filinov IA, Ivanov EV, Kerber EV (2016) Lake morpholithogenesis in the "Valley of the Volcanoes" (Zhombolok lava field, East Sayan). Geography and natural resources 3: 37-48 (in Russian).

Rusol A. V., Dorofeeva V. A. Model of heat distribution in subsurface layers of cometary nuclei: using the 67P/Churyumov-Gerasimenko comet as an example.

V.I. Vernadsky Institute of Geochemistry and Analytical Chemistry RAS, Moscow (fermata@inbox.ru)

Abstract. The goal of this paper is to construct a numerical model of propagation of heat in the subsurface layers of a cometary nucleus that allows the nonuniformity of temperature distribution to be investigated. This is very important, because in zones with a maximum surface temperature chemical and physical transformations of material are possible in subsurface layers. We use the previously proposed 3D model of the geometry and dynamics of a cometary nucleus that takes into account the diurnal rotation and orientation of the rotation axis relative to the Sun to simulate the irradiance to take value of temperature the surface of the nucleus. The paper presents a 1D thermal model of the porous ice-rock body. The results of numerical simulation of heat propagation in the subsurface layers of various regions of the 67P core, obtained for the first 14 days after the perihelion passage, are presented in this paper.

Keywords: propagation of heat, subsurface layers, 3D model of cometary nucleus shapes

Model description. The investigation of physical and chemical processes occurring in subsurface regions of cometary nuclei and surrounding gas-dust structures includes mathematical modeling of their thermal evolution. A necessary stage of this is to construct a model of the temperature distribution over the surface of the cometary nucleus considering its complex topological shape which leads to a significantly non-uniform irradiance of the nuclear surface. In the work (Marov et al., 1987) mathematical formulation and boundary conditions describing the heat energy balance on the surface of the nucleus were proposed

$$c(T)\rho \frac{\partial T}{\partial t} = \nabla(\lambda(T)\nabla T), \quad t \geq 0, r_0 \leq r \leq R_N$$

$$S_{\odot}(1 - A_v)R_H^{-2}e^{-\tau\xi} = (1 - A_{IR})\sigma_B T^4 + \Sigma(nv)_{\alpha}\Delta h_{\alpha}(T) - \lambda(T)\nabla T|_{r=R_N} \quad (1)$$

where S_{\odot} is the solar constant; σ_B is the Stefan–Boltzmann constant; $\Delta h_{\alpha}(T)$ is the sublimation heat of particles of type α at a temperature T ; A_v and A_{IR} are respectively the Bond albedo and the infrared albedo of the nuclear surface; τ is the effective optical depth of the coma; R_H is the heliocentric distance; ξ is the coefficient depending on the local

zenith angle; $(nv)_{\alpha}$ is the rate of the sublimation of particles of type α . The correspondence between the temperature of the nuclear parts and the solar radiation flux arriving at the surface, taking into account the orbital position, the orientation of the rotation axis and the time of day on the nucleus, we investigated in works (Rusol, Dorofeeva 2015; Rusol, Dorofeeva 2016).

As the reliable data necessary to consider all operating factors are not available we adopted in this paper a simplified formulation of the problem of heat distribution in the subsurface layers of the cometary nucleus; however, it doesn't break the generality and entirety of the results obtained. Firstly, since the nucleus of 67P/Churyumov-Gerasimenko comet (hereafter 67P) has no spherical symmetry a one-dimensional formulation of the equation in Cartesian coordinates was accepted

$$c\rho \frac{\partial T}{\partial t} = \lambda \frac{\partial^2 T}{\partial x^2}, \quad t \geq 0, \quad 0 \leq x \leq L \quad (2)$$

Secondly, a simpler statement of the boundary conditions was adopted

$$\frac{\partial T}{\partial x}\Big|_{x=0} = T_{surf} \quad \text{and} \quad \frac{\partial T}{\partial x}\Big|_{x=L} = 0 \quad (3)$$

where T_{surf} is the surface temperature determined in the work (Marov et al., 2017) from the simplified state of the energy balance on the surface $\sigma_B T^4 S_{el} = (1 - A)S_{el}W_R \cos \alpha$; W_R is the energy of solar radiation per unit area at the heliocentric distance R ; A is the optical albedo of the nucleus; S_{el} is the area of the surface element and α is the angle between the outward normal to the surface element and the direction toward the Sun.

The thermophysical characteristics of the material of the cometary nucleus are determined by the properties of the ice-rock porous body (Cheremskoy P.G. et al., 1990). For the numerical solution of problem (2) with boundary conditions (3), an implicit finite-difference scheme was realized.

Figure 1 shows the characteristic positions of the comet 67P nucleus during the diurnal rotation at perihelion; the duration of the day at 67P is 12.4 hours.

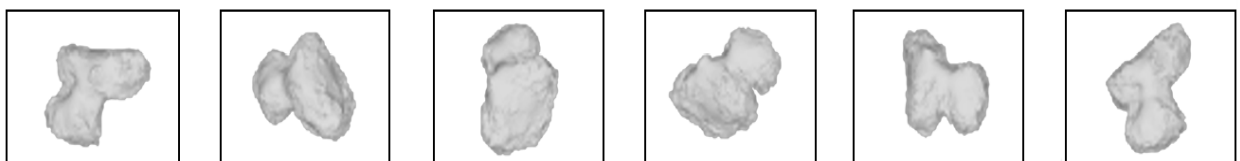


Fig. 1. The diurnal rotation of the comet 67P nucleus at perihelion

We chose several parts of the comet 67P nucleus, located in different regions (HATHOR, MA'AT, SETH) and in the region conventionally named SOBEK for numerical simulation. The choice of parts is dictated by the need to investigate the thermal evolution of the substance of the cometary nucleus under different light conditions. The parts

located in the regions of HATHOR, MA'AT and SETH are characterized by a change of day and night, with differing durations and peak daytime temperatures. The part located in the SOBEK region is constantly illuminated (Fig. 2). As a range of account time, a time period corresponding to 14 days of the cometary nucleus was adopted.

Temperature of surface in selected regions

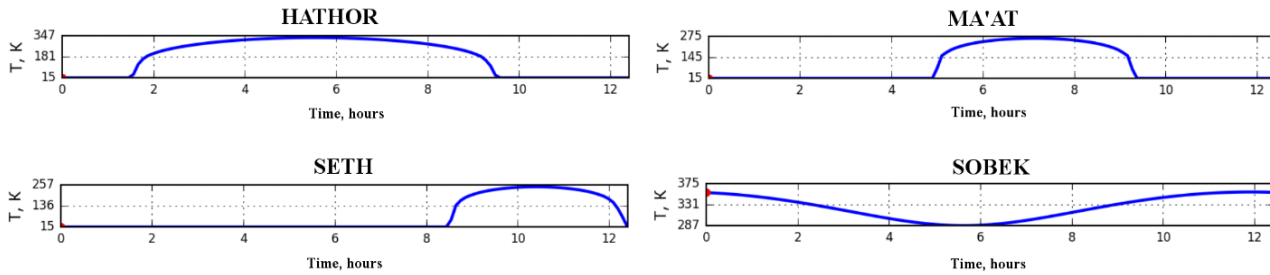


Fig. 2. Dependence of temperature of selected parts on time of day

Results of numerical simulation. For all the investigated parts of simulation an initial temperature distribution was taken as a uniform temperature level of 15 K. The thermophysical properties of the substance for all parts are assumed to be temperature independent and calculated as properties of the porous ice-rock body. Let us consider in more detail the results of a numerical simulation of the thermal evolution of matter in cometary nuclei.

HATHOR region. The comet day in the HATHOR region consists for the most part of a "day" with a maximum temperature of 347 K (as shown in Fig. 2). Numerical simulation demonstrates that because of the features of the thermophysical

properties of the porous ice-rock body at the first stage of simulation a zone of accumulating of thermal energy at a depth of ~ 0.5m is forming in the subsurface layer of the comet 67P nucleus. Further simulation showed that over 14 comet days, the heating front propagated deeper into the subsurface layers (Fig. 3). From the results of the modeling it can be seen that within 14 days of comet 67P the nucleus being at perihelion, the heating region of subsurface layers in the HATHOR region spread to values of ~ 1.5 m, and the maximum of internal temperatures ~ 160 K was at the level of ~ 0.15–0.2 m.

Temperature of sub-surface layers in HATHOR region

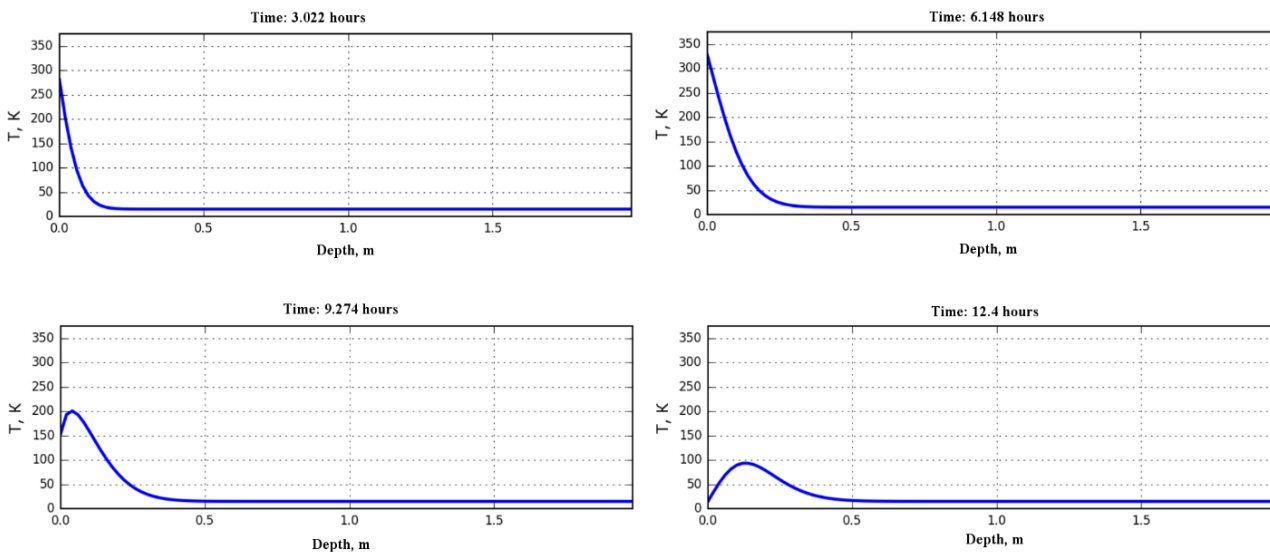


Fig. 3. The depth temperature distribution in the HATHOR region for the 14th model day

Temperature of sub-surface layers in SOBEK region

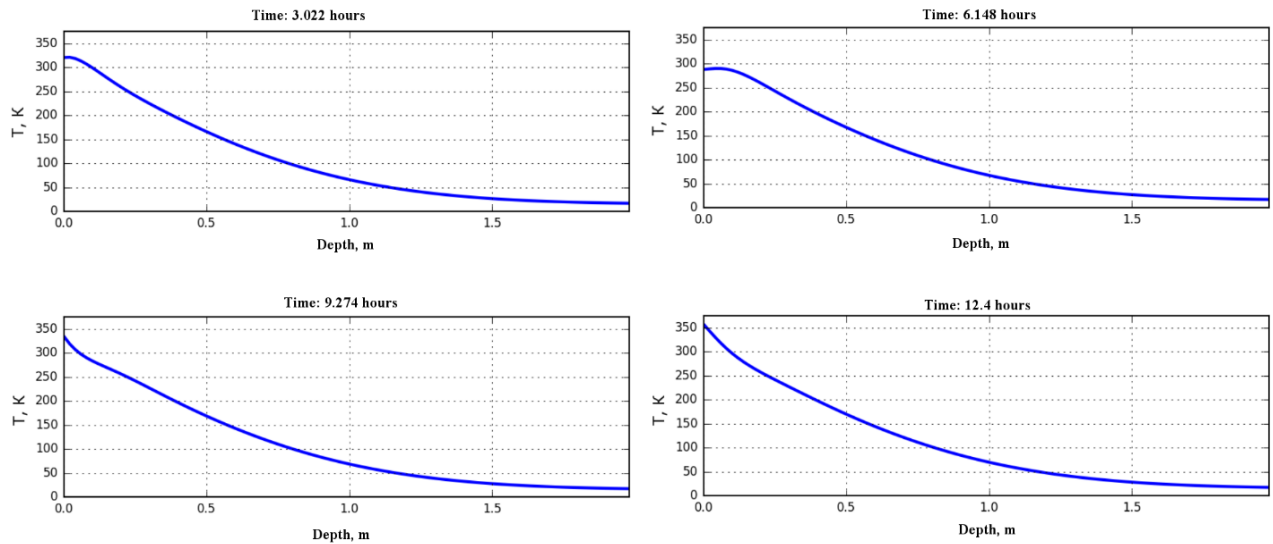


Fig. 4. The depth temperature distribution in the SOBEK region for the 14th model day

MA'AT region. Numerical simulation showed that in the MA'AT region, approximately one third of the comet day is a "day" with a maximum temperature of 275 K. The obtained results show that in the MA'AT region the same temperature distribution evolution occurs as in the HATHOR region. The area of heating of the subsurface layers in the MA'AT region on the 14th model day spread to ~ 1.25 m, and the maximum of the internal temperatures of ~ 90 K was at the level of ~ 0.12 - 0.13 m.

SETH region. Referring to Fig. 2, about one third of the comet day is occupied by a "day" with a maximum temperature of 257 K, what leads to results that are close to the MA'AT region's qualitative level. The area of heating of subsurface layers in the SETH region on the 14th model day spread to values of ~ 1.0 m, and the maximum of internal temperatures ~ 150 K was at the level of ~ 0.06-0.07 m.

SOBEK region. As illustrated in Fig. 2, the part from the SOBEK region is always on the illuminated side and the surface temperatures range from 287 to

357 K. Such illumination of the surface leads to a heating mode of the subsurface layers of the nucleus which differs significantly from the regions considered previously. Figure 4 shows the temperature distribution in the subsurface layers of the comet 67P nucleus on the 14th model day of stay at perihelion.

In the SOBEK region, the heating area of the subsurface layers on the 14th model day spread to values of ~ 1.75 m, and the maximum of internal temperatures of ~ 352 K was on the surface of the nucleus.

Conclusions. Numerical simulation demonstrated that as the thermal evolution of the comet 67P nucleus occurs, the thermal energy accumulates in the subsurface layers of matter. If we assume that the conditional critical temperatures are 25 K (T of sublimation of one of the ice fraction's main components – CO ice), 90 K (sublimation of CO₂ ice), and 140 K (sublimation of H₂O ice), then, according to the calculations, layers with significantly different temperature conditions can be distinguished in the subsurface regions (Table 1).

Table 1. Critical temperatures distribution.

Region	Temperature, °K	Depth, m	Region	Temperature, °K	Depth, m
HATHOR	25	1.3	SETH	25	1.0
	90	0.6		90	0.13
	140	0.3		140	0.1
MA'AT	25	0.9	SOBEK	25	1.5
	90	0.13		90	0.85
	140	not attain.		140	0.65

This type of accumulation of thermal energy provides the possibility of intensive production of the gas component of the coma in the part of the orbit after the passage of perihelion. We can also estimate the depth of possible sublimation of various ices in

regions where the outer layer will have significant defects (faults, cracks): to a depth of 0.1 to 0.65 m the layer will be almost completely degassed, to a depth of 0.13 to 0.85 m it will be substantially depleted of CO₂. The distribution of the most volatile

macro component of the cometary nucleus, CO, should change to the greatest degree. CO could be completely degassed from the layer to a depth of 0.9-1.5 m, but if the outer layer does not have the defects mentioned above, CO, subliming in relatively *deep* layers, can be redeposited in the outer layers as crystalline hydrate $\text{CO} \cdot 5.75\text{H}_2\text{O}$; its sublimation temperature is approximately 20 K higher than that of CO ice.

This work was partially supported by the Basic Research Program no. 7 of the Presidium of the Russian Academy of Sciences.

References:

1. Marov M.Ya., Kolesnichenko A.V., Skorov Yu.V. 1987. Thermal and Photometric Model of a Cometary Nucleus // *Astron. Vestn.* Vol. 21, No. 1, P. 47.
2. Marov M.Ya, Rusol A.V., Dorofeeva V.A. 2017. Three-dimensional model of the irradiance of cometary nuclei: Using the nucleus of comet 67P/Churyumov–Gerasimenko as an example // *Doklady Physics*, 62(5), pp. 273-277, DOI: 10.1134/S1028335817050019
3. Rusol A.V., Dorofeeva V.A. 2015. Modeling the Process of Thermal Evolution of Cometary Nuclei: Using the Nucleus of Comet 67/P Churyumov–Gerasimenko as an Example. In *All-Russian Annual Seminar on Experimental Mineralogy, Petrology and Geochemistry. VESEMPG–2015*, pp. 317–323.
4. Rusol A.V., Dorofeeva V.A. 2016. Thermal Model of a Cometary Surface: Using the Nucleus of Comet 67/P Churyumov–Gerasimenko as an Example. In *All-Russian Annual Seminar on Experimental Mineralogy, Petrology and Geochemistry. VESEMPG–2016*.
Cheremskoy P.G. et al. 1990. *Pores in Solid State*. – M.: Energoatomizdat

Tselmovich V.A.¹, Kurazhkovskii A.Yu¹, Blyakharchuk T.A.². Burst changes of the cosmogenic substance entrance in the "Tundra" Peatbog UDC 523.161

¹ Borok Geophysical Observatory Shmidt Institute of Physics of the Earth, RAS, Borok, Yaroslavl' Region, tselm@mail.ru, ksasha@borok.yar.ru,

² Institute of Monitoring of Climatic and Ecological Systems, Siberian Branch of the RAS, Tomsk, tarun5@rambler.ru

Abstract. Microprobe determinations of mineral composition, as well as remanent saturation magnetization - Irs and ash content - A of peat samples taken from a natural peat outcrop with a thickness of 270 cm (54.78649° N, 88.27233° E) were carried out. It was found that the tendencies of the change in the mass of the investigated samples (cubes with an edge of 2 cm) and ash content, basically coincide - their values increase from the upper horizons to the lower ones. The behavior of these parameters is mainly controlled by endogenous

factors: a change in the species composition of vegetation and compaction of peat during its accumulation. Measurements of the Irs did not reveal the apparent influence of endogenous factors on the behavior of this parameter. Microprobe studies have shown that periodic short-term Irs bursts are associated with sharp increases in the entrance of mineral (mainly cosmogenic) matter in peat deposits. The intervals between Irs bursts on the oligotrophic (last 1200 years) stage of swamp development, on the average, were about 100 years. The maximum burst of the cosmogeneous substance concentration (4-5 times higher than other bursts) was noted about 5000 years ago.

Keywords: Holocene, disasters, magnetism, microprobe, cosmic dust, peat

Introduction

The results of the study of collisions of the Earth with large space objects leaving many kilometers of craters are summarized in review articles and catalogs, for example [Goncharov and Orlov, 2003]. Based on these data, studies of the impact of impact events on a wide range of processes occurring on the Earth's surface can be carried out. The influence of such events on the biota turned out to be clearly significant (catastrophic), while the intervals between the falls of large meteorites are great and considerably exceed the time of the existence of our civilization.

Dusty cosmic matter enters the earth's surface continuously and, probably, also can influence the changes in biota and climate. The dynamics of the arrival of cosmic dust on the earth's surface, even in the Holocene, remains, practically, unexplored. At the same time, the first experience of research on a dust cosmogenic substance formed in connection with known events, for example, the Tunguska catastrophe [Lvov, 1967; Boyarkina, 1983; Vasiliev, 1986] already exists. This work is the next step in studying the regional dynamics of the arrival of a dust cosmogenic substance on the Earth's surface in the Holocene. Peat deposits, which fix dust particles of different origin, are chosen as the object of study.

Object of research and methodology

An attempt to determine the dynamics of the arrival of dust cosmogenic particles on the earth's surface was carried out on the basis of research on peat deposits. The peat monolith cross section of 10x10 cm was selected in the "Tundra" swamp (Kemerovo region, Mezhdurechensky district) at the coordinates: 54.78649° N, 88.27233° E. The thickness of the peat deposits at the point of extraction was 2.65 m. The top 2.5 m of the monolith was divided into 125 samples of 2 cm. According to radiocarbon dates, peat formation occurred during the last 6915 years. The peat accumulation conditions can be broken down into two stages: eutrophic (lower 1.4 m, 6915 - 1200 years) and oligotrophic (upper 1.1 m, 1200 years - modernity). In accordance with these

stages (approximately twice), the average peat accumulation rate in the oligotrophic stage has increased in comparison with the eutrophic stage.

The search for horizons enriched with mineral (terrigenous or cosmogenic) matter was carried out in two ways: by determining the dynamics of ash content - A and the parameter Irs - the remanent magnetization of saturation with respect to the power of the core. Then, using the TESCAN VEGA 2 microprobe, the composition and genesis of mineral particles in horizons with increased values of A and Irs was determined. It should be noted that carrying out quantitative determinations of the mineral and, especially, of the cosmogenic substance in the horizons of peat deposits, the problem is complex and finally not solved. Nevertheless, the values of the parameters (A and Irs) are certainly related to the amount of mineral matter contained in the peat samples. The combination of petrophysical and micromineralogical methods makes it possible to determine the horizons enriched, mainly, by cosmogenic substance, and also to make conclusions about changes in its quantity.

Results of the study

In Fig. 1a, b shows the results of the determinations of the parameters A and Irs in accordance with the depth and age of the investigated horizons of peat deposits. In the behavior of these parameters, one can distinguish between background (low) and burst (high) values. For example, Irs values less than 0.12 A / m were considered as background ones, and short-term increases of this parameter more than three times - as bursts. The results of the measurements showed that the behavior of the values of the parameters A and Irs in the mineralotrophic and oligotrophic stages of the development of the bog (Fig. 1a) differ somewhat. Thus, the background values of the parameter A decrease in accordance with the age of peat samples during the transition from the mineralotrophic stage to the oligotrophic

stage. Parameter Irs with the age of peat practically did not change. In addition, the bursts (high values) of A and Irs in a number of cases did not occur simultaneously. Probably, changes in ash content in the mineralotrophic stage of mire existence were strongly influenced by floods and biota.

In the course of the oligotrophic stage of peat accumulation (Fig. 1b), synchronism appears in the behavior of the parameters A and Irs. Thus, the outbursts of ash content and saturation magnetization begin to occur simultaneously. Investigations carried out with a microprobe showed that in cases where the A and Irs bursts coincided, an increase in the concentration of particles of cosmogenic genesis took place in peat samples. They were represented by magnetite balls with a detrital surface structure; (Figure 2a, b), taenite (Figure 2c), carbonaceous microspheres, native metals: Zn, W, Ni, Cu, intermetallides: FeCr, FeCrNi, WTiCo. Ilmenite (probably volcanic), melted at impact (Figure 2d) These bursts are likely to indicate episodes of regional impact on the landscape. Asynchronous bursts of A and Irs most likely reflect climatogenic phenomena (in the first case) and global impact background In the second case.

The main results of the paper are as follows. Studies of changes in parameters A and Irs make it possible to comprehend the dynamics of the arrival of a cosmogenic substance in peat deposits. The most significant surge in the amount of cosmogenic material occurred in about 5000 thousand years ago. Probably, this event had ecological consequences, since after it within the next 150 years the speed of peat accumulation significantly increased. A series of less significant bursts A and Irs (the arrival of cosmogenic particles) is noted in the interval 1000-600 years. In this series of bursts, a quasiperiodicity is observed with characteristic times of the order of 100 years.

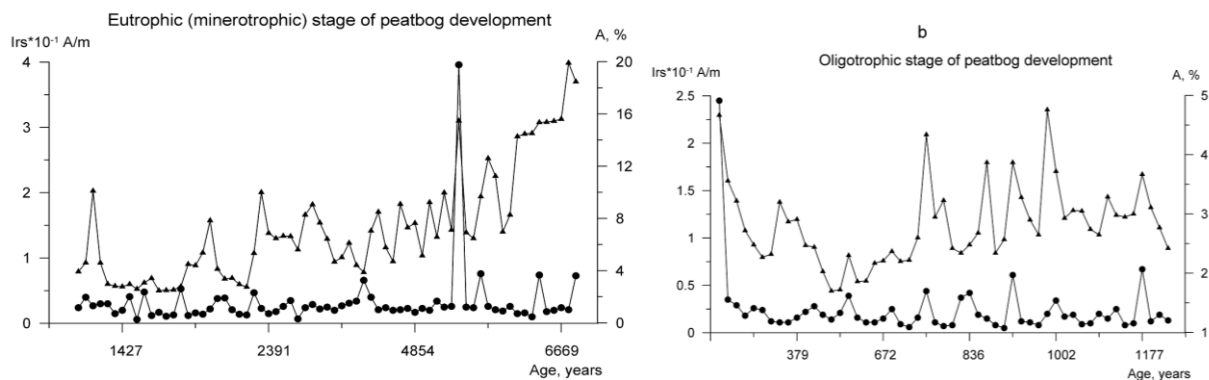


Fig. 1. Distribution of values of Irs (circles) and ash content of peat A (triangles) by age of peat deposits.

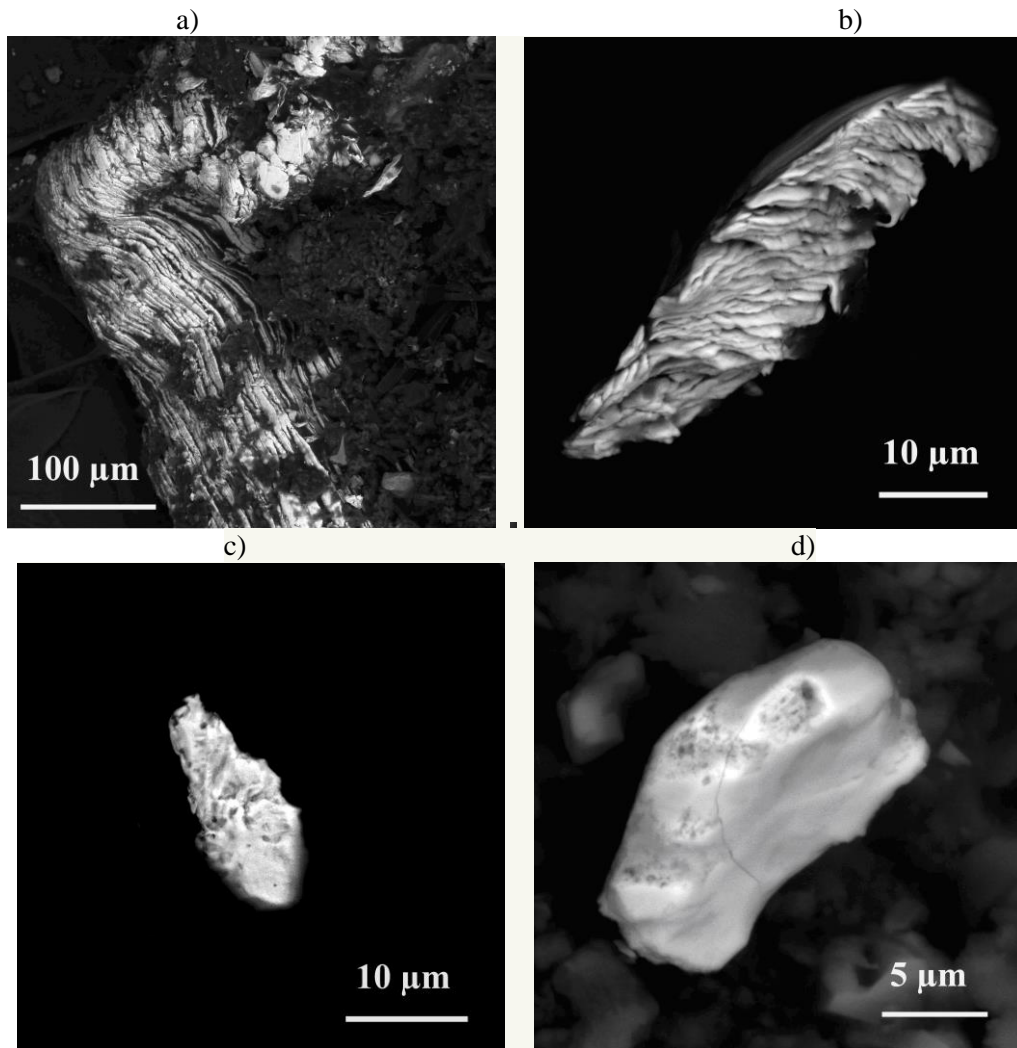


Fig.2. a, b - native scaly Fe; c is a piece of taenite; d - melted as a result of the impact of volcanic ilmenite.

The work was supported by the Russian Foundation for Basic Research, project No. 16-05-00703a

References:

1. Boyarkina A.P. Investigation of the ratio of cosmic and technogenic aerosol spheres in peat. *Sat. Meteorite and meteoric research*. Ed. "Science" Siberian Branch. Novosibirsk. 1983. P. 216-222.
5. Golenetsky, S.P., Stepanyuk V.V. To the search for the substance of the Tunguska cosmic body. In the book. *Interaction of a meteoritic substance with the Earth*. Ed. Yu.A. Dolgov. Novosibirsk: Nauka, 1980. P. 102-114.
6. Goncharov G.N., Orlov V.V. Global recurring events in the history of the Earth and the movement of the Sun in the galaxy // *Astronomical Journal*. 2003. T.80. №11. 1002-1012.
7. Lviv Yu.A. On the discovery of cosmic matter in peat. In: *Problems of the Tunguska meteorite*. Issue. 2. Publishing house Tomsk. University of Tomsk. 1967. P. 140-144.
8. Vasilyev N.V. History of the study of the problem of the Tunguska meteorite (1970-1980). In the book. *Space matter and Earth*. Ed. A.P. Boyarkina, N.V. Vasilyeva and G.M. Ivanovo. Novosibirsk: Nauka, 1986. P. 3-34.

Ustinova G.K., Alexeev V. A. Cosmogenic radionuclide production rates in chondrites with known orbits and their dependence on phase of the solar activity.

V.I. Vernadsky Institute of Geochemistry and Analytical Chemistry RAS, Moscow (ustinova@dubna.net.ru)

Abstract. The results of study of cosmogenic radionuclide production rates of ^{54}Mn , ^{22}Na and ^{26}Al in 7 chondrites of known orbits, which have fallen to Earth during different years of solar cycles in 1959-2013, are presented. Information is obtained on galactic cosmic ray (GCR) distribution and variations conditioned by temporal accumulation of a layer of the solar wind magnetic irregularities with GCR efficient modulation for the years of high solar activity on $\sim 2-4$ AU in the Solar system. Results demonstrate the highest sensitivity of cosmogenic radionuclide production rates to short time changes of the heliosphere structure, i.e. the high-resolution possibility of this method of study of magneto hydrodynamic processes in the Solar system and even a possibility of their forecast.

Key words: chondrites, cosmogenic radionuclides, cosmic rays, solar activity, heliospheric processes

Introduction: Under irradiation of chondrites by cosmic rays in space cosmogenic radionuclides of different half lives $T_{1/2}$, are produced, being thus natural detectors of cosmic rays along the chondrite orbits for $\sim 1.5 T_{1/2}$ of the radionuclides before the chondrite falls onto the Earth. Investigation of the radionuclides of different $T_{1/2}$ in the chondrites of different dates of fall, having orbits of different size and inclination provides us an unique set of homogenous data on cosmogenic radionuclides production rates and their variations in 3-dimension heliosphere. Direct proportionality of cosmogenic radionuclide production rates to GCR intensity allows us to obtain some indirect information on distribution and variation of GCRs ($E > 100$ MeV) in the Solar system over a long time scale (from some average values in the contemporary solar cycles up to the average status for the last ~ 1 Myr), which is not inaccessible to direct measurements in the interplanetary space (see description of the method in [Lavrukhina, Ustinova, 1990; Alexeev, Ustinova, 2006] and references there).

Cosmogenic radionuclides in the chondrites of known orbits: Especial value presents radionuclides in the chondrites of known orbits (which falls are photographed and velocity is fixed that allow to determine exactly all the elements of their orbits) [Meier, 2016]. The first such chondrites are Pribram and Lost City, fallen in 1959 and 1970, respectively. Their orbits in coordinates of dependence of heliocentric distance on time, during which the chondrite is on orbit before its fall onto the Earth are presented in Fig.1. Strokes on curves mark beginnings of accumulation of radionuclide contents ($\sim 1.5 T_{1/2}$), measured on the moment of the chondrite falls. There is seen that short-lived radionuclides ^{32}P и ^{37}Ar are produced practically by the GCR intensity near the Earth, whereas the radionuclides with longer $T_{1/2}$ are produced at the corresponding average heliocentric distances of their accumulation by the corresponding average GCR intensity in the heliosphere.

Table. Contents of ^{54}Mn , ^{22}Na and ^{26}Al measured in 7 chondrites of known orbits, which have fallen in 1957-2013. (see references in [Lavrukhina and Ustinova, 1990; Alexeev and Ustinova, 2006; Alexeev et al., 2015])

№	Chondrite	Type	Date of fall	Q, AU	^{54}Mn	^{22}Na	^{26}Al
					dpm/kg		
1	Pribram	H5	April 7, 1959	4.05	-	99±11	53±5
2	Lost City	H5	January 3, 1970	2.35	88±9	75±8	58±6
3	Innisfree	L5	February 5, 1977	2.76	92±9	97±10	64±6
4	Peekskill	H6	October 9, 1992	2.10	-	116±15	71±6
5	Moravka	H5	May 6, 2000	2.71	112±11	92±9	57±6
6	Košice	H5	February 28, 2010	4.5	162±16	95±10	60±2
7	Chelyabinsk	LL5	February 15, 2013	2.78	45±5	30±3	28±4

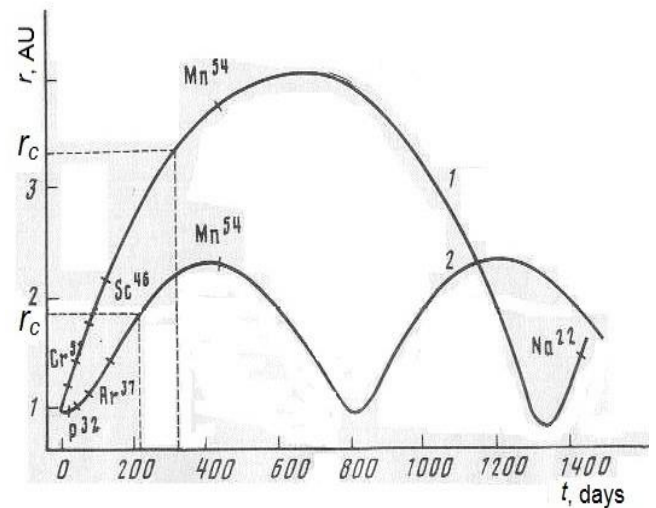


Fig. 1. Dependence of heliocentric distance r on time t before falling to Earth of the Pribram (1) and Lost City (2) chondrites. Starts of accumulation of cosmogenic radionuclide contents measured on time of the chondrite fall are marked by strokes; r_c – average heliocentric distances of the orbits.

For instance, ^{54}Mn is produced by the average GCR intensity over the last 450 days before the chondrite fall, and ^{22}Na is produced under the average GCR intensity during the last ~ 4 years, i.e., practically, under the average GCR intensity for the solar hemi-cycle, whereas ^{26}Al is produced by the average GCR intensity over the last ~ 1 Myr sat the average heliocentric distances r_c of the chondrite orbits (marked on the ordinate). Such set of average GCR intensities at different heliocentric distances according to the data of chondrites with different dates of fall in addition to the existence of corresponding homogenous stratospheric data on the GCR intensity at 1 AU [Stozhkov et al., 2009] allows us to estimate integral gradients of GCRs ($E > 100$ MeV) along the meteorite orbits (at 2-4 AU from the Sun) for about 5 solar cycles already [Alexeev, Ustinova, 2006]. By nowadays 7 chondrites of known orbits, in which the contents of cosmogenic radionuclides are measured at the moment of the chondrite falls, are studied (see Table).

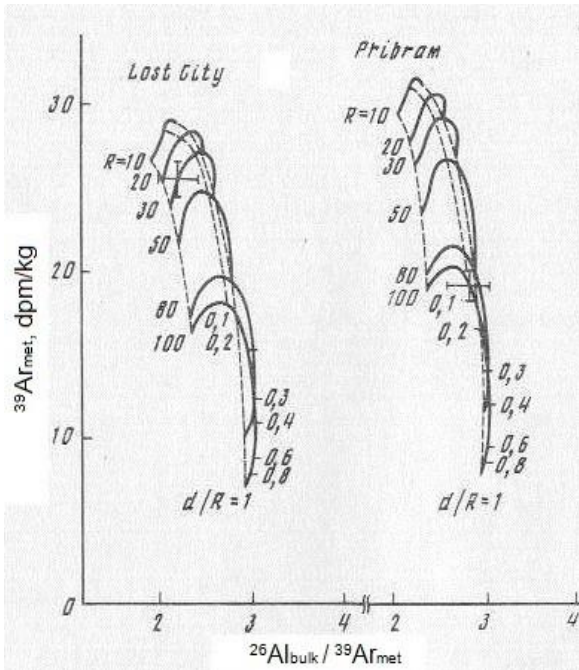


Fig.2. Nomograms for estimation of pre-atmospheric sizes of the Pribram and Lost City chondrites (experimental data are from [Lavrukhina et al., 1974; Forman et a., 1971])

Beside of the direct proportionality to the GCR intensity, cosmogenic radionuclide production rates depend also on many factors, in particular, on chemical composition of the chondrites, on their pre-atmospheric sizes, on shielding depth of the investigated specimens, on size of the orbits, if the GCR space variations exist in the heliosphere (and therefore, on average heliocentric distances, at which their contents, measured at the moment of the chondrite falls, are accumulated), on inclination of the orbits, if the GCR heliolatitude variations exist, and lastly, on dates of the chondrite falls due to the GCR modulation by the solar activity and its possible dependence on heliocentric distance.

All the questions are considered in detail in the book by Lavrukhina and Ustinova [1990], in which an analytical method of calculation of cosmogenic radionuclide production rates (of any $T_{1/2}$) at any depth of cosmic bodies of any size and composition

$$H_i(R,r) = \left[I_p(R,r) \sum_{j=1}^n \frac{N}{A_j} m_j \bar{\sigma}_{ij}^p + \sum_s I_s(R,r) \sum_{j=1}^n \frac{N}{A_j} m_j \bar{\sigma}_{ij}^s + \sum_t I_t(R,r) \sum_{j=1}^n \frac{N}{A_j} m_j \bar{\sigma}_{ij}^t + \dots \right], \quad (1)$$

where N is Avogadro number; $I_{p,s,t}(R,r)$ are integral fluxes of primary, secondary and tertiary particles; $\bar{\sigma}_{ij}^{p,s,t}$ are mean weighted production cross sections of i -radionuclide from j -target element of mass number A_j in accordance with spectra of primary, secondary and tertiary particles, and m_j is a content of j -target element in the chondrite. On such grounds cosmogenic radionuclide production rate $H_{\tilde{r}}$ at the heliocentric distance \tilde{r} is proportional to the integral

under their irradiation by cosmic rays of any spectrum and intensity is presented is presented. Determination of pre-atmospheric sizes of chondrites and shielding depths of investigated samples is of paramount importance. The analytical method has provided with knowledge of some regularities of depth distribution of cosmogenic radionuclide production rates inside cosmic bodies of different size and composition, which allow us to elaborate more than 10 independent approaches to estimation of pre-atmospheric sizes of chondrites [Ustinova et al., 1988]. As shown, the most efficient method of the pre-atmospheric size estimates is use of a combination of the data on ^{60}Co or $^{60}\text{Co}/^{26}\text{Al}$ depth distribution in chondrites with the data on depth track density profile of VH -ядер under the chondrite surface (see, for instance, such way of determination of pre-atmospheric sizes of the Kosice and Chelyabinsk chondrites [Alexeev et al., 2015]). If such data are absent, the data of some other radionuclides with strongly distinguished excitation functions might be used. For instance, in Fig.2 the nomograms for determination of the pre-atmospheric sizes of the Pribram chondrite ($R \sim 100$ cm) and Lost City chondrite ($R \sim 30$ cm) are presented, in which the $^{39}\text{Ar}_{\text{MET}}$ content in the metal phase of the chondrites and $^{26}\text{Al}_{\text{bulk}}/^{39}\text{Ar}_{\text{MET}}$ ratio is used.

Analytical method (cascade-evaporation model) of cosmogenic radionuclide production rate calculation in isotropically irradiated chondrites: When pre-atmospheric sizes of chondrites and shielding depths of the investigated samples are determined, the cosmogenic radionuclide production rates in the samples can be calculated, using the average GCR intensity ($E > 100$ MeV) at 1 AU, according to stratospheric balloon measurements, the long set of homogenous data of which exist from 1957 [Stozhkov et al., 2009].

Indeed, production rate of i -radionuclide in stony chondrites might be approximated by the following general form

GCR intensity $I_{\tilde{r}}(>E)$ at the heliocentric distance \tilde{r} , as well as its production rate near the Earth H_{\oplus} is proportional to the integral GCR intensity $I_{\oplus}(>E)$ at 1 AU, so that a gradient of cosmogenic radionuclide production rate between 1 AU and \tilde{r} might be presented as:

$$G_{\tilde{r}}^H = \frac{H_{\tilde{r}}/H_{\oplus} - 1}{\tilde{r} - 1} \cdot 100\%, \quad (2)$$

where $H_{\tilde{r}}$ is a content of the radionuclide measured on the moment of the chondrite fall, and H_{\oplus} is its content in the identical chondrite, which is calculated using GCR intensity at 1 AU for the same period of time. It is clearly seen that the gradient of the cosmogenic radionuclide production rate in (2) is

directly proportional to the gradient of the integral GCR intensity between 1 AU and \tilde{r} :

$$G_{\tilde{r}}(>E) = \frac{I_{\tilde{r}}(>E)/I_{\oplus}(>E) - 1}{\tilde{r} - 1} \cdot 100\% \quad (3)$$

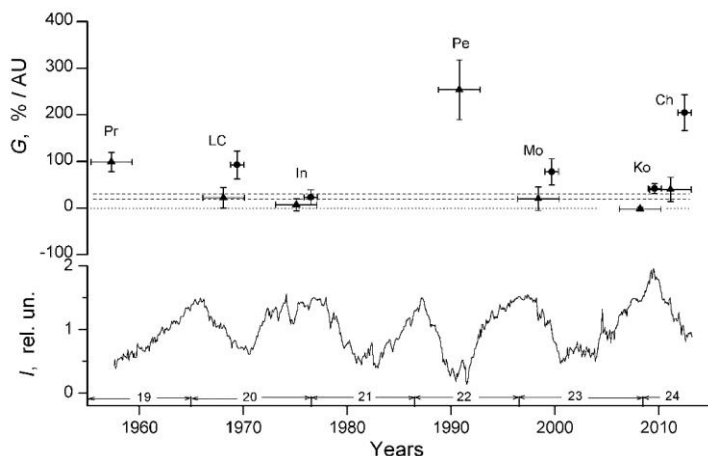


Fig.3. Variations of the gradients of ^{54}Mn (circles) и ^{22}Na (triangles) production rates along the orbits of 7 chondrites of known orbits in 1957–2013. Dashed horizontal lines mark average gradients of 20-30%/AU for ~ 1 Myr, according to the data of ^{26}Al production rates. Curve below describes variations of GCR intensity ($E>100$ MeV), according to stratospheric data [Stozhkov et al., 2009], just which is used in calculation of cosmogenic radionuclide production rates at 1 AU, using Eq.(1).

Discussion: Thus, the possibility to measure contents of cosmogenic radionuclides in the chondrites with known orbits and simultaneously to calculate their production rates, using the GCR intensity near the Earth allows us to reveal the spatial variations of cosmogenic radionuclide production rates, as well as of the GCR intensity, respectively, in the heliosphere for the different years of the solar activity, which is inaccessible for direct measurements at the different heliocentric distances in the interplanetary space. The results obtained are demonstrated in Fig. 3. It is clearly seen that ^{22}Na content in the Lost City chondrite, as well as ^{22}Na and ^{54}Mn contents in the Innisfree chondrite, as well as ^{22}Na content in the Moravka chondrite, as well as ^{22}Na and ^{54}Mn contents in the Kosice chondrite, and as well as ^{22}Na content in the Chelyabinsk chondrite, which were accumulated during the periods of minimum solar activity or near those minima, demonstrate small (0-20)%/AU gradients of their production rates, because GCR intensity along the orbits of the chondrites for those periods was as high as near the Earth (see the lower curve in Fig.3). It is in quite accordance with the direct measurements inside 4 AU for such the periods (McKibben et al., 1977; Venkatesan et al., 1987). On the other hand, ^{22}Na content in the Pribram chondrite, as well as ^{54}Mn content in the Lost City chondrite, as well as ^{22}Na content in the Peekskill chondrite, and as well as ^{54}Mn contents in the Moravka and Chelyabinsk chondrites, which were accumulated during the periods of maximum or near maximum of the solar activity, demonstrate much higher gradients, conditioned by strong decrease of the GCR intensity near the Earth, according to the stratospheric balloon measurements (Stozhkov et al., 2009), as well as to the neutron monitor data (Moraal and Stocker, 2010). Finally, average values of the gradients for the

contemporary solar cycles (~20–30%/AU, according to ^{22}Na) correspond to the average gradients over the last 1 Myrs (according to ^{26}Al , see Fig.3), which testifies to the constancy of the solar modulation mechanism over, at least ~ 1 Myrs.

Direct proportionality of cosmogenic radionuclide production rates to the GCR intensity testifies to existence of spatial GCR variations within the chondrite orbits (2-4 AU), which are conditioned by temporary accumulation in that range during the years of high solar activity a layer of magnetic irregularities of the solar wind modulated efficiently GCRs (Lavrukhina, Ustinova, 1990). At the stage of the solar activity decline influx of the magnetic irregularities into the transient layer suspends and that is gradually resolve, moving towards the external boundary of the heliosphere and forming some distinctive barriers of worse diffusive conditions for the GCR penetration into the Solar system, which was registered by the Voyager 1 and 2 missions (Venkatesan et al., 1987).

It should be noted, that cosmogenic radionuclide production rates in chondrites demonstrate extremely high sensitivity to the smallest alterations of the magneto hydrodynamic conditions in the heliosphere (Ustinova, 2016). It is especially clear revealed due to the extremely large gradient of the ^{54}Mn production rate in the Chelyabinsk chondrite. Indeed, during all the period of ^{54}Mn accumulation (12.2011 – 02.2013) both the polar regions of the heliosphere were positive [<http://wso.stanford.edu>], i.e., the heliosphere was closed for penetration of the positively charged GCRs (protons on the whole), so that their intensity near the Earth was much lower, than at $r_c=2.35$ AU, where, on the average, ^{54}Mn was accumulated in the Chelyabinsk chondrite, and just that led to the extremely high gradient of its production rate, conditioned by the high GCR

intensity gradient. Apparently, it occurs stochastically at the change of the magnetic cycles in the maximum of the even solar cycles. In particular, similar situation was observed in the maximum of the 22nd even solar cycle, according to the ^{22}Na data in the Peakskill chondrite (see. Fig.3). It demonstrates the highest sensitivity of the cosmogenic radionuclide production rates in the chondrites to dynamical variations of the heliosphere structure, and provides us a high-resolution method of study processes of the GCR modulation at any stage of the solar activity at any heliocentric distances within the chondrite orbits.

This work is partly supported by the Program 7 of the fundamental researches of Presidium of the Russian Academy of Sciences

References:

1. Alexeev V. A., Ustinova G. K. // *Geochem. Intern.* 2006. V.44. No. 5. P. 423-438.
2. Alexeev V. A., [Laubenstein](#) M., Povinec P. P., Ustinova G. K. // *Adv.Space Res.* 2015. V. 56/4. P. 766-771.
3. Forman M. A., Stoenner R.W., Davis R. // *J.Geophys.Res.* 1971. V. 76. N 17. P. 4109-4120.
4. McKibben R.B., O'Gallagher J.J., Pyle K.R., Simpson J.A. // *Proc. XV Intern.Cosm. Ray Conf. Plovdiv*, 1977. V.3. P. 240-245.
5. Meier M.M.M. Meteorites with photographic orbits (<http://www.meteoriteorbits.info>)
6. Moraal H., Stocker P.H. // *J. Geophys. Res.* 2010. V. 115: A12109. doi 10.1029/2010JA015413.
7. Lavrukhina A. K., Ustinova G. K. Meteorites as probes of cosmic ray variations. Nauka, Moscow. 1990. 262 p.
8. Lavrukhina A.K., Fisenko A.V., Kolesnikov E.M. // *Bull. Astron. Inst. Czech.* 1974. V.25. P.122-126.
9. Stozhkov, Yu.I., Svirzhevsky, N.S., Bazilevskaya, G.A., et al. // *Adv. Space Res.* 2009. V. 44. No. 10. P. 1124-1137.
10. Ustinova G.K. // *Doklady Physics*, 2016. V. 61. No. 11. P. 571-575.
11. Ustinova G.K., Alexeev V.A., Lavrukhina A.K. // *Geochem. Intern.* 1989. V.26. No. 5. P. 1379-1395.
12. Venkatesan D., Decker R.B., Krimigis S.M. // *Proc. XX Intern. Cosm. Ray Conf.* 1987. Moscow. V. 3. P. 385-388.

Voropaev S.A.¹, Korochantsev A.V.¹, Dushenko N.V.¹, Kocherov A.V.², Kuzina D. M.³, Nugmanov I.I.³ Experimental study of destruction of the Chelyabinsk meteorite components under compression.

¹V.I. Vernadsky Institute of Geochemistry and Analytical Chemistry RAS, Moscow;

²Chelyabinsk State University, Chelyabinsk; ³Kazan Federal University, Kazan, RF (Voropaev@geokhi.ru)

Abstract. Stone meteorites usually are impact breccias of the surface layers of the parent bodies and their properties provide important information about the composition and evolution of asteroids and small bodies of the Solar system. In ordinary

chondrites there are two main petrological components, which differed in genesis. This is the original chondrite material (A) composed of crystal grains-chondrules, and impact melt solidified with partial recrystallization (B). To identify the different failure mechanisms, we experimentally investigated the strength properties of the main components of the Chelyabinsk meteorite, type LL4, S3, W0. The elastic mechanical values under determination were the Poisson's ratio, Young's modulus and ultimate strength in tension and compression. Features of fracture under triaxial load, shows a significant difference in the development of cracks for component A and B.

Keywords: Meteorites, chondrites, impact, asteroids, fracture, elastic properties

Stone meteorites usually are impact breccias of the parent body's surface and their properties provide important information about the composition and evolution of asteroids and small bodies of the Solar system [Yomogida et al., 1983]. In ordinary chondrites there are two main petrological components, which differed in terms of genesis. This is the original chondrite material (A) composed of crystal grains-chondrules, and impact melt solidified with partial recrystallization (B). Their physico-mechanical characteristics are very different, which leads to significant variations in studies of properties of chondrite meteorites [Medvedev and others, 1985]. To identify the origin of different failure mechanisms, we experimentally investigated the strength properties of the main components of the Chelyabinsk meteorite, type LL4, S3, W0 [Galimov, 2013]. The obtained values of elastic mechanical quantities is the Poisson's ratio, Young's modulus and ultimate strength in tension and compression. Focuses on the features of fracture under triaxial load, shows a significant difference in the development of cracks for component A and B.

To adequately estimate the variations of physico-mechanical properties of the Chelyabinsk meteorite we studied samples consisting of different proportions of the two main component of the Chelyabinsk meteorite - chondrite predominantly light material (component A) and dark impact melt (component B). The tests were performed at the Institute of geology and petroleum technologies of Kazan Federal University. Part of the test was made on the installation of uniaxial compression GT 0.5.1 construction of GEOTEK (Penza) with a measurement accuracy of displacement sensors 0.00001 mm, and a force sensor to 0.0001 MPa. Characteristics determined were the modulus of deformation, the coefficient of lateral deformation (Poisson) and the tensile strength in uniaxial compression. Determination of deformation and strength properties of the meteorite samples under uniaxial and axisymmetric triaxial compression were performed on the test installation of rocks in terms of

Problems of Planetology, Cosmochemistry and Meteoritica

lithostatic pressure - GTYAN.441179.050 (GEOTEK). The installation ensures functional compliance with all technical requirements and conditions of standards, namely GOST 21153 mechanical test: measuring stress and deformation, consolidation ratios, and the limits of strength under conditions of axisymmetric triaxial loading. Preparation of cylindrical samples with an average diameter of 25 mm and height 50 mm was carried out

using the abrasive cutting tool of the original fragment of the meteorite with instrumental control of the parallelism of ends and perpendicularity of the side surface.

Series of three tests (see table. 1) were performed: uniaxial tension, uniaxial compression with free lateral surface and triaxial compression of samples with different lateral pressure (5 MPa and 10 MPa).

Table 1. Elastic and strength properties of the meteorite' Chelyabinsk components

Sample, type/N	Density (g/sm ³)	The modulus of deformation / elasticity Md / Me (MPa)	Poisson ratio, v	Angle of main cracks (α °)	The ultimate strength of the 1-axis compression (lateral pressure) / tensile (MPa)
A-0	3.21	-	-	81° (90°)	- 3.4 ÷ -3.8 / -
A-1	3.215	- / 8621	0.2	-	45.2 / -
A-2	3.245	- / 17940	0.17	0°	141.99 / 10
B-0	3.31	-	-	90° (излом)	- 1.68 ÷ -4.84 / -
B-1	3.297	7132 / 8776	-	11°	73.66 / -
B-2	3.315	15214 / 16839	0.21	32°	124.02 / 5

Figure 1 shows a typical graph of the cyclic load 0-10 MPa, which is built for samples of type B in the cell of triaxial compression.

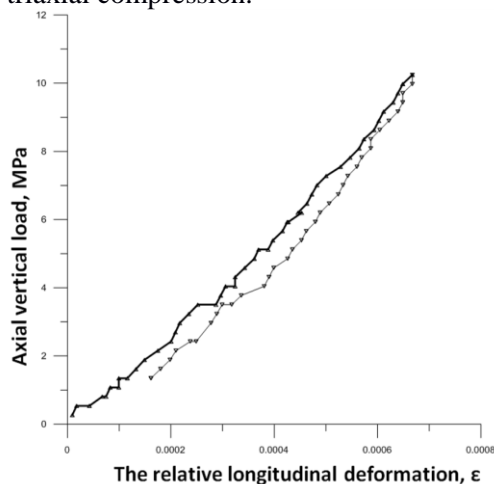


Fig.1. "Stress-Strain curves", type B

This stage is preceded by a standard triaxial test to estimate the degree of fracture. The deviation of the lines of loading and unloading for compressed samples is due to the incomplete closure of cracks of various size and partly plastic behavior of the material. For samples of type A such an effect also exists, but is much less pronounced. Apparently, this is due to the relatively fine grained chondrite matter and, as a consequence, a much larger number of microscopic defects such as pores. Linear sections of the graphs, the relative longitudinal and lateral deformation were successfully determined modulus of elasticity (Young, E) and the ratio of transverse strain (Poisson ratio, v), the values of which are given in table 1.

A widely used criterion to estimate the strength of rocks (certificate of strength) is based on the Mohr' hypothesis about the dependence of the limiting shear stress and average normal stress as the

hypothesis that the named dependency is caused by internal friction in solids [Nicolas, 1992]. The equation of Coulomb-Mohr is a representation of the dependence of the limiting shear stresses (τ) from the intensity of the applied normal stress (σ) in linear form

$$\tau = \text{tg}(\varphi) * \sigma + \tau_0, \quad (1)$$

where τ_0 is the cohesion shear in the absence of lateral pressure, φ is the angle of internal friction for the rigid body. For the mechanical strength tests of various samples of the Chelyabinsk meteorite was built passport strength of the composing components. In the linear approximation, the graphical visualization may be presented in the form of a straight line - tangent to graph Mohr-Coulomb based on experimental values of the ultimate loads only uniaxial tension and compression. At the same time, such characteristic values as the angle of internal friction, φ and cohesion of the crack, σ_0 , determined by the experimental ultimate strength of the rock in compression (σ_c) and tensile (σ_p) using expressions

$$\text{tg}(\varphi) = (\sigma_c - \sigma_p) / 2 \sqrt{(\sigma_c * \sigma_p)}, \quad (2)$$

$$\sigma_0 = (\sigma_c * \sigma_p) / (\sigma_c - \sigma_p), \quad \tau_0 = \text{tg}(\varphi) * \sigma_0 \quad (3)$$

In the real approximation given the data, to represent the strength of the chondrite substances it is necessary to involve a more complex nonlinear expression [Voropaev, 2017].

For some types of chondrites, presumably also significant are the effects of the anisotropy of the strength properties, detected for the meteorite Tsarev [slyuta, 2017]. Measuring the strength of samples of two major components of the Chelyabinsk meteorite showed a significant difference in the development

of cracks (see Fig.2). If the type And the characteristic longitudinal crack stretching, for type B – crack cut to different angles depending on the ratio of the longitudinal and lateral loads. The dependence of the formation and development of cracks on the mineralogical and petrological composition is the subject of further study.

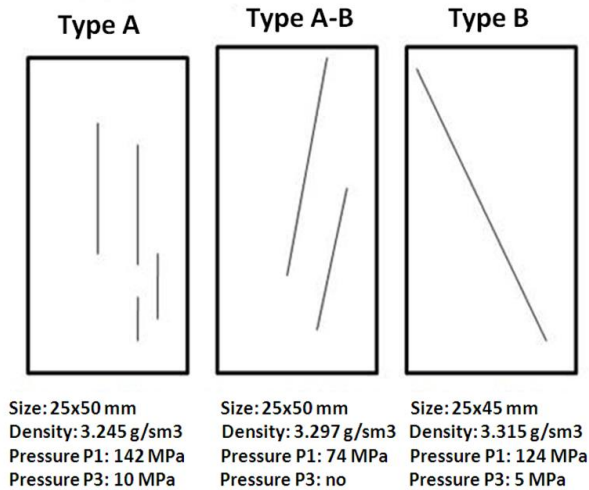


Fig. 2. The mechanisms of cracking, by types

It is important that the proportion of the components in the sample of the meteorite, as well as the morphology and number of defects that can be obtained by non-destructive method of x-ray microtomography. The equipment used allows, in parallel with the experiments on triaxial compression, measurement of the speed of acoustic waves. Of course, there remains the question of extrapolation of the strength characteristics of samples of small size of the meteoroid (asteroid) in general, the so-called scale factor. Due to limitations on the article size, this important issue has not received sufficient space. However, the obtained expressions are useful for evaluating the failure mechanisms of asteroid bodies S-types and their fragments, as studied in detail the strength of the main component composing the LL chondrite. The data of the tests important for the correct assessment of parameters of natural processes in which there are inhomogeneous spatial stress in asteroids and meteoroid (shock metamorphism, fragmentation of the meteoroid in the atmosphere) and man-made impacts on small bodies (e.g., the destruction of the asteroid directed blast).

Of particular importance are data on the strength characteristics of ordinary and, especially, carbonaceous, chondrites for problems planetesimal growth and development of the internal structure of the growing planets in the early Solar system. The formation of the crust of the moon, Earth and other Terrestrial planets inevitably accompanied by mechanical destruction of primary substances

chondrite global processes during deformation under gravity. The resulting geological formations, tectonics, the formation of a primary atmosphere was controlled many strengths and the development of the main cracks in large blocks of growing bark. Therefore, the application of this approach to mechanical tests of meteorites of other types of major practical importance, and should be the subject of further research.

The study was supported by the program 22 of Presidium of RAS (project No. 137-215-0105).

References:

- Galimov E.M. Chelyabinsk meteorite – an LL5 chondrite // *Solar System Research*, 2013, 47(4), 255-259.
- Marov M.Y., Shustov B.M. Chelyabinsk event as astronomical phenomenon // *Geochemistry International*, 2013, 51(7), 587-589.
- Medvedev R. V. et al., Determination of physical properties of stone meteorites with application to the processes of their destruction // *Meteoritika*, 1985, 44, 105-110 (in Russian).
- Nicolas A. Principles of rock deformations // D. Reidel Publ. Company, 1990, pp.186.
- Slyuta E.N. Physico-mechanical properties of stone meteorites // *Solar System Research*, 2017, 51(1), 1-23 (in Russian).
- Voropaev S.A., Kocherov A.V., Lorenz C.A., Korochantsev A.V., Dushenko N.V., Kuzina D. M., Nugmanov I.I., Jingao Y. Constructing passport strength of extraterrestrial matter on the example of the Chelyabinsk meteorite // *Doklady Astronomy*, 2017 (in print).
- Yomogida K., Matsui T. Physical properties of ordinary chondrites and their implications. *Journal of Geophysical Research*, 1983, 88(10), 9513-9533.

Shpekin M.I.¹, Barenbaum A.A.² On mechanism and time-formation of Lunar mascons

¹Kazan Federal University, Kazan (michaels1@yandex.ru), ²Oil and Gas Research Institute RAS, Moscow (azary@mail.ru)

Abstract. Questions of the origin and age of the mascons are discussed based on data of the GRAIL and LRO missions. The analysis of the actual data is carried out from the positions of the Galactocentric paradigm, connecting the formation of mascons, large craters and mares with the cyclical bombardment of the Moon by galactic comets. A preliminary conclusion is reached by the fact that most of the mascons on the Moon have a Cenozoic age.

Keywords: mascons, craters, mares, galactic comets, Galactocentric paradigm, formation mechanism, time-formation

Introduction. Large formations in the lunar crust, creating positive gravitational anomalies call the mascons. Most often, the mascons are located under the extensive lunar seas, the origin of which is associated with the fall of large space bodies creating giant basins flooded with basalts, under which the substance of increased density is located.

An international group of researchers [Melosh et al., 2013] on the bases of a detailed study of the Moon by the GRAIL and LRO missions, concluded that the mascons arose as a result of the rise to the surface of a heavier substance of the lunar mantle, due to the fall of cosmic bodies 4-3 billion years ago. It turned out, however, that the mascons can not be explained by the falls of bodies with a diameter distribution similar to that of the bodies of the modern asteroids belt [Neumann et al., 2015].

In this paper, the hypothesis [Barenbaum, Shpekin, 2017] is discussed, according to which the lunar mascons do not arise from the fall of asteroids and comets of the solar system, but from the imposition of impact effects [Barenbaum, 2016; Barenbaum, 2015; Barenbaum, Shpekin, 2016] in the massive bombardment of the Moon by high-speed galactic comets. These bombardments have a duration of ~ 1-5 million years and are repeated each 20-37 Ma. For one bombardment, ~ 10^3 - 10^6 comets can fall to the Moon. Moreover, each 150 million years, comets predominantly and alternately bombard the southern or northern lunar hemisphere. The last bombardment occurred between 5 and 1 million years ago. The density of falls was ~ 3-5 comets per area of $100 \times 100 \text{ km}^2$, and the falls themselves mainly occurred in the southern hemisphere of the Moon [Barenbaum, 2010].

To argument the hypothesis we used a new approach to the interpretation of crater data.

New approach to the interpretation of crater data. It is established [Barenbaum, 2010] that all craters on the Moon with diameter $D \geq 10 \text{ km}$ are created by the fall of two different types of cosmic bodies: 1) asteroids and comets of the solar system and 2) galactic comets. The former have an inverse quadratic distribution in size, and the latter are exponential. The impact structures formed by their fall are distributed in size according to the same laws.

This circumstance makes it easy to distinguish the structures created by the incidence of bodies of different types, analyzing their size distributions in graphs or in a double logarithmic coordinate system in the form of an R-function [Melosh, 1990], or in a semilogarithmic coordinate system in the form of a cumulative number of structures $N(D)$ with a diameter $> D$. As a result, the structures created by asteroids on the R-graph will give a straight line parallel to the abscissa, and the galactic comets in semilogarithmic coordinates $N(D)$ -distribution in the form of an oblique line.

The origin of lunar mascons. When discussing this issue, we use the data in Fig. 1-4. In Fig. 1 shows the R-distribution functions for the diameters of large craters (and seas) with $D \geq 10 \text{ km}$ on elevated (continents) and low (sea) sections of the surface of the Moon, Mars and Mercury [Voronov et al., 1986]. And in Fig. 2 shows $N(D)$ -distributions of continental craters on the Moon and planets in a semi-logarithmic coordinate system [Barenbaum, 2010].

Almost all continental craters with $D = 10$ - 160 km , judging by their $N(D)$ -distributions (Fig. 2), are created by the fall of the galactic comets. The lower limit of this range is explained by $\approx 100\%$ saturation of the continents with craters with $D \geq 10 \text{ km}$, which "erase" all smaller craters. And the upper limit of the range is that larger-diameter structures on the Moon are interpreted not as craters, but as "sea basins". The limiting saturation of such craters on the surface of the Moon, Mercury and Mars is almost the same and amounts to ≈ 100 per 1 million km^2 [Barenbaum, 2010]. On the Moon and Mercury, which are atmosphere-free, the $N(D)$ dependences are identical. On Mars, the largest craters are smaller due to the ablation of the nuclei of galactic comets in its atmosphere.

The relationship between the magnitude of the central gravitational Bouguer anomaly and the diameter of lunar craters is shown in Fig. 3 [Soderblom et al., 2015]. The authors state that this dependence is constructed for craters on the continents of the Moon. However, since $D \approx 160 \text{ km}$, these are not craters, but lava seas. So, a positive gravitational anomaly is observed only over sea basins of diameter $D \geq 213 \text{ km}$. With an increase in the size of the basin, the Bouguer anomaly size is also increasing.

A positive gravitational anomaly above the seas indicates the presence under the bottom of the basin of large masses of a heavier substance than the material of the lunar crust. This material, according to the authors [Melosh et al., 2013, Neumann et al., 2015, Soderblom et al., 2015], is a mantle of the Moon that rose to the surface due to the impact of the cosmic body.

We resulted the $N(D)$ -distributions of the seas on both sides of the Moon from paper [Neumann et al., 2015], approximating them by the exponentials (dotted lines) in Fig. 4 in a semilogarithmic coordinate system. The solid line shows the average dependence. The authors found that on the visible side of the Moon there are more marine basins with $D > 350 \text{ km}$, while on the reverse side there are more seas of smaller size. According to the authors, this is due to the different thickness of the crust on both sides of the Moon, as well as differences in the porosity and temperature of the lunar rocks.

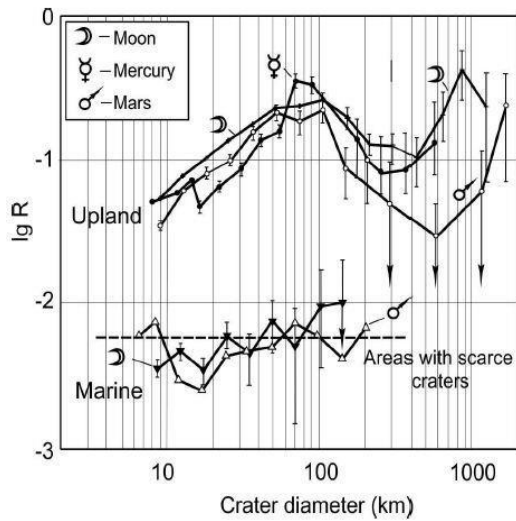


Figure 1. R-distribution of large craters on upland (continental) and lowered (marine) areas on surface Moon, Mars and Mercury [Voronov, Strom and Garkis,1986]

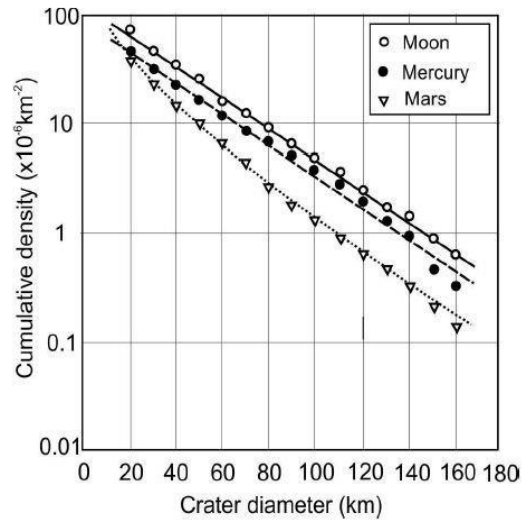


Figure 2. Cumulative N(D) distributions of upland craters on the Moon, Mercury and Mars in semi-logarithmic coordinate system [Barenbaum, 2010]

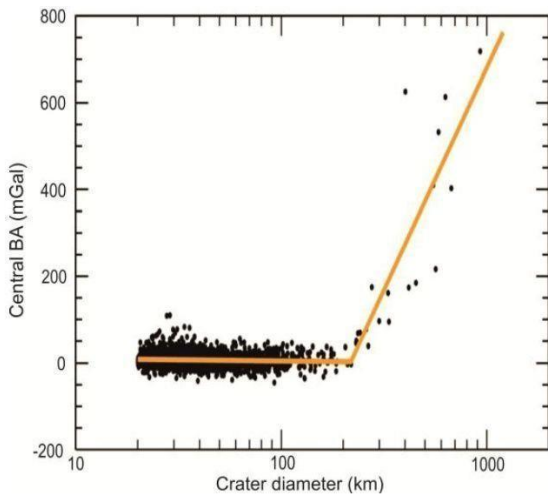


Figure 3. Amplitude of the central gravitational Bouguer anomaly versus D for craters formed in the lunar upland. Yellow line shows the approximation of the measurements data of the proposed model [Soderblom et al.,2015].

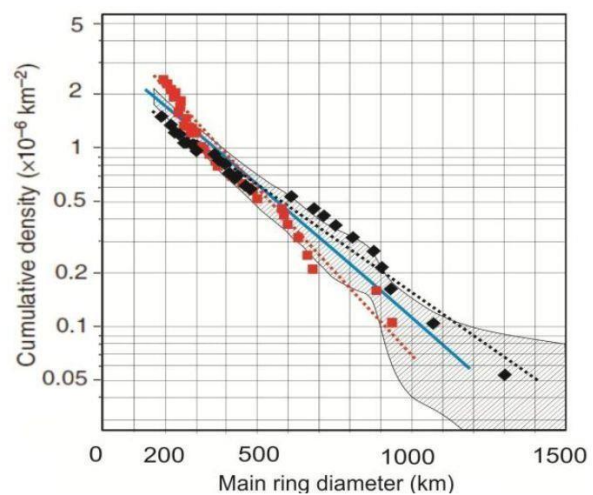


Figure 4. Cumulative size-frequency distributions for complex craters and basins [Neumann et al.,2015]

Fig. 2 and 4 allow us to establish that the transition to Fig. 1 from continental craters to sea basins with mascons is not monotonous. Thus, if the number of craters of diameter $D > 160$ km is $N_{cr}(160) < 1$ per million km^2 (see Figure 2), then the number of seas with mascons (see Figure 4) of the same diameter is $N_m(160) \approx 2$ by million km^2 . This discrepancy is explained by different physical mechanisms of the formation of craters and seas by galactic comets [Barenbaum, Shpekin, 2017].

According to [Barenbaum, 2016], craters are formed in sections of the "thick" lithosphere from the fall of single comets, while lava seas create by magma which pours out from asthenospheric lenses formed under conditions of "thin" lithosphere with a high density of cometary falls.

In addition to heating the asthenosphere by comets, the processes of cooling the rocks of the lithosphere and tectonic relaxation of the lunar surface during the time between cometary bombardings also participate in the formation of the modern relief of the Moon. Therefore, when analyzing the actual data, one should also take into account: 1) the periods of cometary bombardments, 2) the orientation of the Moon rotation axis relative to the direction of galactic comets arrival, and 3) the time of tectonic relaxation of the lunar surface [Barenbaum, 2015; Barenbaum, 2016].

A joint consideration of these factors makes it possible to estimate the time of formation of lunar mascons.

Age of the lunar mascons. We [Barenbaum, 2010; Barenbaum and Shpekin, 2011] have shown

that the surface of the Moon, Mars and Mercury, the bombing of which is one of the leading relief-forming factors on all the terrestrial planets, has now been plowed repeatedly by the galactic comets fall. In the epochs of cometary falls, along with the formation of craters, there is a rise in the surface bombarded by comets, which are largely leveling by means of the relaxation processes during periods between bombings.

The data (Figure 1) indicate that most craters with $D = 10-160$ km on the continents of the Moon, Mars and Mercury, like continents themselves, arose with the last bombardment of the solar system by galactic comets. The same conclusion can be drawn about the seas of the Moon and Mars, with the only difference that outflows of sea basalts occurred at the end of this bombardment or immediately after its termination.

The situation with the mascons is somewhat more complicated. According to [Neumann et al., 2015], the mascons on the Moon are both under the seas and on the continents, where they are clearly not connected with large craters. Sea mascons, as a rule, have a certain topographic structure and are characterized by high values of the central gravity anomaly, which allows them to be divided into 6 groups. While mascons on the continents are more difficult to identify, they are characterized by smaller gravitational anomalies, and many of them are left without classification.

Unlike sea mascons, which we consider "young", the unstructured ones formed under the sea basins, which arose earlier, but they have been completely leveled and ceased to exist at present.

Since in the Cenozoic the galactic comets predominantly bombarded the southern hemisphere of the Moon, it should be expected that in its southern hemisphere there are more young mascons.

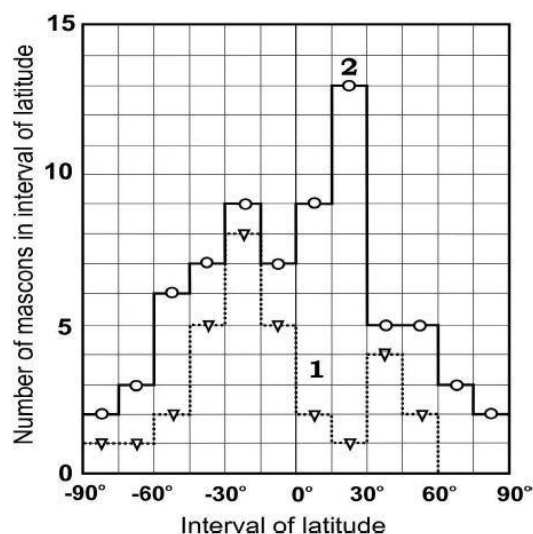


Figure 5. Latitudinal distributions of mascon basins: 1—"young" basins; 2—"old" basins.

While in the northern hemisphere must prevail old mascons.

In Fig. 5, according to [Neumann et al., 2015], we constructed distributions over 15-degree latitude intervals for 16 off-the-sea "peak-ring" mascons, which by many attributes refer to young, as well as for 71 mascons with unclassified structure, which we consider old. It is clearly seen that young mascons dominate in the southern hemisphere of the Moon, while the number of old structures in the northern hemisphere is predominant.

References:

1. Barenbaum A. A. (2010) Galaxycentric paradigm in geology and astronomy (Moscow: Librokom) 546 c. (Rus.)
2. Barenbaum A. A. and Shpekin M. I. (2011) Vestnik Otdelenia Nauk o Zemle RAN 3 NZ6011, doi:10.2205/2011NZ000141.
3. Barenbaum A. A. (2016) The formation of asthenosphere by galactic comets as a new trend in tectonophysics // Tectonophysics and topical issues of Earth sciences. Conference materials: M.: IPE RAS, vol. 2. Section 5, p. 430. (Rus.)
4. Voronov A., Strom R.G. and Garkis M. (1986) Interpretation of the crater chronicle: from Mercury to Ganymede and Callisto // Satellites of Jupiter, Edited D. Morrison, vol. 2 (Moscow: Mir) p 5.
5. Melosh H. J. (1989) Impact Cratering. A Geological Process (New York: Oxford Univ. Press Inc.) 336 p.
6. Barenbaum A.A. (2015) On the mechanism of energy dissipation of galactic comets bombarding terrestrial planets // Journal of Physics: Conf. Ser. 653 012073, doi:10.1088/1742-6596/653/1/012073.
7. Barenbaum A.A., Shpekin M.I. (2016) To the development of the mechanism of interaction of galactic comets with the terrestrial planets // Journal of Physics: Conf. Ser. 774 012096 doi:10.1088/1742-6596/774/1/012096.
8. Barenbaum A.A., Shpekin M.I. (2017) To the formation mechanism of the lunar mascons by galactic comets // XXXII International Conference on Interaction of Intense Energy Fluxes with Matter (March 1-6.2017, Elbrus Russia) Book of Abstracts. Moscow & Chernogolovka & Nalchik. P. 223.
9. Melosh H.J., Freed A.M., Johnson B.C. et al. (2013) The origin of lunar mascon basins // Science. Vol. 340, Issue 6140, pp. 1552-1555, doi:10.1126/science.1235768.
10. Neumann G.A., Zuber M.T., Wieczorek M.A. et al. (2015) Lunar impact basins revealed by Gravity Recovery and Interior Laboratory measurements // Science Advances. 1, e1500852, doi:10.1126/sciadv.1500852.
11. Soderblom J.M., Evans A.J. Johnson B.C. et al. (2015) The fractured Moon: Production and saturation of porosity in the lunar highlands from impact cratering // Geophys. Res. Lett., 42, 6939–6944, doi: 10.1002/2015GL065022.